

https://dspace.org/

The effect of intrauterine alcohol exposure on postnatal skeletal development in Sprague Dawley rats

Pillay, Diana Subramony

2019

https://hdl.handle.net/10539/29877

Pillay, Diana Subramony, The effect of intrauterine alcohol exposure on postnatal skeletal development in Sprague Dawley rats, University of the Witwatersrand, Johannesburg, <http://hdl.handle.net/10539/29877>

Downloaded from a DSpace repository. https://dspace.org/

THE EFFECT OF INTRAUTERINE ALCOHOL EXPOSURE ON POSTNATAL SKELETAL DEVELOPMENT IN SPRAGUE DAWLEY RATS

Diana Subramony Pillay

A Thesis submitted to the Faculty of Health Sciences, University of the Witwatersrand, Johannesburg, in accomplishment of the requirements for the degree of Doctor of Philosophy.

Johannesburg, 2019

DECLARATION

I, Diana Pillay declare that this dissertation entitled “The effect of intrauterine alcohol exposure on postnatal skeletal development in Sprague Dawley rats” is my own work. It is being submitted for the Degree of Doctor of Philosophy at the University of The Witwatersrand, Johannesburg. It has not been submitted before for any degree or examination at any other University.

_____

Diana Subramony Pillay

31th day of October 2019, Parktown

PRESENTATIONS ARISING FROM THIS THESIS

1. **PILLAY, D.S**., NDOU, R. Microarchitecture and tensile strength of the rat femur (Sprague Dawley) at 12 weeks postnatally following maternal gestational alcohol treatment. 47th Annual Conference, Anatomical Society of Southern Africa (ASSA), April 2019. Oral presentation

2. **PILLAY, D.S**., NDOU, R. The effects of intrauterine alcohol exposure on the growth plate of 3-week rat humerus: An immunohistochemical investigation. 46th Annual Conference, Anatomical Society of Southern Africa (ASSA), April 2018. Oral presentation

3. **PILLAY, D.S**., NDOU, R. The effects of gestational alcohol treatment on the microarchitecture of the rat humerus (*Sprague Dawley*) at 3 weeks postnatally. 46th Annual Conference, Anatomical Society of Southern Africa (ASSA), April 2018. Poster presentation

4. **PILLAY, D.S**., NDOU, R. Intrauterine alcohol exposure affects bone epiphyseal plate chondrocyte proliferation by inhibiting transforming growth factor beta-1 (TGFβ1) in 3-week-old rat (*Sprague Dawley*) humerus. 6th World Congress on Controversies, Debates & Consensus in Bone, Muscle & Joint Diseases (BMJD), Bangkok, Thailand, November 2018. Poster presentation

5. NDOU, R**., PILLAY, D.S**. Effects of prenatal alcohol exposure on Sprague Dawley rat growth and development. 45th Annual Conference, Anatomical Society of Southern Africa (ASSA), April 2017. Oral presentation

6. **PILLAY, D.S**., NDOU, R. The effects of gestational alcohol treatment on the rat femur (*Sprague Dawley*): A three-dimensional micro focus X-ray computed tomography (3D-µCT) investigation. 45th Annual Conference, Anatomical Society of Southern Africa (ASSA), April 2017. Oral presentation

7. NDOU, R**., PILLAY, D.S**. The Effects of Prenatal Alcohol Exposure on Sprague Dawley Rat Femur: A Three-Dimensional Micro Focus X-Ray Computed Tomography (3D-µCT) Investigation. XXIV International symposium of morphological sciences, Xian, China, 26th – 30th July 2017. Oral presentation

8. **PILLAY, D.S.,** NDOU, R. The Effects of Prenatal Alcohol Exposure on Sprague Dawley Rat Femur: A Three-Dimensional Micro Focus X-Ray Computed Tomography (3D-µCT) Investigation. The 3rd conference on imaging with radiation (IMGRAD), University of Witwatersrand, 14-15 Sep 2017. Oral presentation

ABSTRACT

The detrimental effects of intrauterine alcohol exposure are well known, however, many women around the world continue to drink alcohol while pregnant. The deleterious effects include neurological deficiencies, intrauterine and postnatal growth retardation as well as craniofacial and skeletal deformities in addition to short stature and osteoporosis, with high propensity to fracture. The central nervous system disturbances related to intrauterine alcohol exposure are intensively studied in the scientific literature, with relatively scanty data on the postnatal skeletal development in children exposed to alcohol during gestation.

The few studies on how intrauterine alcohol exposure affects skeletal development are on fetuses and newly born animals, mostly rodents. There is debate as to whether gestational alcohol exposure effects on the skeletal system persist into adulthood or whether there is skeletal recovery in postnatal life. Therefore, this study aims to investigate whether the effects of prenatal alcohol exposure persist through postnatal life in rats (3 and 12-week-old) regarding long bone (humerus and femur) development and strength.

To achieve our aim, animals were time-mated (n=15), then randomly allocated to three groups; ethanol group (n=6), saline controls (n=6) and untreated controls (n=3). The appearance of a vaginal plug was considered day one of gestation; on this this day treatment was started. The former two groups were treated with 0.015ml/g of 25.2% ethanol and 0.9% saline for the first 19 days of gestation, respectively. The treatment was through oral gavage. The untreated group received no treatment. Once born, two pups from each dam were used so that the ethanol and saline control group had 12 pups each while the untreated control had 6 pups.

Bilateral humeri and femora were harvested then fixed in 10% buffered formalin before scanning using a 3D-µCT scanner (Nikon XTH 225L) to analyse trabecular thickness, number, and spacing were. The left proximal and distal extremities of the humeri and femora at 3 weeks of age were processed for routine histology. These sections were stained with Haematoxylin and Eosin (H&E) for normal morphology and immunolabelled with the anti-Ki-67 antibody for cell proliferation as well as immunolocalization of chondrocytes

expressing Transforming Growth Factor Beta-1 (TGFβ1) at 3 weeks of age. The right humeri and femora at 12 weeks of age were subjected to 3-point bending tests using a universal tensile tester to obtain the maximum force, displacement and time, as well as the breaking force.

The crown rump length (CRL) was reduced in postnatal day 1 and 3-week-old pups belonging to the ethanol group. Using Ki-67 showed that exposure to alcohol during gestation results in decreased chondrocyte proliferation coupled with smaller epiphyseal growth plates containing fewer chondrocytes in both the femur and humerus on ethanol treated rats. We also found that TGFβ1 immunopositive chondrocytes were fewer in the alcohol group. With these findings, we propose that intrauterine alcohol exposure inhibits TGFβ1 expression, leading to fewer chondrocytes that also proliferate at a slower rate in the epiphyseal growth plates. With respect to trabecular morphometric parameters obtain through Micro CT, disturbances in the number, thickness and spacing of trabeculae were detected in both the 3 and 12-week old humeri and femora of the ethanol group. However, there were no differences in bone strength detected.

We conclude that gestational alcohol exposure has more severe consequences in bone development during the early stages afterbirth which may improve in postnatal life. This may be more applicable if the offspring does not take alcohol in postnatal life in our study in which alcohol exposure was only in the gestational phase with no postnatal alcohol intake.

ACKNOWLEDGEMENTS

Writing this note of thanks is the finishing touch on my dissertation after three years of extensive work. It has been a period of intense learning for me, not only in the scientific arena but also on a personal level. I would like to reflect on the people who have supported and helped me so much throughout this period.

Firstly, I would like to express my sincere gratitude to my supervisor Prof Robert Ndou for the continuous support, ideas, funding, for his patience, motivation, and immense knowledge making my PhD experience productive and stimulating. His guidance helped me in all my research and writing of this thesis. I could not have imagined having a better supervisor and mentor for my PhD study than him.

My sincere thanks and appreciation to Mrs Ali for all her technical assistance. My master students, Vaughan Perry and Nura Bello, thank you for all your laboratory support during the pursuit of this thesis. I also wish to thank Dr Kudakwashe Jakata who assisted me with scanning and reconstruction of the rat bones.

Nobody has been more important to me in the pursuit of this PhD than the members of my family. Your prayer and support are what sustained me thus far. Most importantly; I wish to thank my loving and supportive husband, Craig, and son, Jordan, who provide unending inspiration. I would like to thank my parents, Benny and Pushpa and siblings whose love and guidance are with me in whatever I pursue. To my in-laws, Philip and Rita, thank you for praying and supporting me throughout this journey.

Special thanks to my friends who supported me and encouraged me during this time. Also, a huge thanks go to the staff in the School of Anatomical Sciences for your encouragement and support.

Above all, I owe it all to the Lord, Jesus Christ, for granting me the wisdom, health and strength to undertake this research task and enabling me to its completion.

TABLE OF CONTENTS

DECLARATION		i
PRESENTATIONS		ii
ABSTRACT		iii
ACKNOWLEDGEMENTS		v
LIST OF FIGURES		viii
LIST OF TABLES		xii
LIST OF ABBREVIATIONS		xiii
CHAPTER 1	Introduction, Literature Review, Aims and Objectives	3
CHAPTER 2	A Sprague Dawley rat model for studying postnatal growth and development associated with prenatal alcohol exposure in a binge drinking setting	25
CHAPTER 3	Intrauterine alcohol exposure inhibits Transforming Growth Factor Beta-1 (TGFβ-1) expression in epiphyseal growth plate chondrocytes and disturbs trabecular morphology, in the Sprague Dawley rat humerus epiphysis	44
CHAPTER 4	Intrauterine alcohol exposure delays growth and disturbs trabecular morphology through inhibiting epiphyseal plate chondrocyte Transforming Growth Factor Beta-1 (TGFβ1) expression in 3-week-old Sprague Dawley rat femur	83
CHAPTER 5	Trabecular morphometry and bone strength in postnatal life (12 weeks) of Sprague Dawley rats exposed to intrauterine alcohol	123
CHAPTER 6	General discussion and conclusions	156
REFERENCES		162
APPENDICES		

LIST OF FIGURES

Figure	Description	Page
Figure 1.1	Facial dysmorphology seen in FAS children	8
Figure 1.2	Features of a long bone	11
Figure 1.3	Electron micrograph of Haversian canal	12
Figure 1.4	Schematic representation of bone microarchitecture	13
Figure 1.5	Schematic representation of endochondral ossification	16
Figure 1.6	Zones of the growth plate	16
Figure 1.7	Bone remodelling	18
Figure 1.8	TGF β Signalling pathway/Smad pathway	19
Figure 1.9	Force-displacement curve	21
Figure 2.1	Allocation of groups	29
Figure 2.2	Food consumption	31
Figure 2.3	Mass gained	31
Figure 2.4	Chow calories	32
Figure 2.5	Total FER (dams)	33
Figure 2.6	Body mass of the pups on postnatal day 1	35
Figure 2.7	The crown-rump length of the pups at postnatal day 1	35
Figure 2.8	Weight of the pups at 3 weeks of age	36
Figure 2.9	The crown-rump length of the pups at 3 weeks of age	37
Figure 2.10	Weekly mass (3-12 weeks)	37
Figure 3.1	Three-dimensional reconstruction of the humerus showing the parts that were investigated	47
Figure 3.2	Humerus length at 3 weeks of age	51
Figure 3.3	Humerus epiphysis volume at 3 weeks of age	52
Figure 3.4	Humerus total bone to volume ratio (BV/TV) at 3 weeks of age	53
Figure 3.5	Humerus trabecular thickness (TbTh) at 3 weeks of age	54
Figure 3.6	Humerus trabecular thickness (TbN) at 3 weeks of age	55
Figure 3.7	Humerus trabecular spacing (TbSp) at 3 weeks of age	56
Figure 3.8	Trabecular morphology in the humerus at 3 weeks of age	57
Figure 3.9	Humerus proximal cross-sectional area, medullary area and cortical thickness at 3 weeks of age	58
Figure 3.10	Humerus midshaft cross-sectional area, medullary area and cortical thickness at 3 weeks of age	59
Figure 3.11	Humerus distal cross-sectional area, medullary area and cortical thickness	60
Figure 3.12	Histomorphometry of the epiphyseal growth plate surface area in the humerus at 3 weeks of age	61
Figure 3.13	Photomicrograph of the Haematoxylin and Eosin stained section epiphyseal growth plate of the humerus	62

Figure 3.14	Epiphyseal growth plate proliferative zone number of chondrocytes in the humerus	63
Figure 3.15	Epiphyseal growth plate hypertrophic zone number of chondrocytes in the humerus	64
Figure 3.16	Ki-67 immuno-positive proliferative chondrocytes of the humerus	65
Figure 3.17	Photomicrograph of humerus proliferative zone chondrocytes immunolabeled with the anti-Ki-67 antibody	66
Figure 3.18	Ki-67 immuno-positive hypertrophic chondrocytes of the humerus	67
Figure 3.19	Photomicograph of humerus hypertrophic zone chondrocytes immunolabeled with the anti-Ki-67 antibody	68
Figure 3.20	TGFβ-1 immuno-positive proliferative chondrocytes in the epiphyseal growth plate of the humerus	69
Figure 3.21	Photomicograph of humerus proliferative zone chondrocytes immunolabeled with the anti-TGFβ1 antibody	70
Figure 3.22	TGFβ-1 immuno-positive hypertrophic chondrocytes in the epiphyseal growth plate of the humerus	71
Figure 3.23	Photomicograph of humerus hypertrophic zone chondrocytes immunolabeled with the anti-TGFβ1 antibody	72
Figure 4.1	Three-dimensional reconstruction of a 12-week old femur showing the parts that were investigated	85
Figure 4.2	Femur length at 3 weeks of age	89
Figure 4.3	Femoral shaft volume at 3 weeks of age	90
Figure 4.4	Femoral bicondylar length at 3 weeks of age	91
Figure 4.5	Femoral epiphysis volume at 3 weeks of age	92
Figure 4.6	Femoral bone to total volume ratio (BV/TV) at 3 weeks of age	93
Figure 4.7	Femoral trabecular thickness (TbTh) at 3 weeks of age	94
Figure 4.8	Femoral trabecular number (TbN) at 3 weeks of age	95
Figure 4.9	Femoral trabecular spacing (TbSp) at 3 weeks of age	96
Figure 4.10	Proximal (25^{th} percentile mark) dimensions of the femur at 3 weeks of age	97
Figure 4.11	Midshaft (50th percentile mark) dimensions of the femur at 3 weeks of age	98
Figure 4.12	Distal (75th percentile mark) dimensions of the femur at 3 weeks of age	99
Figure 4.13	Histomorphometry of the epiphyseal growth plate surface area in the femur at 3 weeks of age	100
Figure 4.14	Photomicrograph of the Haematoxylin and Eosin stained section epiphyseal growth plate of the femur	102
Figure 4.15	Epiphyseal growth plate proliferative zone number of chondrocytes in the femur	103
Figure 4.16	Epiphyseal growth plate hypertrophic zone number of chondrocytes in the femur	104
Figure 4.17	Ki-67 immuno-positive proliferative chondrocytes of the femur	105

Figure 4.18	Photomicrograph of femur proliferative zone chondrocytes immunolabeled with the anti-Ki-67 antibody	106
Figure 4.19	Ki-67 immuno-positive hypertrophic chondrocytes of the femur	107
Figure 4.20	Photomicrograph of femur hypertrophic zone chondrocytes immunolabeled with the anti-Ki-67 antibody	108
Figure 4.21	TGFβ-1 immuno-positive proliferative chondrocytes in the epiphyseal growth plate of the femur	109
Figure 4.22	Photomicrograph of femur proliferative zone chondrocytes immunolabeled with the anti-TGFB1 antibody	110
Figure 4.23	TGFβ-1 immuno-positive hypertrophic chondrocytes in the epiphyseal growth plate of the femur	111
Figure 4.24	Photomicrograph of femur hypertrophic zone chondrocytes immunolabeled with the anti-TGFβ1 antibody	112
Figure 5.1	Three-dimensional reconstruction of a 12-week old humerus showing the parts that were investigated	127
Figure 5.2	Three-dimensional reconstruction of a 12-week old femur showing the parts that were investigated	127
Figure 5.3	Three-point bending test	129
Figure 5.4	Humerus osteometric measurements at 12 weeks of age	130
Figure 5.5	Humerus bone to total volume ratio (BV/TV) at 12 weeks of age	131
Figure 5.6	Humerus trabecular thickness (TbTh) at 12 weeks of age	132
Figure 5.7	Humerus trabecular number (TbN) at 12 weeks of age	133
Figure 5.8	Humerus trabecular spacing (TbSp) at 12 weeks of age	134
Figure 5.9	Trabecular morphology in the humerus at 12 weeks of age	135
Figure 5.10	Humerus proximal cross-sectional area, medullary canal area and cortical thickness at 12 weeks of age	136
Figure 5.11	Humerus midshaft cross-sectional area, medullary canal area and cortical thickness at 12 weeks of age	137
Figure 5.12	Humerus distal cross-sectional area, medullary canal area and cortical thickness at 12 weeks of age	138
Figure 5.13	Femur osteometric measurements at 12 weeks of age	140
Figure 5.14	Femur bone to total volume ratio (BV/TV) at 12 weeks of age	141
Figure 5.15	Femur trabecular thickness (TbTh) at 12 weeks of age	142
Figure 5.16	Femur trabecular number (TbN) at 12 weeks of age	143
Figure 5.17	Femur trabecular spacing (TbSp) at 12 weeks of age	144
Figure 5.18	Trabecular morphology in the femur at 12 weeks of age	145
Figure 5.19	Femur proximal cross-sectional area, medullary canal area and cortical thickness at 12 weeks of age	146
Figure 5.20	Femur midshaft cross-sectional area, medullary canal area and cortical thickness at 12 weeks of age	147
Figure 5.21	Femur distal cross-sectional area, medullary canal area and cortical thickness at 12 weeks of age	148
Figure 5.22	Principal component analysis	151

LIST OF TABLES

Table	Description	Page
Table 2.1	Gestation duration and litter size for the ethanol group, saline and untreated controls	34
Table 3.1	Scanning parameters	47
Table 3.2	Osteometric parameters taken from 3-week-old humeri	48
Table 3.3	Trabecular parameters assessed	48
Table 3.4	Humerus osteometric and proximal epiphysis trabecular morphometric parameters in the equation	73
Table 3.5	Group membership classification from humerus osteometric and proximal epiphysis trabecular morphometric parameters	74
Table 3.6	Humerus osteometric and distal epiphysis trabecular morphometric parameters in the equation	75
Table 3.7	Group membership classification from humerus osteometric and distal epiphysis trabecular morphometric parameters	75
Table 4.1	Osteometric parameter descriptions	86
Table 4.2	Femur osteometric and proximal epiphysis trabecular and cortical morphometric parameters in the equation	113
Table 4.3	Group membership classification from osteometric and proximal epiphysis trabecular morphometric parameters of the femur	114
Table 4.4	Femur osteometric and distal epiphysis trabecular and cortical morphometric parameters in the equation	115
Table 4.5	Group membership classification from osteometric and distal epiphysis trabecular morphometric parameters of the femur	115
Table 5.1	Scanning parameters of 12-week old bones.	126
Table 5.2	Osteometric parameter descriptions	128
Table 5.3	Osteometric measurements and tensile strength of the humerus	139
Table 5.4	Osteometric measurements and tensile strength of the femur	149
Table 5.5	Principal components analysis of femur and humerus	150

LIST OF ABBREVIATIONS

%:	Percent
^{o}C:	Degree celsius
β:	Beta
µm:	micrometer
dl:	deciliter
g:	gram
kg:	kilogram
kcal:	Calories
ml:	milliliter
mg:	milligram
mm:	millimeter
nm:	nanometer
µCT:	Microfocus x-ray computed tomography
3D:	Three-dimensional
AESC:	Animal Ethics Screening Committee
ANOVA:	Analysis of variance
AP:	Alkaline phosphatase
APES:	3-aminopropyltriexothysilane
ARBD:	Alcohol-related birth defects
ARND:	Alcohol related neurodevelopmental disorder
BDMP:	Birth Defects Monitoring Program

BAC:	Blood alcohol concentration
BMD:	Bone marrow density
BMU:	Basic multicellular unit
BV/TV	Bone volume to total volume
CAS:	Central animal services
CNS:	Central nervous system
CRL:	Crown rump length
DAB:	3-3’ di-amino benzidine
DNA:	Deoxyribose nucleic acid
EDC:	Ethanol-derived calories
EDTA:	Ethylenedeamine tetraacetic acid
FAS:	Fetal alcohol syndrome
FASD:	Fetal alcohol spectrum disorder
FER:	Feed efficiency ratio
Fig:	Figure
H_2O_2:	Hydrogen peroxide
H&E:	Haematoxylin and eosin
IHC:	Immunohistochemistry
PBS:	Phosphate buffer solution
pFAS:	Partial fetal alcohol syndrome
TbTh:	Trabecular thickness
TbN	Trabecular number

TbSp: Trabecualr spacing

TGFβ1: Transforming Growth Factor Beta 1

Chapter 1

Introduction, Literature Review,

Aims and Objectives

Table of Contents

1.0 INTRODUCTION 3

1.1 Background to the research question 3

1.2 LITERATURE REVIEW 6

1.2.1 Overview of effects of prenatal alcohol exposure 6

History of FAS 7

1.2.2 Prevalence of FAS 8

Worldwide Prevalence 8

Prevalence in South Africa 8

1.2.3 Binge drinking and a history of alcohol abuse 9

1.2.4 Alcohol metabolism 10

1.2.5 Bone structure and function 10

Cortical bone 12

Trabecular bone (cancellous or spongy bone) 13

1.2.6 The effects of alcohol on the internal bone architecture 14

1.2.7 Development and remodelling of bone 14

Long bone formation and elongation 14

1.2.8 The role of transforming growth factor beta 1 (TGFβ1) in signalling in bone 18

1.2.9 Bone biomechanical properties 20

AIM 22

OBJECTIVES 22

1.0 INTRODUCTION

1.1 Background to the research question

Alcohol is the most abused legal substance worldwide Olivier et al. (2016), and in some communities is often consumed during pregnancy. This is despite the fact that the dire consequences to the fetus are widely known (Abel and Dintcheff, 1978; Day et al., 1989; Chaudhuri, 2000; Simpson et al., 2005). In South Africa, the rate of alcohol consumption during pregnancy is among the highest in the world at 13% (Peltzer and Pengpid, 2019) compared to 9.8% on average in the rest of the world (Peltzer and Pengpid, 2019). A range of disorders known as Fetal Alcohol Spectrum Disorders (FASD) may occur because of gestational alcohol exposure. Fetal Alcohol Syndrome (FAS) is the most severe form of this spectrum of disorders. Neurological anomalies, facial dysmorphology and growth retardation (O'Leary, 2004; Olivier et al., 2016) are the main characteristics of FAS. While most research studies emphasize the neurological aspects of FAS (Idrus et al., 2017; Petrelli et al., 2018; Naassila and Pierrefiche, 2019), there is a paucity of literature with respect to the implications for the osseous tissue. The latter presents with short stature, low weight to height ratio, a small head (O'Leary, 2004) and propensity to osteoporosis and increased fracture risk (Simpson et al., 2005).

Existing studies investigating the effects of gestational alcohol exposure on skeletal elements focus mostly on rat fetuses (Simpson et al., 2005; Snow and Keiver, 2007). Consequently, there is limited research on postnatal skeletal development among adolescents and young adults (Miralles-Flores and Delgado-Baeza, 1992; Turner, 2000). It is very important to understand how gestational alcohol exposure affects the skeletal system in postnatal development as peak bone growth occurs during adolescence (Farr and Khosla, 2015). Such research could provide evidence as to whether the effects of gestational alcohol persist through childhood and adolescent stages or if there are restorative processes to the alcohol effects in postnatal life.

The existing literature on the effects of prenatal exposure to alcohol on bone growth uses animal models that mimic moderate to heavy alcohol drinking (Simpson et al., 2005; Snow and Keiver, 2007). In South Africa, some pregnant women drink in secret to evade detection by their spouses and the social stigma associated with women drinkers (Olivier et al., 2016). This behaviour results in binge drinking. Considering this, a model that mimicked binge drinking was employed in the present study. Binge drinking is defined as consuming four to five glasses of alcohol per occasion (Croxford and Viljoen, 1999; Katwan et al., 2011).

Miralles-Flores and Delgado-Baeza (1992), suggested that intrauterine alcohol exposure results in growth retardation through disturbances of the epiphyseal growth plate in rat long bones due to impaired cell function. However, markers of cell proliferation were not used to establish the number of proliferating chondrocytes in the respective zones. Therefore, this knowledge gap needs further investigation by using markers of cell proliferation such as immunolocalising the Ki-67 protein in epiphyseal growth plate chondrocytes.

Bone lengthening relies on the equilibrium between proliferation and senescence of epiphyseal growth plate chondrocytes (Nilsson and Baron, 2004; Lui et al., 2011). This equilibrium may be disturbed by gestational alcohol exposure causing a delay in bone lengthening. Cytokines such as Transforming Growth Factor Beta (TGFβ) regulate bone development and structural integrity. This is the most abundant cytokine in bone matrix (Bismar et al., 1999) and plays a major role in bone remodelling by regulating migration, proliferation, and differentiation of osteoprogenitors (Tang et al., 2009). Other cytokines found in bone matrix such as BMP's, which are associated with bone lengthening should be considered for future studies.

In summary, previous studies on intrauterine alcohol exposure in rat bone reports shorter bone length (Keiver and Weinberg, 2004; Simpson et al., 2005; Snow and Keiver, 2007), delayed fetal skeletal ossification and low skeletal scores (Keiver et al., 1997; Keiver and

Weinberg, 2004). Additionally, osteoporosis and high fracture risk in postnatal life are common (Snow and Keiver, 2007). This suggests that there may be inadequate postnatal catch-up development if a fetus is exposed to intrauterine alcohol.

Considering the above, this study seeks to investigate whether bone growth, development, and structural integrity disturbances would persist through postnatal life in 3 and 12-week-old humerus and femur in a chronic binge drinking rat model. To achieve this, the body size parameters of the pups exposed to gestational alcohol will be evaluated. To assess whether gestational alcohol causes stunted growth through disturbances of epiphyseal growth plate chondrocyte activity, we will immunolabel these chondrocytes for Ki-67 protein expression. We will then evaluate whether exposure to gestational alcohol affects bone growth and development through inhibiting chondrocyte multiplication by anti TGFβ1 antibody immunolabeling. After this, three-dimensional micro-focus X-ray computed tomography (3D- μCT) will be used to assess trabeculae thickness, volume and spacing in the proximal and distal epiphysis of the femur and humerus. Finally, we will test the theory that gestational alcohol exposure increases fracture risk (weakens bones) by using 3-point bending tests to assess bone strength.

1.2 LITERATURE REVIEW

1.2.1 Overview of the effects of prenatal alcohol exposure

Consumption of alcohol during pregnancy has well known teratogenic consequences on fetal development (O'Leary, 2004). These may include spontaneous abortion, fetal growth inhibition, premature delivery, abruption placentae and breech presentations (Abel and Dintcheff, 1978; Miralles-Flores and Delgado-Baeza, 1992; Chaudhuri, 2000). An offspring exposed to alcohol in utero can suffer an assortment of disorders and disabilities (O'Leary, 2004; May et al., 2013) collectively described as Fetal Alcohol Spectrum Disorder (FASD). This is a non-diagnostic, umbrella term used to describe the range of effects on an offspring that result from gestational alcohol exposure (O'Leary, 2004). These include Alcohol-Related Birth Defects (ARBD), Alcohol-Related Neurodevelopmental Disorder (ARND), Partial Fetal Alcohol Syndrome (pFAS), and Fetal Alcohol Syndrome (FAS) (Streissguth et al., 1991; Koren et al., 2003; O'Leary, 2004; May et al., 2013).

The diagnostic criteria used to measure the severity of these disorders involve assessment of physical, cognitive, behavioural and learning abilities of the child. For a diagnosis of alcohol-related birth defects (ARBD) prenatal alcohol exposure must have been confirmed, with evidence of facial abnormalities and one or more congenital anomalies, including malformations and dysplasias of the heart, bone, kidney, visual, or auditory systems (Streissguth et al., 1991; O'Leary, 2004; May et al., 2013).

The alcohol-related neurodevelopmental disorder (ARND) diagnostic criteria are used when there is alcohol-induced mental impairment without the characteristic facial defects and growth deficiency seen in Fetal Alcohol Syndrome (FAS) (Chudley et al., 2005; Hoyme et al., 2005; Welch-Carre, 2005). FAS is the most severe diagnosis of FASD. The partial Fetal Alcohol Syndrome (pFAS) diagnostic criteria reflect a confirmed history of maternal alcohol exposure (when there is a confirmed history of prenatal alcohol exposure and some components of the full syndrome but not enough to establish the diagnosis of FAS) (Koren et al., 2003; O'Leary, 2004; May et al., 2013).

History of FAS

The history of FAS description and its diagnosis has been reviewed by Koren (2012). In brief, the first documented description of the adverse consequences of gestational alcohol exposure was by Lemoine et al (1968) in a not widely known French journal (*Quest Medical*). Five years later, Jones et al. (1973), made it more widely known after publishing in *The Lancet*, and naming the condition as Fetal Alcohol Syndrome. The English translation of Lemoine's work was republished in 2003 in Therapeutic Drug Monitoring as (Lemoine et al., 2003).

In South Africa, the first documented clinical diagnosis of FAS was in 1978 in a study investigating new-born babies (n=4) from Somerset hospital, Cape Town (Beyers and Moosa, 1978). These authors expressed the view that the condition may be more common than previously thought and that subtle abnormalities may have often been overlooked (Beyers and Moosa, 1978). Therefore, there was a need to agree upon features that characterise FAS in addition to what had been described by Jones et al. (1973). These features of FAS are grouped into three categories (O'Leary, 2004) as follows:

i. Growth retardation - small stature, low weight to height ratio

ii. Facial characteristics - short palpebral fissure, thin upper lip, flattened philtrum and maxillary hypoplasia (Fig. 1.1)

iii. Brain anomalies - delay in development, intellectual disability and microcephaly

Palmer (1985) described characteristics of FAS evident in 14 infants born at the same hospital (Somerset Hospital) that year. This researcher found that one in 281 infants had facial dysmorphology features consistent with prenatal alcohol consumption. Despite the author's recommendation (Palmer, 1985), it was not until the late 1990s that community surveys were conducted to establish FAS prevalence on wine estates in the Western Cape Province of South Africa.



Figure 1.1: Facial dysmorphology seen in FAS children. Short palpebral fissures, smooth philtrum, and relatively thin vermilion border of the upper lip. Adapted from Hoyme et al. (2016).

1.2.2 Prevalence of FAS

Worldwide Prevalence

The overall global FAS prevalence is 1-3 cases per 1000 births (O'Leary, 2004) with some countries recording lower or higher incidence than the world average. In the USA, rates of 10-15 per 1000 have been reported, 10 per 1000 in Canada, 35 per 1000 in Italy, 18 per 1000 in France, 20 per 1000 in Poland and 12 per 1000 in Croatia (Olivier et al., 2016). A study (Fitzpatrick et al., 2012) in a rural area in Australia in 2015 reported a FAS rate of 120 per 1000. This has been the first study outside South Africa to report figures as close to the South African FAS rates.

Prevalence in South Africa

South Africa has the highest prevalence of FAS in the world ranging from 29-290 per 1000 live births (Olivier et al., 2016). In South Africa, most of the FAS studies have been done in the Western Cape (the main wine producing area) and the Northern Cape. In the Western Cape, a study by May and Viljoen in Olivier et al. (2016) reported rates of 46 per 1000 in grade 1 learners in 1997, increasing to 74 per 1000 in 1999 and 89.2 per 1000 in 2001 (Olivier et al., 2016). The most recent study by Urban et al. (2015), reported the prevalence

of FAS to be 63/1000 in first grade learners in Roodepan, Northern Cape; and 52/1000 first grade learners in Galeshewe, Northern Cape (Urban et al., 2015). In another study in the Northern Cape, among primary school children in De Aar (sheep-farming area) and Upington (wine farming area), an overall FAS rate of 67.2 per 1000 was recorded for both regions (Urban et al., 2008). This similar rate of FAS in a sheep farming area (De Aar) compared to a wine producing area (e.g. Upington), shows that high rates of FAS are not limited to wine farming areas. In support of this, another study in the Gauteng province, where wine production is negligible, has a FAS prevalence of 19 per 1000 children. Even though the rate is low in comparison to that of the Western Cape, it is still high compared to worldwide rates (Olivier et al., 2016).

1.2.3 Binge drinking and a history of alcohol abuse

The reasons for the high prevalence of alcohol consumption in the Western and Northern Cape provinces of South Africa are poorly understood but contributing factors may be multifaceted. One of the contributing factors for the high prevalence of FAS in this Cape provinces could be attributed to poverty in this region (Olivier et al., 2016). Poverty is a factor of low socioeconomic status (Abel and Hannigan, 1995; Viljoen et al., 2002). Historically, the Cape provinces had a practice of paying farm workers with alcohol (the 'Dop' system). While this practice has been abolished, generations of families have a history of alcohol abuse and heavy drinking (Viljoen et al., 2002). Additionally, the existence of 'Shebeens" (informal bars) that sell alcohol, at lower prices increases access to alcohol and may contribute to maternal drinking in these farming communities.

Some conservative sectors of societies around the world (Olivier et al., 2016) and in South Africa stigmatise drinking by a woman. Consequently, some women drink in secret to evade detection by their spouses and to avoid the perceived societal stigma associated with women drinkers (Olivier et al., 2016). This behaviour of secluded alcohol consumption results in binge drinking, defined as consuming four to five glasses of alcohol per occasion (Croxford and Viljoen, 1999; Katwan et al., 2011). This pattern of drinking poses a high risk

for FAS (Jacobson et al., 1998) particularly as women may not know that they are pregnant in the initial two months of gestation. Considering this, the current study employed a model that sought to mimic binge drinking. Binge drinking causes more severe brain damage and behavioural changes than heavy chronic drinking in rats (Thomas et al., 1998). This is thought to be due to the high peak blood alcohol concentration produced by consuming large alcohol volumes over a short duration as in binge drinking (Olivier et al., 2016).

1.2.4 Alcohol metabolism

The removal of ethanol from the body occurs mainly through hepatic metabolism (Cederbaum, 2012). This process is governed by the catalytic enzymes, alcohol dehydrogenase (ADH) and aldehyde dehydrogenase (ALDH) (Ramchandani et al., 2001). The rate at which alcohol is metabolised varies between species (Cederbaum, 2012). All mammalian species express the enzymes required to metabolise ethanol, however, the actual rate at which the enzymes function to clear alcohol from the system varies (Ramchandani et al., 2001). Rodents, including rats and mice, metabolise alcohol at a much faster rate (1.5 hours) than humans, while larger animal species such as sheep and non-human primates have similar rates of alcohol metabolism to humans (4 hours) (Zorzano and Herrera, 1990).

1.2.5 Bone structure and function

To investigate the effects of intrauterine alcohol exposure on growth, an understanding of bone structure is essential. The bony skeleton is a remarkable organ that serves a structural function, providing mobility, support, and protection for the body in addition to storage of essential minerals (Chapurlat and Confavreux, 2016). Bone growth and development contribute significantly to the stature and overall body growth. As it has been established that prenatal alcohol exposure results in short stature (Simpson et al., 2005; Snow and Keiver, 2007), and considering that long bones are crucial for height and growth, this study will pay attention to long bones.

In long bones such as the femur and humerus, a diaphysis or shaft consists of cortical bone surrounding a marrow-filled space known as the medullary canal (Fig. 1.2). On either end of the diaphysis are two rounded ends, the epiphyses (Chapurlat and Confavreux, 2016). The epiphysis consists of trabecular bone, covered by a thin layer of compact bone. In juveniles, a cartilaginous epiphyseal plate is known as the growth plate (longitudinal growth) separates the diaphysis from the epiphyses (Robey and Boskey, 2009). The metaphysis is the transitional zone between the diaphysis and epiphysis (Chapurlat and Confavreux, 2016).

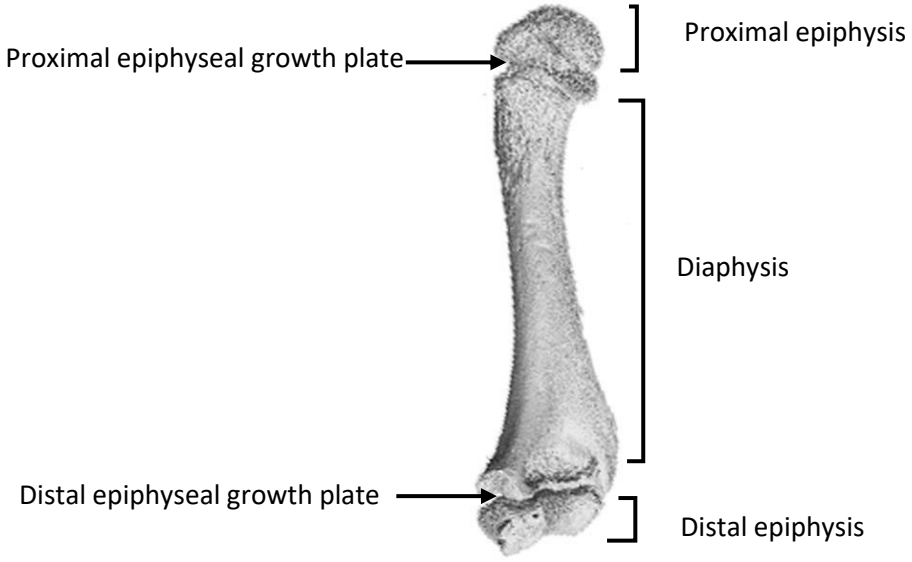


Figure 1.2: Features of a long bone. A 3D reconstruction of a rat humerus obtained from Micro focus X-Ray Computed Tomography (Courtesy of R Ndou).

Cortical bone

Cortical or compact bone consists of several subunits called osteons or the Haversian system (Fig. 1.3). The centre of the osteon has a Haversian canal, containing blood vessels, lymph and nerves (Kierszenbaum and Tres, 2015). Around the Haversian canal, the bone is arranged in concentric layers of calcified matrix called lamellae. The Volkmann's canal interconnects the Haversian canals. The lamellae of the Haversian systems are created by osteoblasts (Fig. 1.3). As these cells secrete matrix, they become trapped in spaces referred to as lacunae (Robey and Boskey, 2009), and become known as osteocytes. These (osteocytes) lie within the lacunae separated from each other, with lengthy cellular processes (canaliculi) extending through the bone matrix. This creates an extensive network for communication with each other and with the bone lining cells and osteoblasts at the bone surface (Bonewald, 2011).

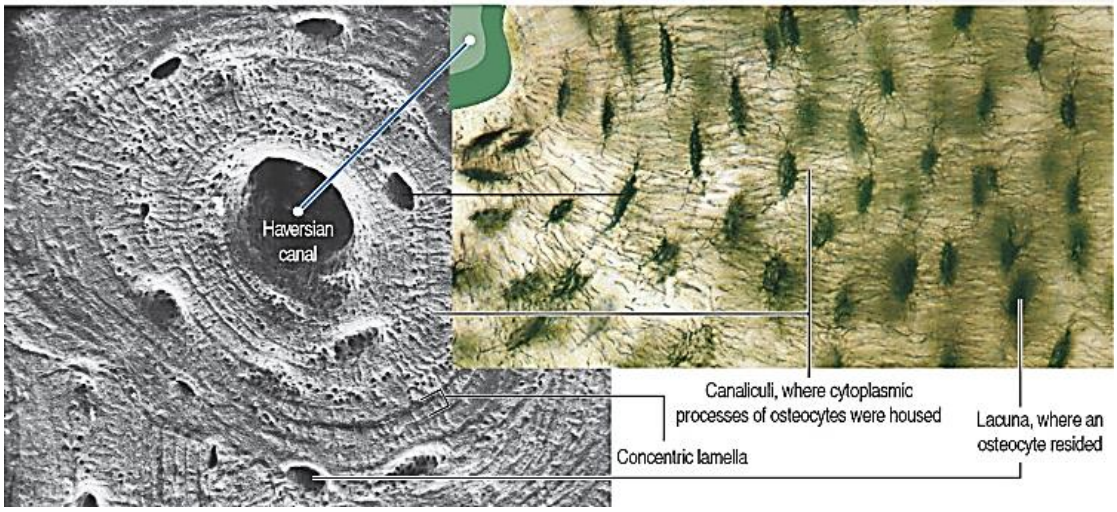


Figure 1.3: Electron micrograph of Haversian canal. Canal surrounded by concentric lamella, with lacuna embedded within. Canaliculi project from lacuna. Adapted from Weiner et al. (1999).

Trabecular bone (cancellous or spongy bone)

A long bone has approximately 20% trabeculae (spongy), found predominantly in the epiphyses, and lining the medullary cavity (Kierszenbaum and Tres, 2015). True osteons and the Haversian systems are absent in spongy tissues. Cancellous or spongy bone has an asymmetrical shape consisting of lamella arranged into an irregular lattice of thin interconnecting partitions called trabeculae (Fig. 1.4). The spaces between the trabeculae are filled with red bone marrow (Hsu et al., 2013). The orientation of trabeculae in spongy bone is along the line of stress similar to the osteons in cortical bone. This feature helps resist stresses and the transfer of force without breaking (Kini and Nandeesh, 2012). Cancellous bone has a higher rate of turnover than compact bone, and so reacts to the changing stresses placed on it more quickly than compact bone does (Hsu et al., 2013). For this reason, osteoporosis is more evident in the cancellous bone compartments than cortical bone.

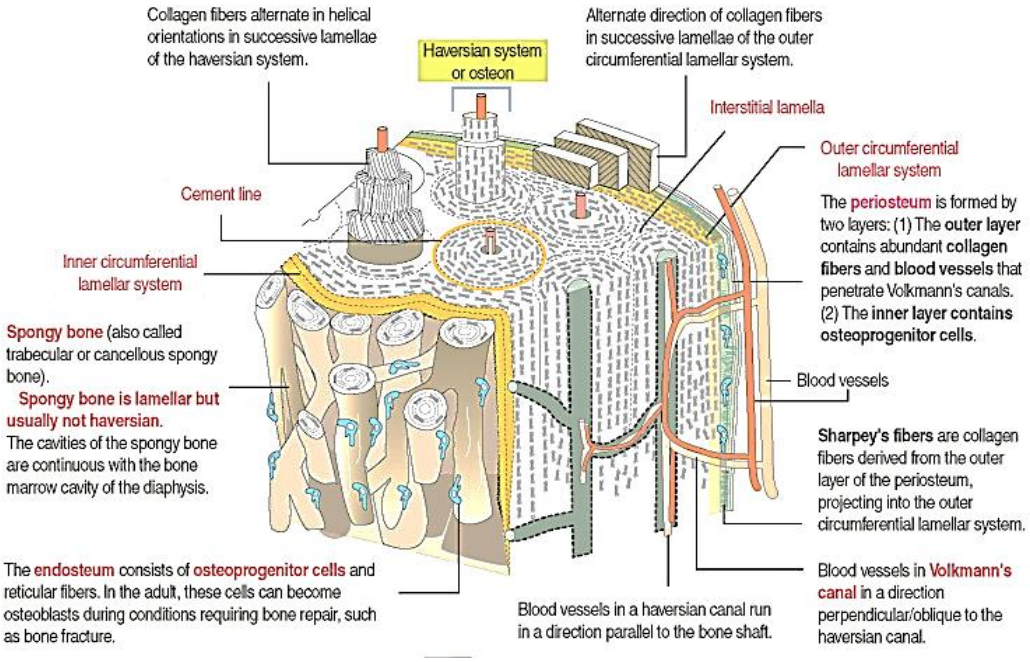


Figure 1.4: Schematic representation of bone microarchitecture. Adapted from Kierszenbaum and Tres (2015).

1.2.6 The effects of alcohol on the internal bone architecture

Alcohol disturbs bone formation, resulting in weaker bones which may be prone to osteoporosis and the increased risk of fracture due to weakness (Turner, 2000; Mikosch, 2014). Therefore, the microarchitecture of the osseous tissue is an important structural property of bone with several factors contributing to bone strength. These factors are (i) bone morphology (size, shape and internal architecture of bone); (ii) bone tissue material properties (density, degree of mineralisation, the extent of micro-damage, collagen traits); and (iii) bone remodelling.

There is limited data on changes in the internal architecture of bone following gestational alcohol exposure. However, research shows that cortical and trabecular thickness is reduced along with a reduction in bone formation rate in alcohol-induced bone disease in postnatal life (Diamond et al., 1989; Hogan et al., 1997; Maurel et al., 2012a). Alcohol consumption modifies bone remodelling, due to a decrease in bone formation (Diamond et al., 1989; Maurel et al., 2011). A decrease in bone formation rate may occur due to the disturbance in proliferation and the activity of osteoblasts (Sampson et al., 1996; Hogan et al., 1997), which may alter the internal integrity of the bone. Although, studies have shown the adverse impact of alcohol consumption on cortical and trabecular parameters, no research has established the effects of gestational alcohol exposure on the internal architecture of postnatal bone development. Knowledge in this area will be useful and will help us understand weaker bones in FAS children.

1.2.7 Development and remodelling of bone

Long bone formation and elongation

Growth retardation and facial dysmorphology are cardinal features which characterize FAS. This may imply that either endochondral or intramembranous ossification may be affected when the fetus is exposed to alcohol. Endochondral ossification is the formation of long bone within a hyaline cartilage model (growth plate), whereas bone forms directly from

mesenchymal cells in intramembranous ossification (Boskey and Coleman, 2010). This process is also involved in the lateral growth of long bones.

Long bone develops by endochondral ossification (Fig. 1.6). This process involves mesenchymal cells condensation, to form clusters of cells. Subsequently, these cells differentiate to become chondrocytes which are the primary cell type of cartilage (Kini and Nandeesh, 2012). A bone collar is formed as mineralisation happens; then the chondrocytes undergo apoptosis. The cell death of the chondrocytes allows (Martini et al., 2015) blood vessels to enter the diaphysis and the outer layer is converted into a primitive form of bone. Blood vessels bring in osteoblasts, which bind to the degenerating cartilaginous matrix and deposit a bone matrix. Bone formation and growth consist of coordinated arrays of proliferating, hypertrophic, and mineralizing chondrocytes. Secondary ossification centres also form as blood vessels enter near the tips of the bone (Sivaraj and Adams, 2016).

The epiphyseal growth plate

The epiphyseal growth plate is responsible for longitudinal growth. The growth plate is a thin layer of cartilage entrapped between the epiphysis and diaphysis, at the ends of long bones (Nilsson and Baron, 2004; Lui et al., 2011). The growth plate comprises three zones (Burdan et al., 2009), viz. the resting, proliferative and hypertrophic zone: (Fig. 1.7).

i. The resting zone is characteristic of immature inactive cartilage cells that anchor the growth plate to the bone.
ii. The proliferation zone contains mature chondrocytes and is the site where rapid cell division and lengthening of the bone occurs.
iii. The hypertrophic zone consists of older chondrocytes which enlarge and signal matrix calcification.

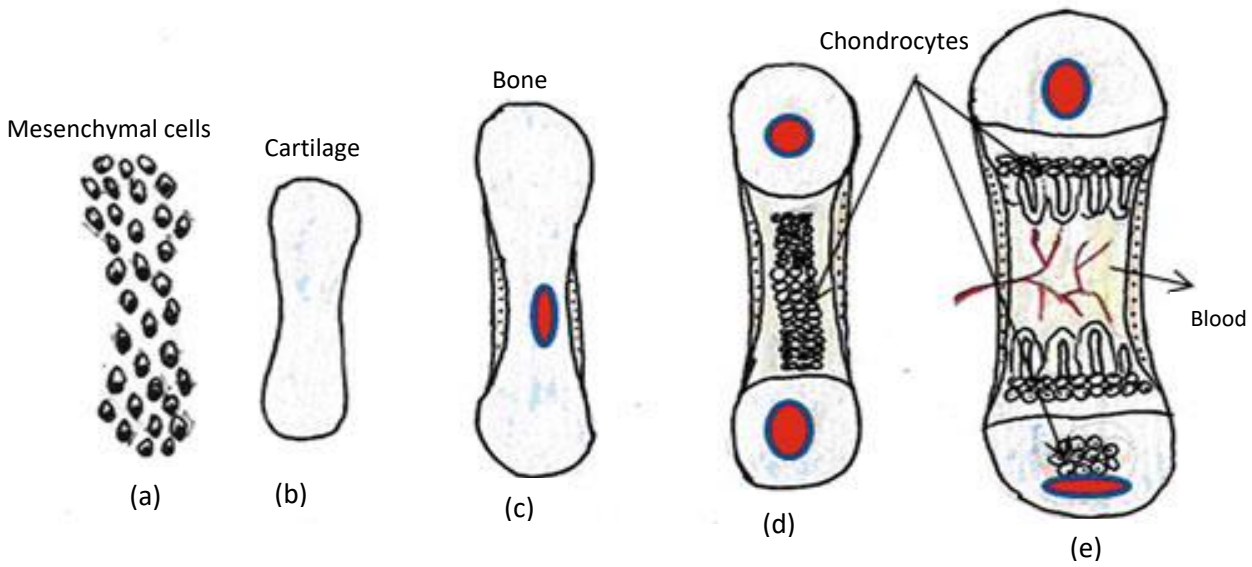


Figure 1.5: Schematic representation of endochondral ossification: (a and b) Condensation of mesenchymal cells, differentiate into chondrocytes which produces the cartilaginous model of the bone (c) primary centre of ossification (d) secondary centre of ossification (e) bone with medullary cavity and epiphyseal ends. Adapted from Kini and Nandeesh (2012).

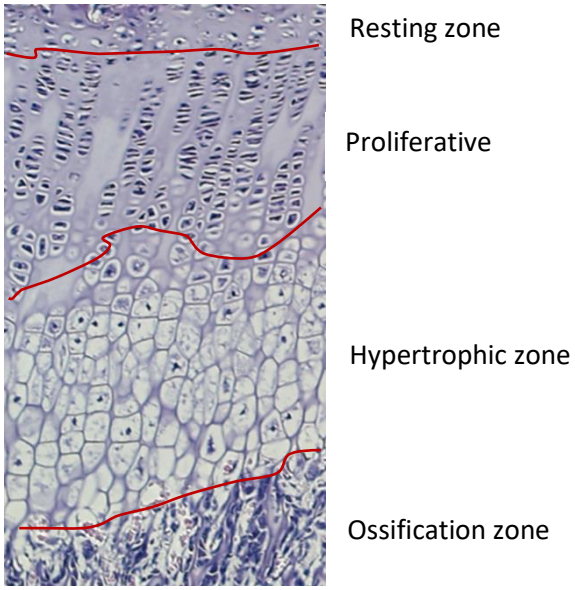


Figure 1.6: Zones of the growth plate (Courtesy of D Pillay).

Bone remodelling and repair

Bone is continuously being remodelled to maintain its integrity throughout life. This process occurs through a sequence of osteoclastic bone resorption followed by osteoblastic new bone formation to repair localized areas of micro-damage (Fig. 1.8) (Raggatt and Partridge, 2010). Disturbances in remodelling, where bone resorption exceeds bone deposition, create imbalances. These imbalances may lead to the fragility in the bone, increasing the propensity of fractures and osteoporosis.

There are four stages involved in bone remodelling are resorption, reversal, formation and quiescence. Micro-damage triggers the activation of the pre-osteoclasts, which differentiate into osteoclasts (Hadjidakis and Androulakis, 2006). This is the resorption stage in which the osteoclasts remove or resorb the damaged bone cells. When resorption ends, the reversal stage is initiated. In this stage, the osteoblast precursors located at the resorption site proliferate and differentiate (Chen et al., 2012; Kini and Nandeesh, 2012). In the formation stage, cytokines such as BMP's and TGFβ, osteoblasts produce collagen and hydroxyapatite to fill the cavities left by osteoclasts (Chen et al., 2012; Kini and Nandeesh, 2012). The osteoblasts now become resting cells in the newly formed bone. Prenatal alcohol exposure may interfere with the balance of the osteoclast and osteoblast activity, hence disturbing the net bone density, resulting in weaker bones. However, the mechanism involved is unknown.

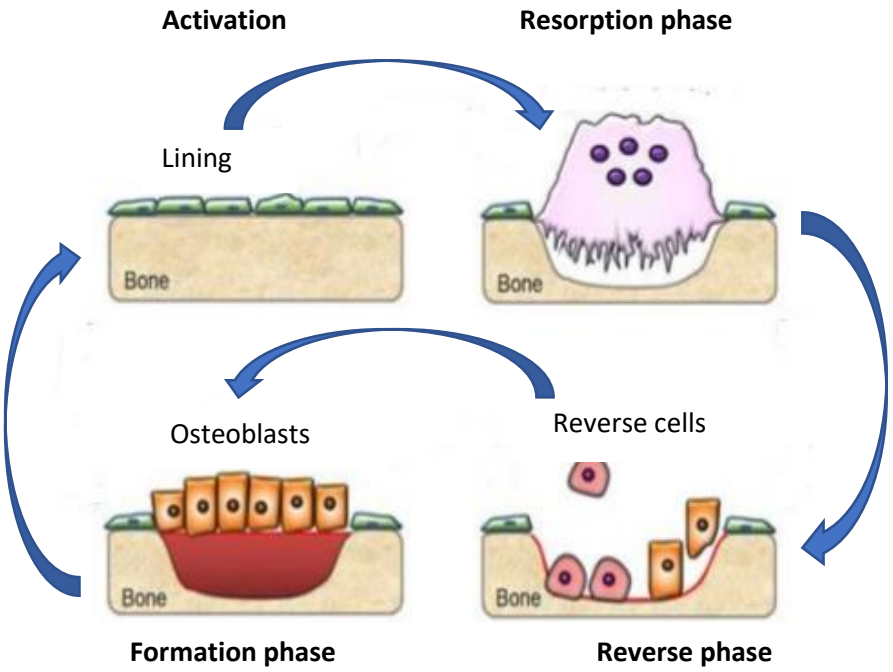


Figure 1.7: Bone remodelling. Schematic representation of the phases of the bone remodelling process. Adapted from Del Fattore et al. (2012).

1.2.8 The role of transforming growth factor beta 1 (TGFβ1) in bone

Transforming growth factor beta 1 (TGFβ1) is crucial in bone development and maintenance and affects both cartilage and bone metabolism (Chen et al., 2012). This cytokine controls proliferation and differentiation of osteoblasts and osteoclasts in bone remodelling (Kasagi and Chen, 2013). The Smad pathway is one of the modes through which TGFβ1 influences bone remodelling. In this pathway, TGFβ1 binds to a complex of type I receptors (TGFβRI) and type II receptor kinase (TGFβRII). The type II receptor kinase transphosphorylates TGFβRI resulting in the subsequent phosphorylation of receptor activated Smads (R-Smads), Smad 2 and 3. The R-Smads then interact with the common Smad (Co-Smad), Smad 4 and translocate to the nucleus. Gene transcription for the osteoblasts then occurs in the nucleus, resulting in increased new bone formation. On the other hand, the involvement of Smad – 7 has an inhibitory effect as it competes for TGFβRII and hinders the transphosphorylation of TGFβRI and subsequently stops the receptor

activated R-Smads (Chen et al., 2012). Also, it interferes with the interaction of R-Smads with Co-Smad (Fig. 1.9).

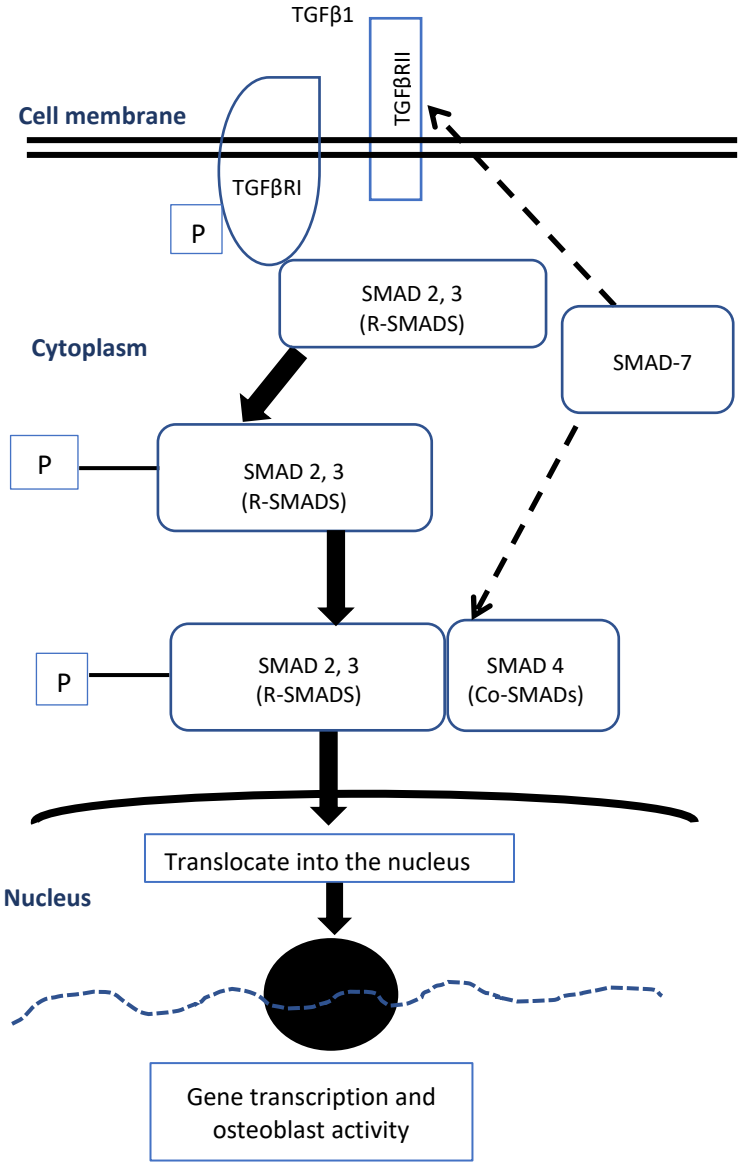


Figure 1.8: TGF β Signalling pathway. Illustration by D Pillay.

1.2.9 Bone biomechanical properties

Alcohol consumption is known to cause secondary osteoporosis (Kanis et al., 2005; Broulik et al., 2010). Osteoporosis is a skeletal disease, characterised by a reduction in bone mass and disruption of trabecular and compact bone structure, causing a loss of mechanical strength and increased fracture risk (Kanis et al., 2005). The ability of osseous tissue to resist mechanical forces and fractures relies not only on the quantity but the quality of bone tissue. Bone quality is established by the structural and material properties which are influenced by the remodelling rate (Martin and Correa, 2010).

The structural properties of bone are determined by bone geometry, i.e. its shape and size and microarchitecture (Martin and Correa, 2010). The microarchitecture of bone is a crucial factor of bone strength, quality, and mechanical properties. It is known that alcohol antagonises the microarchitecture of bone in postnatal life (Schnitzler and Solomon, 1984). However, to date, no studies have investigated the effects of intrauterine alcohol exposure on the mechanical properties of bone in postnatal life.

The quantification of the mechanical properties of bone has been achieved through various experimental testing techniques such as compression testing (McCalden et al., 1993; Yeni et al., 2004), tensile testing (Kotha and Guzelsu, 2007), and bending testing (Bagi et al., 2006; Leppanen et al., 2006; Margolis et al., 2006). The most widely used method for the determination of biomechanical properties of long bones is the three-point bending test (Leppanen et al., 2006). This involves placing the whole bone in a fixture attached to a material testing machine which is then loaded until broken. The three-point bending test provides various parameters that describe different aspects of bone fragility. These parameters are derived from the force displacement curve (Fig. 1.5), accessing the following parameters:

i. Displacement (Deflection) – the amount of vertical deviation from the horizontal plane required to fracture the bone
ii. Maximum force- the amount of force required to cause deformation

iii. Break Force – the amount of force required to fracture the bone

iv. Yield Point-indicates the value of the load at the yield point which is where the load-displacement plot deviates from linearity

v. Time - the duration that the bone withstands the force until a fracture

vi. Work to fracture (Energy-to-fracture)- is defined as the total area under the curve. It represents the work that must be done to fracture the bone. A tough bone requires more work to fracture

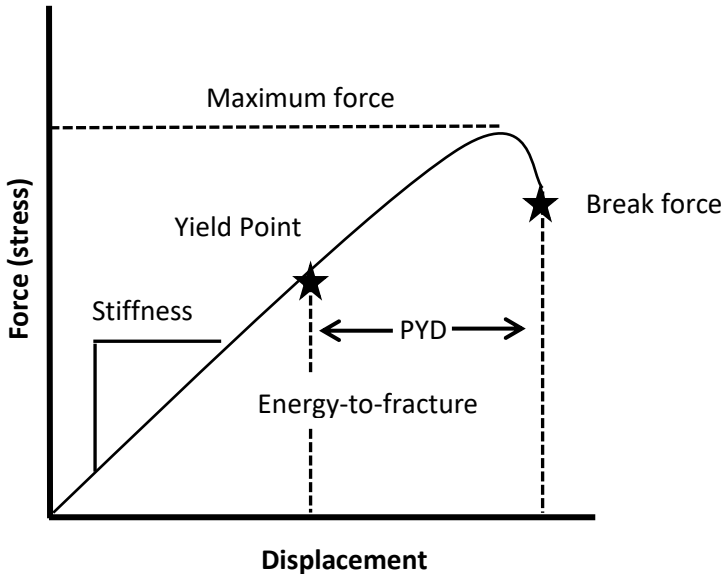


Figure 1.9: Force-displacement curve. A graphical illustration of bone strength properties of compact bone. PYD (post yield displacement). Illustration by D Pillay.

AIM

This study aims to investigate whether the effects of prenatal alcohol exposure persist through postnatal life in (3 and 12-week-old) rats regarding long bone (humerus and femur) development and strength.

OBJECTIVES

1. To study growth and development by evaluating body size parameters of the pups exposed to gestational alcohol in a binge drinking rat model.
2. Immunolabeling chondrocytes for Ki-67 protein expression to assess whether gestational alcohol causes stunted growth through disturbances of epiphyseal growth plate chondrocyte activity.
3. To evaluate whether exposure to gestational alcohol affects bone growth and development through inhibiting chondrocyte multiplication by anti TGFβ1 antibody immunolabeling.
4. To use three-dimensional micro-focus X-ray computed tomography (3D- μCT) for assessment of trabeculae thickness, volume and spacing in the proximal and distal epiphysis of the femur and humerus.
5. To test the theory that gestational alcohol exposure increases fracture risk (weakens bones) by using 3-point bending tests in the assessment of bone tensile strength.

Chapter 2

A Sprague Dawley rat model for studying postnatal growth and development associated with prenatal alcohol exposure in a binge drinking setting

Table of Contents

1.0 INTRODUCTION 25
2.1 MATERIALS AND METHODS 27
2.1.1 Breeding and animal husbandry 27
Treatment with ethanol or saline 27
Determination of maternal blood alcohol levels 27
Allocation of pups 28
2.1.2 Data analysis 28
2.3 RESULTS 30
2.3.1 Blood alcohol concentration 30
2.3.2 Food consumed during the gestation period 30
2.3.3 Body mass gained daily during the gestation period 30
2.3.4 Chow caloric intake 32
2.3.5 Feed efficiency ratio (FER) 33
2.3.6 Gestation duration and litter size 33
2.3.7 Pups weights and crown-rump length (CRL) at Postnatal day 1 34
2.3.8 Pups weights and crown-rump length at 3 weeks of age 36
2.3.9 Weekly mass gained in 12 week old rats. 37
2.4 DISCUSSION 38
2.4.1 Conclusions 40

1.0 INTRODUCTION

It is well known that gestational alcohol exposure causes many neurological and facial abnormalities, as well as low birth weight (Sokol et al., 2003; Simpson et al., 2005; Snow and Keiver, 2007). The latter two are mostly a result of bone developmental abnormalities. Despite this knowledge, most research on the effects of prenatal alcohol exposure focuses on the associated neurodevelopmental deficiencies (Welch-Carre, 2005; Ramadoss et al., 2006; Katwan et al., 2011). As such, there is paucity of literature on the postnatal growth and development associated with prenatal alcohol exposure. Stature depends on skeletal growth and development. This is an important consideration taking into account that gestational alcohol exposure is detrimental to skeletal development.

Several challenges make it difficult to study the effects of prenatal alcohol exposure on skeletal elements using humans. For example, (i) ethical considerations prohibit the administration of alcohol to a pregnant woman, (ii) variable consumption of alcohol, dietary differences and the use of other drugs among humans (Pattern et al., 2014). Consequently, it is necessary to use animals to investigate the effects of gestational alcohol exposure. Animal studies allow for the control of the dose, timing, and the duration of alcohol exposure. Various animal species have been used to investigate the effects of gestational alcohol exposure, including rodents (mice, rats) (Snow and Keiver, 2007), zebrafish (Marrs et al., 2010), chick (Oyedele and Kramer, 2008), sheep (Ramadoss et al., 2006), and primates (Schneider et al., 2011). Rodents are most commonly used as they are inexpensive, have large litter sizes, short gestation duration, and are easy to handle (Pattern et al., 2014).

Rats exhibit numerous similarities to humans regarding bone growth and remodelling. Like in humans, rat bone undergoes endochondral ossification which, slows in magnitude with age and eventually stops (Martin et al., 2003). Both species exhibit basic multicellular unit based endocortical and trabecular bone remodelling (Baron et al., 1984; Erben, 1996). Further, humans and rats show a slow increase in the cross-sectional bone area throughout the lifespan. As is the case in humans, bone remodelling in rats is not constant throughout

life. Therefore, the age of the animal used is vital for investigating the effects of gestational alcohol exposure.

In South Africa, it is common for women to binge drink in secrecy while attempting to conceal this behaviour from their spouses, families and communities to avoid the public disgrace associated with women drinkers (Conover and Jones, 2012; Watt et al., 2014). This behaviour results in binge drinking. Considering this, we have used a binge drinking model to study the effects of fetal alcohol exposure. We sought to understand whether this binge drinking rat model will result in changes in litter size, crown rump length and body mass from birth, 3 weeks and 12 weeks postnatal life.

2.1 MATERIALS AND METHODS

2.1.1 Breeding and animal husbandry

The study received ethics approval from the Animal Ethics Screening Committee, University of the Witwatersrand (AESC 2015/27/15C). A total of fifteen female virgin Sprague Dawley (SD) rats weighing between 260-350g were used. All study animals were bred and kept at the Central Animal Services (CAS), University of Witwatersrand. These animals were maintained under pathogen free conditions, temperature-controlled environment (23°C ±2°C) and a 12-hour light/dark cycle. Pregnant dams were individually housed in plastic cages (L 430 mm x W 220 mm x H 200 mm), with free movement within the enclosures. The animals had unrestricted access to tap water and standard rodent diet.

Treatment with ethanol or saline

The dams (n=15) were allocated into either the ethanol (n=6), saline control (n=6) and untreated control groups (n=3). Fewer animals were used in this group (n=3) to lessen the number of animals required for the study and to reduce study cost. The untreated control group received neither ethanol nor saline. The experimental and saline groups were treated with 0.015ml/g body mass of either 25.2% ethanol in the experimental group or 0.9% in the saline control group (Fig. 2.1). The ethanol administed was to mimic a chronic binge drinking model. The treatment was, administered by oral gavage for 19 days from the first day of gestation as determined by the presence of a vaginal plug. Since a relatively large dose was given once a day, this mimicked binge drinking. Parameters such as, weight and food consumed were recorded to track the health of the dams every day until the pups were born.

Determination of maternal blood alcohol levels

To determine blood alcohol levels in the dams, whole blood was collected from the tail vein into heparinized microcapillary tubes, one hour after alcohol administration. Microcapillary tubes were spun in a microhaematocrit centrifuge (Haematokrit 210, Hetich, Germany) at 3000 rpm for 10 minutes. Plasma alcohol determination was carried out using the BioVision

Ethanol Colorimetric Assay Kit (BioVision incorporation, Milpitas, USA) according to the manufacturer's instructions. All reactions and readings were done in an alcohol-free environment using an iMark Bio-rad Microplate Absorbance Reader (Bio-rad Laboratories Inc, USA).

Allocation of pups

The dams were allowed to litter naturally and allocated into either the 3 groups based on age at termination as follows. These groupings were determined to mimic the effects of gestational alcohol exposure to human offspring at birth, toddler and young adult (Fig. 2.1):

a) postnatal day 1 group

b) 3-week-old group

c) 12-week-old group

From each dam, 2 pups were located into the postnatal day 1 group which were terminated within 24hrs post birth. The pups belonging to the 3-week-old and 12-week-old groups remained with their dams until they were weaned at 3 weeks of age.

2.1.2 Data analysis

The data were managed in Microsoft Excel 2016 (Microsoft Corporation) and analysed using SPSS® version 25 (IBM®). ANOVA with LSD post-hoc was used for multiple group comparisons of means. Significance level was set at $p < 0.05$. Statistical analyses were performed with SPSS® version 25 (IBM®)

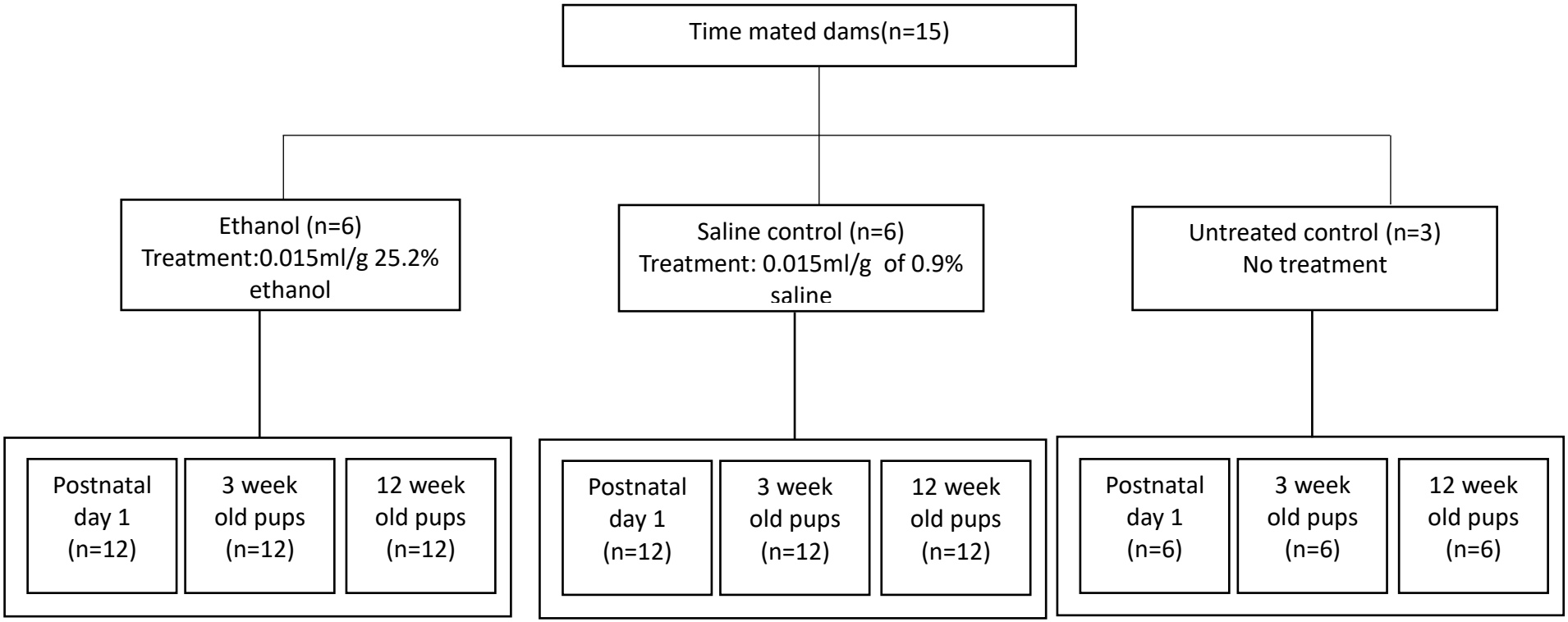


Figure 2.1: Allocation of groups

2.3 RESULTS

2.3.1 Blood alcohol concentration

The mean blood ethanol concentration was 258.77mg/dL in the ethanol group and 81.53mg/dL in the saline controls. The untreated controls were not tested for blood ethanol concentration as they did not receive any treatment.

2.3.2 Food consumed during the gestation period

All three groups studied showed similar daily food consumption by the pregnant dams each week. The pattern was that of food intake increasing every week, being highest in the 3rd week in all the groups (Fig. 2.2). While, the food intake in week 1 was lowest in the ethanol group (mean = 19.63g ±2.80) compared to the saline and untreated controls (mean = 23.45g ±2.34 and mean = 21.38g ±5.51, respectively), no significance was detected among the groups. Again, in week 2, the ethanol group appeared to have the lowest food intake (mean = 21.31 ±5.68) than the saline and untreated groups (mean = 24.81g ±2.51 and mean = 22.69g ±4.23, respectively). However, no group differences were detected. Like in the previous couple of weeks, the ethanol group had the lowest food consumption (mean = 24.23g ±4.50) than the saline (mean = 27.67g ±3.43) and untreated controls (mean = 26.19g ±3.18) in the 3rd week (Fig. 2.2), although not significantly different.

2.3.3 Body mass gained daily during the gestation period

Regarding the body mass gained per week, all groups had a steady body mass from week 1 to 2, with a sharp increase during week 3 (Fig. 2.3). The ethanol group (mean = 4.01g ±1.88) had the least daily mass gained in week 1 compared to the saline and untreated controls (mean = 5.02g ±2.87 and mean = 4.19g ±0.64, respectively) although not statistically significant. The animals did not gain considerable mass in week 2 (ethanol, mean=4.02g ±1.97; saline control, mean = 4.88g ±1.55; untreated control, mean = 4.98 ±1.08). In contrast, week 3 had the most daily mass gain recorded (Fig. 2.3). The ethanol group (mean = 8.80g ±3.35) made a significantly smaller mass gain that the saline (mean = 11.55g ±1.03)

and untreated (mean = 14.02g ±0.89) controls (p=0.03 and 0.001, respectively). No significance was detected between the controls (p=0.10).

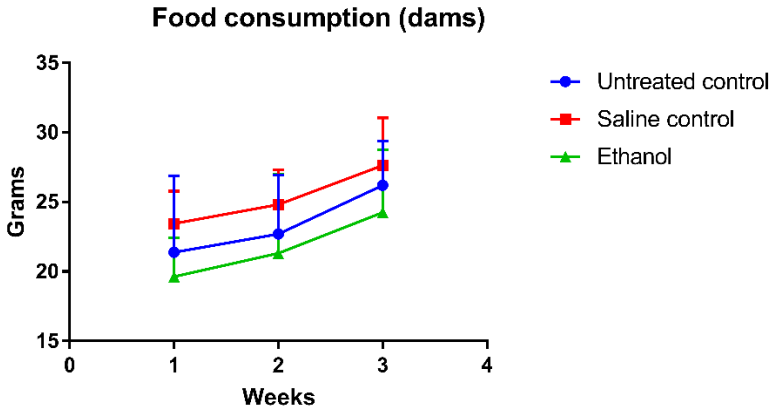


Figure 2.2: Food consumption. The daily food consumption in grams is shown as an average per week for all three groups in the study. Error bars represent standard deviation.

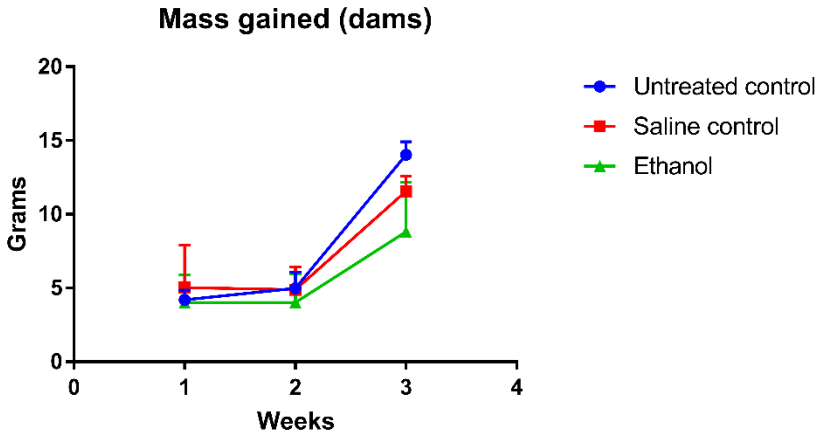


Figure 2.3: Mass gained. The daily mass gained in grams is shown as an average per week for all three groups in the study. Error bars represent standard deviation.

2.3.4 Chow caloric intake

The calories derived from rat chow increased from weeks 1 to 3 in all the groups (Fig. 2.4) In the 1st week, the ethanol group (mean = 66.75kcal ±9.53) appeared to have had the lowest chow caloric intake than the saline and untreated groups (mean = 79.33kcal ±8.59 and mean = 72.70kcal ±18.75, respectively). However, no group differences were detected. In week 2 there was a slight increase in the chow caloric intake among the dams in all the groups (ethanol, mean = 72.46kcal ±19.33; saline control, mean = 84.34kcal ±8.53; untreated control, mean = 77.15kcal ±14.38) with no group differences. The chow caloric intake was greatest in week 3 among the dams of all 3 groups (ethanol group, mean = 82.39kcal ±15.30; saline control, mean = 92.71kcal ±11.57; untreated control, mean = 89.04kcal ±10.83). Again, no significance was detected among the groups.

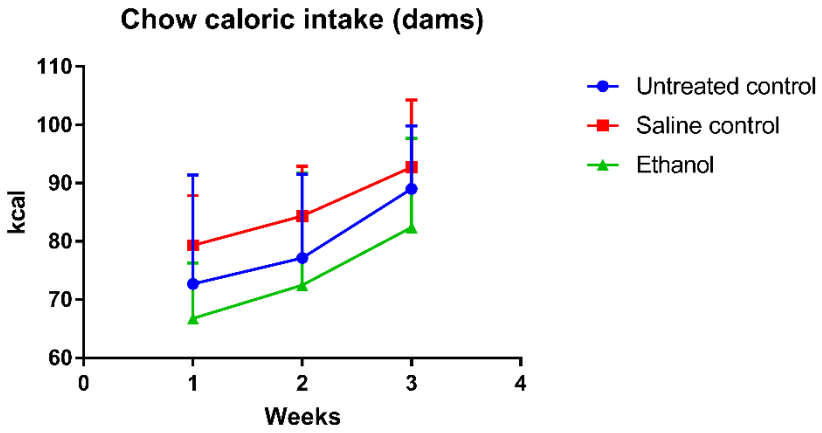


Figure 2.4: Chow calories. The daily chow calories are shown as a weekly average in all three groups in the study. Error bars represent standard deviation.

2.3.5 Feed efficiency ratio (FER)

With regards to total FER, the ethanol group had the highest total FER from week 1 to week 3 (Fig. 2.5). In week 1 the ethanol group (mean = 0.90g/kcal ±0.28) had a significantly higher total FER than the saline (mean = 0.08g/kcal ±0.07) and untreated (mean = 0.05g/kcal ±0.01) controls ($p<0.001$ for both comparisons). No significance was detected between the controls ($p=0.89$). In week 2, again the ethanol group (mean = 0.64 ±0.38) had a significantly higher total FER than the saline (mean = 0.06g/kcal ±0.04) and untreated controls (mean = 0.07g/kcal ±0.01) ($p=0.003$ and $p=0.01$, respectively) (Fig. 2.5). Again, no significance was detected between the controls ($p=0.89$). In week 3 the pattern was like of week 1 and 2 were the ethanol group (mean = 1.23g/kcal ±0.69) had a significantly higher total FER than the saline (mean = 0.10g/kcal ±0.03) and untreated (mean = 0.17g/kcal ±0.05) controls ($p<0.001$ and $p<0.001$, respectively) (Fig. 2.5). However, no significance was detected between the controls ($p=0.74$).

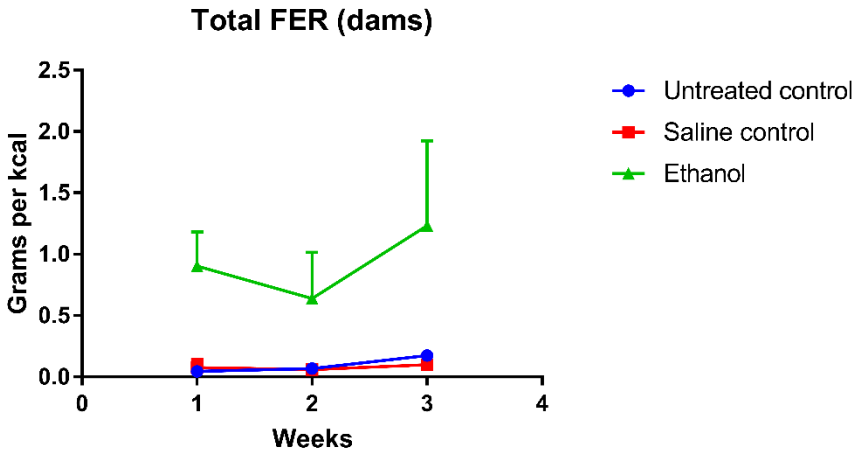


Figure 2.5: Total FER (dams). The weekly total FER (dams) in grams is shown for all three groups in the study. Error bars represent standard deviation.

2.3.6 Gestation duration and litter size

The gestation duration ranged from 19 to 24 days for all the three groups combined (Table 2.1). When stratified by group, this range was 21-24 days in the ethanol group and 19-23 days in the saline controls whereas it was 23 days for the untreated controls. There were

no statistical group differences in gestation duration among the three groups (p=0.37). The litter size showed a wide range among the three groups, with the smallest observed in the ethanol group (3 pups) and the largest observed in the untreated controls (17 pups) (Table 2.1). This group (untreated controls) also had the smallest range of 14 -17 pups in each litter. In contrast, the ethanol group (litter size 3-16) and the saline controls (litter size 5-16) had a wider litter size range. However, no significant differences in litter size were observed between the groups (p=0.28 for ethanol vs saline control). Each of the three groups in the study had two pups found dead at birth from different dams within a group.

Table 2.1: Gestation duration and litter size for the ethanol group, saline and untreated controls. The number of dead pups (n = 2) in each group is included in litter size.

Group		N	Minimum	Maximum	Mean	SD
Ethanol	Gestation	6	21	24	23.00	1.095
	Litter size	6	3	16	9.83	4.916
Saline Control	Gestation	6	19	23	22.00	1.732
	Litter size	6	5	16	12.14	3.671
Untreated Control	Gestation	3	23	23	23.00	0.000
	Litter size	3	14	17	15.33	1.528

2.3.7 Pups weights and crown-rump length (CRL) at Postnatal day 1

The weight of the pups at postnatal day 1 was lower in the ethanol (mean = 4.71g ±1.45) compared to the saline (mean = 5.48g ±0.63) and untreated (mean = 5.41g ±1.12) controls (Fig. 2.6). However, these differences were not statistically significant between the groups (p=0.442). The ethanol group (mean = 4.34mm ±0.34) had a significantly smaller CRL (Fig. 2.7) in comparison to the saline (mean = 4.95mm ±0.62) and untreated (mean = 4.92mm

±0.57) controls (p=0.023 and p=0.009, respectively). The saline and untreated groups did not show significant differences in CRL (p=0.9)

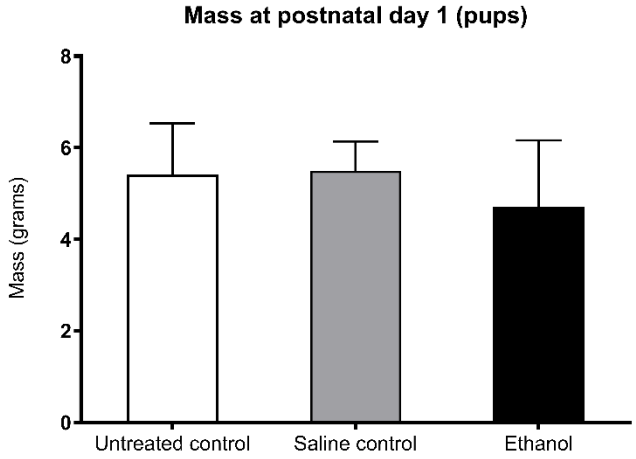


Figure 2.6: Body mass of the pups on postnatal day 1. The values are means in millimetres for all three groups in the study. Error bars represent standard deviation.

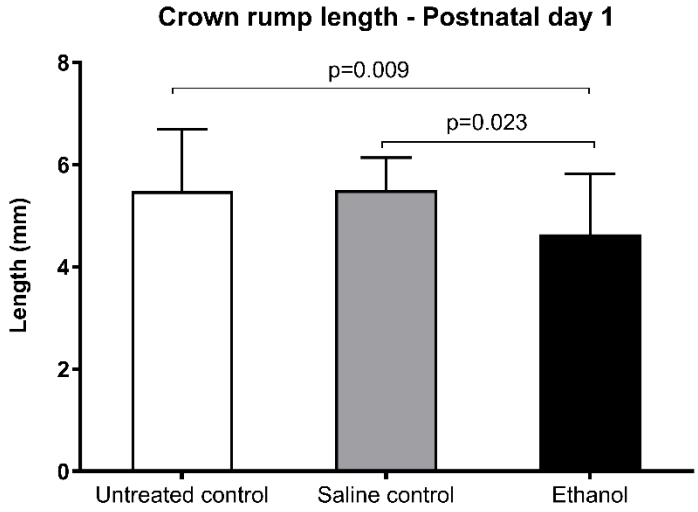


Figure 2.7: The crown-rump length of the pups at postnatal day 1. The values are means in millimetres for all three groups in the study. Error bars represent standard deviation.

2.3.8 Pups weights and crown-rump length at 3 weeks of age

Minor differences in the weight of the pups at 3 weeks of age were observed. The ethanol group (mean = 47.41g ±4.26) weighed marginally lower than the saline (mean = 48.20g ±5.94) and untreated controls (mean = 50.83g ±6.35) (Fig. 2.8). These differences were not statistically significant (p=0.45). The crown-rump length was similar in the ethanol group and the saline controls (mean = 9.70mm ±0.86 and ±0.68, respectively), being significantly higher in the untreated control group (mean = 10.7mm ±0.36) (p=0.01 for untreated control against the ethanol and saline groups) (Fig. 2.9).

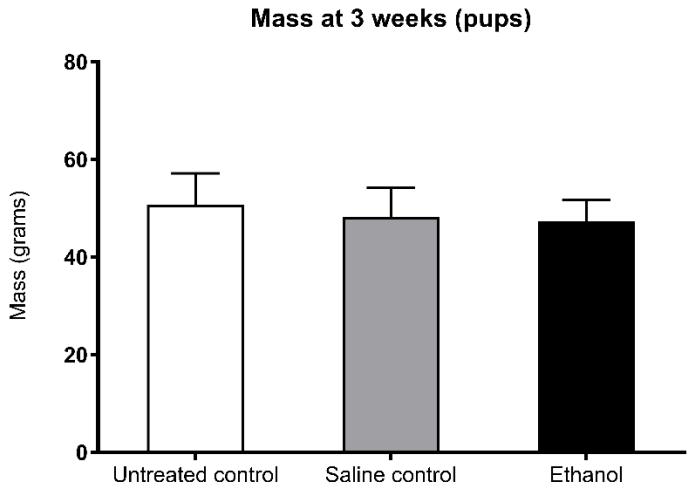


Figure 2.8: Weight of the pups at 3 weeks of age. The mean mass is given in grams for all three groups in the study. Error bars represent standard deviation.

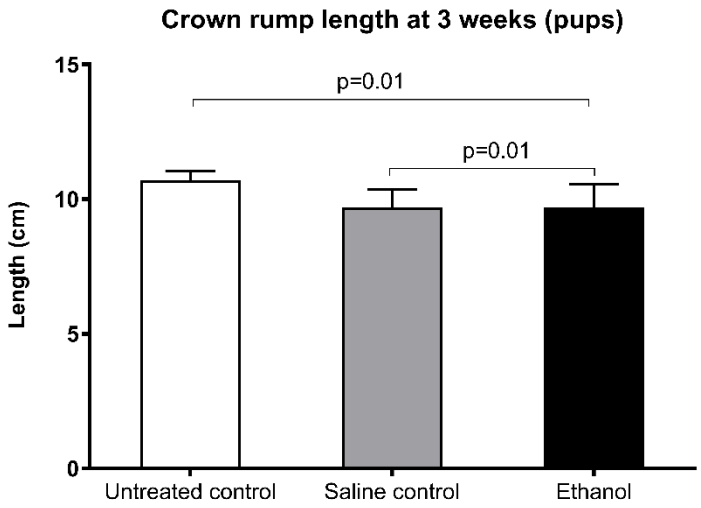


Figure 2.9: The crown-rump length of the pups at 3 weeks of age. The values are means in millimetres for all three groups in the study. Error bars represent standard deviation.

2.3.9 Weekly mass gained in 12 week old rats.

The initial mass of the three groups were similar at 3 weeks (ethanol, mean = 50.29g ±11.69); saline, mean = 46.00g ±7.87 and untreated mean= 47.42g ±5.51). However, no significant differences were observed among the groups ($p>0.05$). There was a steady increase in mass between the 3 groups from 3 to 12 weeks. Again, no significant differences were observed among the groups ($p>0.05$) (Fig. 2.10).

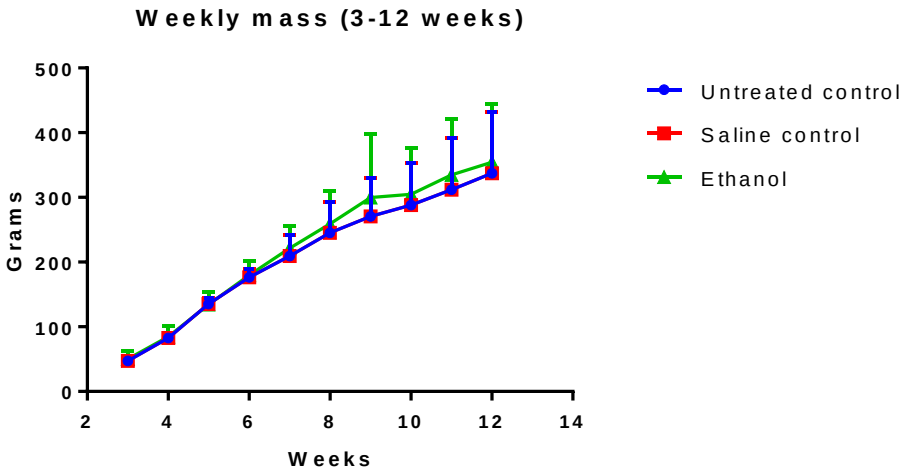


Figure 2.10: Weekly mass (3-12 weeks). The values are means in grams for all three groups in the study. Error bars represent standard deviation.

2.4 DISCUSSION

We investigated the effects of prenatal alcohol exposure on growth and development in a model of a chronic binge drinking rat model. Binge drinking is defined as having 4-5 glasses of alcohol within a short space of time (Sokol et al., 2003). Food consumption and calories obtained from the rat chow increased weekly in all groups, but the FER was better in the ethanol group. Similarly, there was a similar extent of mass gain in all three groups despite one group receiving alcohol. The gestation duration and litter size were not significantly different among the groups although there was a wide range within groups. The ethanol group had smaller pups at birth and at 3 weeks of age with no group differences at 12 weeks.

In the ethanol group, we expected either low food intake or higher mass gained. However, we did not find any group differences in food intake or mass gained. Our expectation was based on the higher calories in alcohol which yields 7.1kcal per each gram of ethanol (Liangpunsakul et al., 2010) in contrast to rat feed which has 3.4kcal per gram. The lack of differences in food intake and mass gained in our study may be attributed to the study design. In the present study, we administered ethanol only for 19 days of gestation. Conversely, other studies (Keiver and Weinberg, 2004; Simpson et al., 2005; Snow and Keiver, 2007) administered ethanol three weeks prior to pregnancy and throughout gestation. Additionally, the dosage used in these studies were higher (36% of ethanol) in comparison to the 25.2% of ethanol which was given in our study.

The feed efficiency ratio (FER) was higher in the ethanol group in all 3 weeks although this group was not significantly different in respect of chow intake and mass gained across the 3 weeks. A higher FER suggests an ability to convert the given calories into body mass. The ethanol group may have had the best FER in the present study owing to the ease of converting ethanol calories into mass relative to rat chow.

In the present study, pups belonging to the ethanol group had the smallest CRL for postnatal day 1 and 3-week old groups whereas no differences were detected at 12 weeks of age. This suggests that gestational alcohol exposure affected intrauterine growth as well as postnatal development to some extent. These effects may have been minimal by the age of 12 weeks as no significant differences were detected in this age group. Researchers have long debated whether there is a possibility of catch-up growth in children of mothers who drink in pregnancy (Day et al., 1989; Cooper et al., 2001; Godfrey et al., 2001). Our study supports the suggestion that catch-up growth takes place following gestational alcohol exposure.

Rosett (1980) reported that alcoholic women who abstained or markedly reduced their intake of alcohol before the third trimester of gestation gave birth to offspring that were less growth-stunted than those born to mothers who continued to consume alcohol heavily during their pregnancy. Catch up growth and development rely on the removal of an insult and continued nutrition. In the present study, the pups were only exposed to alcohol during gestation, with no postnatal alcohol exposure. Also, all the pups in the 3 and 12-week-old groups had access to breastmilk and unlimited food. Considering that maternal milk is highly nutritious and rat feed provided a balanced diet, it is possible that these factors played a role in ameliorating the detrimental effects of gestational alcohol in the 12-week-old group.

Alcohol intake during gestation lengthens gestation duration and decreases fetal viability (Sebastiani et al., 2018). In the present study, the gestation duration did not show statistical differences between the groups. Also, the number of pups born alive and that of dead pups was similar among all 3 groups as in previous studies (Abel and Dintcheff, 1978; Lee and Leichter, 1980). However, this contradicts the findings of (Abel, 1982; Sanchis et al., 1986; Nwaogu, 2002) that found reduced litter size at birth in rodents exposed to prenatal alcohol

2.4.1 Conclusions

Binge drinking at the dosage we gave (0.015ml/g of 25.2%) does not affect maternal food intake although it resulted in smaller weekly mass gained in the ethanol group. However, this group had the best FER meaning that it was more efficient in converting calories into the mass. No significant differences in CRL at 12 weeks of age means that the effects of prenatal alcohol exposure at our dosage and frequency diminish with time in postnatal life (birth to 12 weeks). The present study did not use the same pups at the 3 age groups. A longitudinal study that follows up the same pups from postnatal day 1, up to 3 and 12 weeks would yield more conclusive results.

Chapter 3

Intrauterine alcohol exposure inhibits Transforming Growth Factor Beta-1 (TGFβ-1) expression in epiphyseal growth plate chondrocytes and disturbs trabecular morphology, in the Sprague Dawley rat humerus epiphysis

Table of Contents

3.1 INTRODUCTION 44

3.2 MATERIALS AND METHODS 46

3.2.1 Study sample 46

Skeletal harvesting 46

3.2.2 Three-dimensional Micro-focus X-ray Computed Tomography (3D- µCT) 46

Parts of the humerus and trabecular parameters studied 47

3.2.3 Tissue processing for histology and immunohistochemistry 48

Immunohistochemistry for Ki-67 and TGFβ1 in the humerus epiphyseal growth plate 49

Photography and quantification of chondrocytes 50

3.2.4 Data analysis 50

3.3 RESULTS 51

3.3.1 Humerus Length 51

3.3.2 Humerus epiphyseal morphological parameters at 3 weeks of age 52

Epiphysis volume 52

Humerus bone to total volume ratio (BV/TV) 53

Humerus trabecular thickness (TbTh) 54

Humerus trabecular number (TbN) 55

Humerus trabecular spacing (TbSp) 56

3.3.3 Humerus cross-sectional area, cortical area (thickness) and medullary canal area at 3 weeks of age 58

Proximal (25th percentile mark) 58

Midshaft (50th percentile mark) 59

Distal (75th percentile mark) 60

3.3.4 Humerus epiphyseal growth plate histological and immunohistochemical characterization at 3 weeks of age 61

Humerus epiphyseal growth plate surface area 61

Humerus proliferative zone Ki-67 immuno-positive chondrocytes 65

Humerus hypertrophic zone Ki-67 immuno-positive cells 67

Humerus proliferative zone TGFβ-1 immuno-positive cells 69

Humerus hypertrophic zone TGFβ-1 immuno-positive cells 71

3.3.5 Humerus (3 weeks) trabecular morphometric parameters most affected by gestational ethanol 73

Proximal humerus 73

Distal humerus 74

3.4 DISCUSSION 76

Bone osteometry and epiphyseal trabecular morphometric parameters 76
The role of TGFB1 in maintaining the epiphyseal growth plate and its cellular components 78
Parameters most affected by prenatal ethanol exposure 79
3.4.1 Conclusion 79

3.1 INTRODUCTION

Knowledge about the risks associated with alcohol consumption in pregnancy is widely disseminated (Abel and Dintcheff, 1978; Day et al., 1989; Chaudhuri, 2000; Simpson et al., 2005). However, members of many communities continue to drink in pregnancy. This is the case both in developed and developing countries. For example, in Canada (10%) and the United States (15%) women drink alcohol in pregnancy, with approximately 3% binge drinking during pregnancy in both countries (Popova et al., 2017). In South Africa, a developing country, a prevalence of 25% drinking in pregnancy was reported (Tomlinson et al., 2014).

Fetal alcohol spectrum disorder (FASD) affects most children born to mothers who consume alcohol during pregnancy (Abel and Dintcheff, 1978; Chaudhuri, 2000; Simpson et al., 2005). The neurological aspects and facial dysmorphology associated with this condition have been widely investigated. Despite short stature being a major characteristic of FASD, the literature on bone development in prenatal alcohol exposure has received relatively less attention. The few studies that investigate the skeletal aspects of gestational alcohol exposure (Abel and Dintcheff, 1978; Day et al., 1989; Chaudhuri, 2000; Simpson et al., 2005; Snow and Keiver, 2007) do not explore the mechanisms in which intrauterine alcohol exposure exerts its detrimental effects in postnatal life.

Studies (Simpson et al., 2005; Snow and Keiver, 2007) have established that gestational alcohol exposure suppresses the longitudinal growth of fetal bone and affects fetal osseous tissue mineralization. In support of this, Miralles-Flores and Delgado-Baeza (1992), suggested that intrauterine alcohol exposure antagonises the growth plate in long bones due to impaired cell function in rats. These authors reported a shorter epiphyseal plate in 2-week-old pups exposed to gestational alcohol. In addition, these same researchers also found the height of the proliferative and hypertrophic zones to be reduced, and with fewer chondrocytes compared to the controls. Similar findings were also made in newborn rats (Simpson et al., 2005; Snow and Keiver, 2007).

It is not clear how prenatal exposure to alcohol affects the growth plate leading to the observed smaller epiphyseal growth plate with fewer chondrocytes. We propose that the expression of cytokines that promote cell proliferation may be inhibited. One such cytokine is the Transforming Growth Factor β1 (TGFβ1) which is involved in fetal development as well as in postnatal growth skeletogenesis (Kanaan and A Kanaan, 2006). This cytokine induces cell differentiation into either chondrocytes or osteoblasts (Kanaan and A Kanaan, 2006) and influences bone remodelling in postnatal life (Bismar et al., 1999; Kanaan and A Kanaan, 2006).

Prenatal alcohol exposure affects the balance of osteoclasts and osteoblasts resulting in weak bones and developmental disturbances in the offspring (Chen et al., 2012). It is suggested that the bone weakness is owed to the trabecular morphological properties. Once osteoclasts outperformed the bone deposition by osteoblasts, it is envisioned that trabecular may be thinner, fewer and more spaced out. However, we have not found studies that investigate this proposition using Micro CT in rats exposed to alcohol during gestation.

Considering the above, we sought to understand whether exposure to alcohol during the prenatal duration would affect bone postnatal development. This was achieved by assessing epiphyseal growth plate chondrocyte proliferation and TGFβ1 expression using immunohistochemical methods. Then, we used three-dimensional micro-focus X-ray computed tomography (3D- μCT) to assess trabeculae thickness, volume and spacing in the proximal and distal epiphysis of the humerus.

3.2 MATERIALS AND METHODS

3.2.1 Study sample

Fifteen dams treated as in section 2.1.1 were used to obtain 30 pups allocated into the ethanol (n=12), saline-treated (n=12) and untreated controls (n=6). These pups remained with their respective dams till 3 weeks of age.

Skeletal harvesting

The rats were terminated by a lethal pentobarbital intraperitoneal injection. The entire animal was then immediately immersed in 10% buffered formalin after an abdominal incision was made to allow for the penetration of the fixative. To expose the humeri, skin incisions were made on the respective limbs and muscles were meticulously teased away. The skeletal samples were then individually immersed and stored in 10% buffered formalin to continue fixation until further processing. The left side bones were used for histological and immunohistochemical investigations. Bilateral humeri were used for three-dimensional Micro-focus X-ray Computed Tomography (3D- µCT).

3.2.2 Three-dimensional Micro-focus X-ray Computed Tomography (3D- µCT)

A Nikon XTH 225/320 LC X-ray microtomograph was used to scan bilateral 3-week old humeri for 3D-µCT examination. To keep the samples steady during scanning, the bones were mounted in low-density Styrofoam, placed in plastic tubes while allowing the X-rays to get to the sample with negligible absorption. The plastic container with the sample inside was then positioned on a rotating manipulator in the scanning chamber for the scanning. The scanning parameters used are shown in table 3.1.

Table 3.1: Scanning parameters

Parameter	Value
X-ray voltage	70kv
X-ray current	400µa
Filter	1mm aluminium
Scanning resolution	15µm
Tomographic rotation	360 degrees
Rotation step	1 degree
Frame averaging	4
Scan duration	8 minutes

Parts of the humerus and trabecular parameters studied

Following reconstruction, VG studio Max ®3.2 was used for data analysis as previously described (Bouxsein et al., 2010) (Fig. 3.1 and Table 3.2). The trabecular morphometric parameters were studied in the proximal and distal epiphysis of the bone (Table 3.3). The following trabecular parameters were assessed: bone volume to total volume (BV/TV), trabecular thickness (TbTh) trabecular number (TbN) and trabecular spacing (TbSp) (Table 3.3).

A cross-sectional slice from each percentile mark was then saved for further analysis on Fiji image J. From these slices, the cross-sectional area, cortical area and medullary canal area of the shaft were measured at 3 positions; 25th (proximal), 50th (midshaft) and 75th (distal) percentile marks of the humerus (Fig. 3.1 and Table 3.2) (See Appendix).

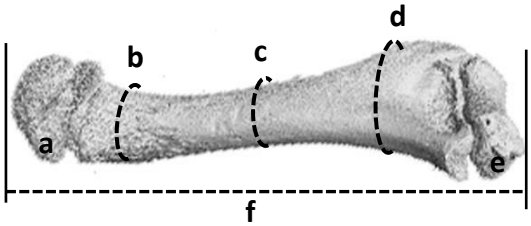


Figure 3.1: Three-dimensional reconstruction of the humerus showing the parts that were investigated. (a), proximal epiphysis; (b), (c), and (d) respectively: shaft circumference at the 25th, 50th, and 75th percentile marks of the humerus length; (e), distal epiphysis; (f), full humerus length (Image courtesy of R. Ndou).

Table 3.2: Osteometric parameters taken from 3-week-old humeri

Parameter	Description
Proximal epiphysis	The part of the bone above the proximal epiphyseal growth plate
Distal epiphysis	The part of the bone below the distal epiphyseal growth plate
Full humerus length	The maximum length that can be measured between the top of the humeral head and the most distant point on the distal humerus.
Cross-sectional area	the area of a slice taken from the outer margins encompassing the shaft at the 25th, 50th and 75th percentile marks
Medullary cavity area	the area of a slice taken from the outer margins encompassing the medullary canal at the 25th, 50th and 75th percentile marks
Cortical thickness	the difference between the cross-sectional area and the medullary cavity area at the shaft 25th, 50th and 75th percentile marks.

Table 3.3: Trabecular parameters assessed adapted from (Bouxsein et al., 2010)

Parameter	Definition
$\frac{\mathrm{BV}}{\mathrm{TV}}$ (bone volume to total volume)	Represents the ratio of material (bone) volume to total volume.
TbTh (mean trabecular thickness)	Specifies the mean thickness of trabecular (column-like) structures in the material (bone), calculated as follows: $\mathrm{TbTh} = \frac{\frac{2}{\mathrm{BS}}}{\mathrm{BV}}$ Where $\frac{\mathrm{BS}}{\mathrm{BV}}$ is the ratio of material (bone) surface (BS) to material (bone) volume (BV)
TbN (mean trabecular number)	Shows the mean number of trabecular (column-like) structures per unit length, calculated as follows: $\mathrm{TbN} = \frac{\frac{\mathrm{BV}}{\mathrm{TV}}}{\mathrm{TbTh}}$
TbSp (mean trabecular spacing)	Indicates the mean distance between trabecular (column-like) structures, calculated as follows: $\mathrm{TbSp} = \frac{1}{\mathrm{TbN}} - \mathrm{TbTh}$

3.2.3 Tissue processing for histology and immunohistochemistry

Bone samples were removed and fixed in 10% buffered formalin for a minimum of 14 days. They were then decalcified in 14% w/v ethylenediaminetetraacetic acid (EDTA, pH 7.4) for 10 days in an incubator with regular gentle shaking at 45˚C. The bones were then rinsed and divided into proximal and distal samples and immersed in 10% buffered formalin for 24 hours. An automatic processor (Citadel 2000, Thermo Fischer Scientific) was then used to take the samples through ascending grades of ethanol prior to embedding in paraffin wax. When embedding, care was taken to ensure that the bone samples were orientated longitudinally to minimise differences in the sectioning angle. Bone sections were cut at 5µm thickness using a microtome (Leica RM2125 RTS, Leica Biosystems, USA) and placed on silane-coated glass slides. Sections in a sequence of 1 in 3 were stained with Haematoxylin and Eosin (H&E) to assess epiphyseal growth plate morphology and chondrocytes or immunolocalization of the Ki67 protein (cell proliferation maker) or Transforming growth factor beta 1 (TGFβ1) (See Appendix).

Immunohistochemistry for Ki-67 and TGFβ1 in the humerus epiphyseal growth plate

Immunolocalization of epiphyseal growth plate chondrocytes expressing the Ki-67 protein and TGFβ1 was performed using an anti-Ki-67 antibody (ab66155) or anti-TGFβ1 antibody (ab215715). Both antibodies were sourced from Abcam. In summary, sections were deparaffinized, rehydrated and subsequently, immersed in a citrate buffer solution (pH=6) kept in a water bath set at a temperature of 60^0C overnight. The next morning, tissue sections were allowed to cool to room temperature for 20 minutes and then washed in phosphate buffer solution (PBS) (pH=7.4) for 5 minutes. Endogenous peroxidase was blocked with 1% hydrogen peroxide (H_2O_2), washed with PBS for 3 x 5 minutes, incubated with normal goat serum for 10 minutes, incubated with primary antibody (anti-ki-67 in 1:1200 or TGFB1 in 1:250 dilution factor) overnight at 4^0C. On the 3rd third day, sections were allowed to reach room temperature, washed in PBS for 3 x 5 minutes. A biotinylated secondary antibody (Biotinylated Goat Anti-Rabbit IgG (H+L) (ab64256) was applied for 10 minutes and then washed in PBS for 3 x 5 minutes. To reduce nonspecific staining background while enhancing antibody binding, sections were incubated with streptavidin

HRP for 10 minutes (ab64269) and washed in PBS for 3 x 5 minutes. For visualisation under a light microscope, sections were then incubated with 3-3' di-aminobenzidine (DAB) working solution for 5 minutes, rinsed in running tap water for 5 minutes. Finally, the sections were dehydrated through alcohol grades, cleared in xylene and eventually mounted in entellen (See Appendix).

Photography and quantification of chondrocytes

A light microscope (Zeiss Axioscope 2 plus) fitted with an axiocam HRC digital camera was used to take photomicrographs of the stained slides. These were taken under ×10 magnification. Photomicrographs were imported into Fiji Image-J software and the parameters measured were delineated based on cell morphology. The proliferative zone was delineated by the first flattened chondrocyte on the epiphyseal end and the first hypertrophic chondrocyte on the metaphyseal side. The hypertrophic zone was delineated by the first hypertrophic chondrocyte from the epiphyseal side and by the last transverse septum on the metaphyseal side.

The built image J tool for estimation of area was used to estimate the area of the respective epiphyseal growth plate zones. For quantification of chondrocytes, the manual counting method from the images was employed (See Appendix).

3.2.4 Data analysis

The data were managed in Microsoft Excel 2016 (Microsoft Corporation) and analysed using SPSS® version 25 (IBM®). ANOVA with LSD post-hoc was used for multiple group comparisons of means. Statistical analyses were performed with SPSS® version 25 (IBM®). Binary logistic regression was used to predict group membership into either the ethanol or saline control group. Significance level was set at $p < 0.05$.

3.3 RESULTS

3.3.1 Humeral Length

All three groups in the study exhibited similar humerus bone length the ethanol group had a mean of 15.49mm ±0.46 compared to the saline (mean=15.29mm ±0.57) and untreated controls (mean=15.56 ±0.36) (p=0.29) (Fig. 3.2).

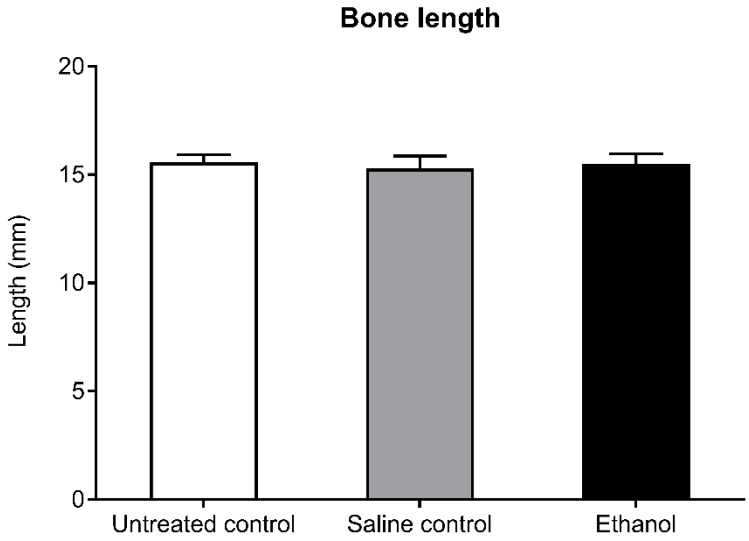


Figure: 3.2. Humerus length at 3 weeks of age. The mean values for the bone length are given for the untreated, saline controls and the ethanol group. Error bars indicate standard deviation.

3.3.2 Humerus epiphyseal morphological parameters at 3 weeks of age

Epiphysis volume

The size of the epiphysis showed regional similarity in the proximal and distal epiphysis with respect to study groupings. In the proximal epiphysis the largest volume was seen in the untreated (mean = 10.94mm^3 ±0.99) and saline controls (mean = 10.11mm^3 ±1.89) compared to the ethanol group (mean = 7.96mm^3 ±1.33 ($p<0.001$ for both comparisons). The control groups had a negligible difference ($p=0.17$) (Fig. 3.3). In the distal epiphysis, the untreated group (mean = 9.65mm^3 ±2.27) had the largest volume compared to the saline controls (mean = 8.2mm^3 ±0.92) and the ethanol group (mean = 7.7mm^3 ±1) showing the smallest volume ($p=0.001$, for both comparisons) (Fig. 3.3). There were no significant differences detected for the ethanol and saline groups ($p=0.28$) (Fig. 3.3).

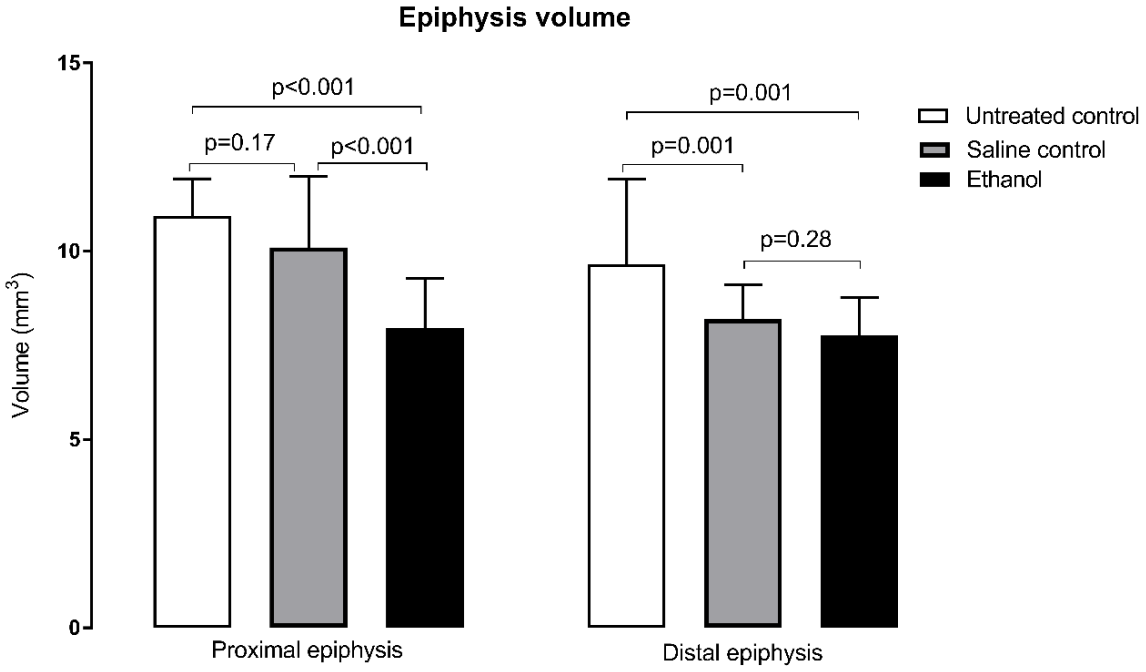


Figure 3.3: Humerus epiphysis volume at 3 weeks of age. The mean volume of the epiphysis is given for the untreated, saline controls and the ethanol group for the proximal and distal epiphysis. Error bars represent standard deviation.

Humerus bone to total volume ratio (BV/TV)

In the proximal region, the bone to total volume ratio (BV/TV) was the smallest in the ethanol group whereas no group differences were observed in the distal region. The untreated (mean = 80.13% ±5.47) and saline controls (mean = 79.08% ±8.72) had similar BV/TV in the proximal epiphysis (p=0.76). The ethanol group (mean = 71.59% ±10.76) had less BV/TV compared to the saline controls (p=0.01) or untreated group (p=0.002) (Fig 3.4). In contrast, the distal epiphysis showed similarities in the saline (mean = 79.48% ±7.30) and untreated controls (mean = 80.21% ±6.62) which were only marginally lower than the ethanol group (mean = 74.64% ±10.14) (p=0.149) (Fig 3.4).

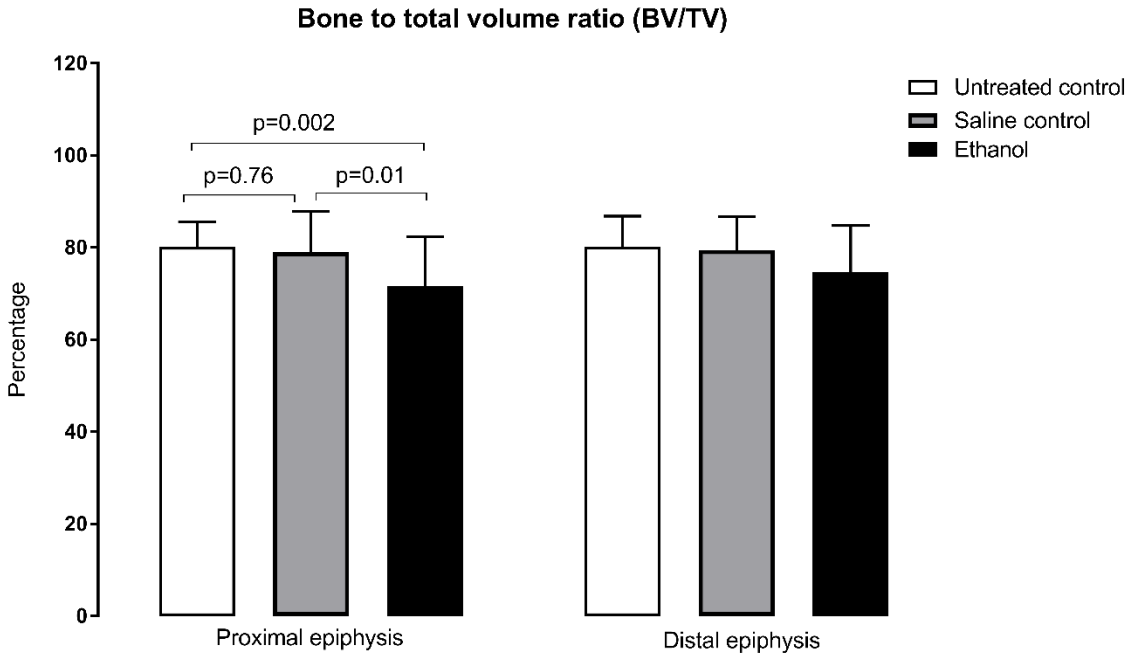


Figure: 3.4: Humerus total bone to volume ratio (BV/TV) at 3 weeks of age. The mean percentages are given for the proximal and distal epiphysis in the untreated, saline controls and the ethanol group. Error bars indicate standard deviation.

Humerus trabecular thickness (TbTh)

Trabeculae were thinnest for the ethanol group in the proximal region, with no group differences in the distal region. In the proximal epiphysis, the ethanol group (mean = 0.14mm ±0.05) exhibited thinnest trabeculae (TbTh) of all three groups in the study (Fig. 3.5), being significantly lower than the saline (mean = 0.20mm ±0.08) and untreated group (mean = 0.19mm ±0.06) (p=0.006 and p=0.05, respectively) (Fig. 3.5). Although the ethanol group (mean = 0.19mm ±0.09) seemed to have thinner trabecular in the distal epiphysis than the saline (mean = 0.23mm ±0.09 and untreated controls (mean = 0.21mm ±0.09), there were no statistical group differences detected (p=0.394) (Fig. 3.5).

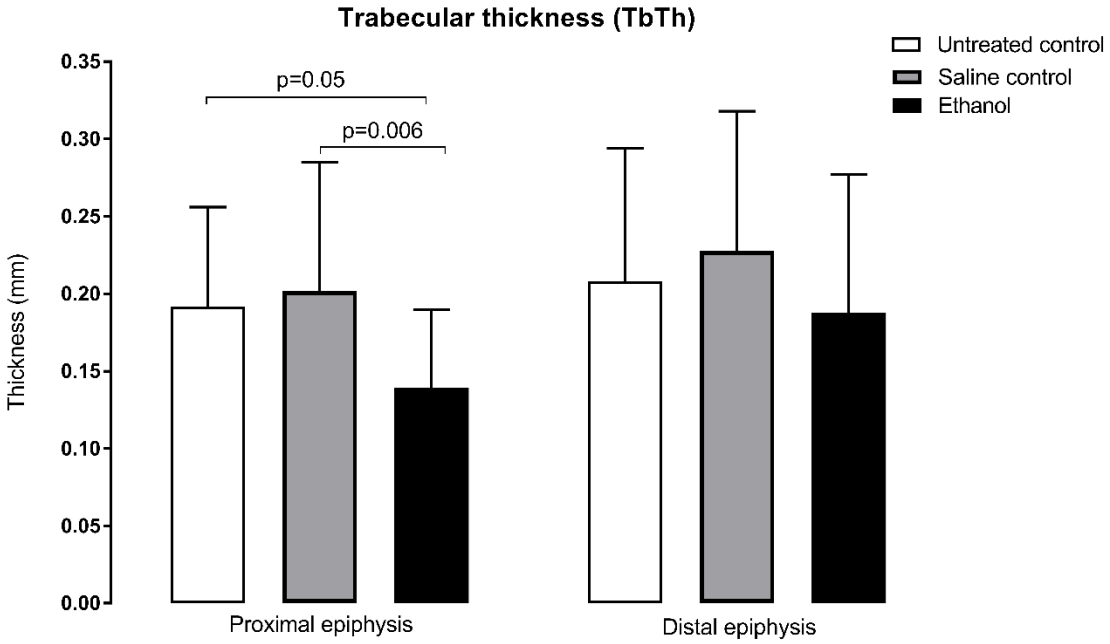


Figure 3.5: Humerus trabecular thickness (TbTh) at 3 weeks of age. The mean values are given for the proximal and distal epiphysis in the untreated, saline controls and the ethanol group. Error bars indicate standard deviation.

Humerus trabecular number (TbN)

Trabecular distribution by the study groups showed a similar pattern when stratified by the epiphyseal end (proximal and distal). In the proximal region, the trabecular number (TbN) was highest in the untreated controls (mean = 6.83mm^{-1} ± 1.68) followed by the saline (mean = 5.63 mm^{-1} ±0.52) and was lowest in the ethanol group (mean = 5.10mm^{-1} ±0.99). These differences were significant between the ethanol and untreated controls ($p<0.001$) and between the controls ($p=0.004$) (Fig. 3.5). However, no significance was detected between the ethanol and saline controls ($p=0.113$). (Fig 3.6). Similarly, the distal epiphysis revealed that the number of trabecular (TbN) was highest in the untreated controls (mean = 6.23mm^{-1} ±0.75) compared to the saline (mean = 5.39mm^{-1} ±0.42) and ethanol group (mean = 4.53mm^{-1} ±0.1.52). This difference was significant for the untreated group compared to the ethanol ($p<0.001$) or the saline group ($p=0.017$). A comparison of the control groups showed no significant differences ($p=0.06$) (Fig. 3.6).

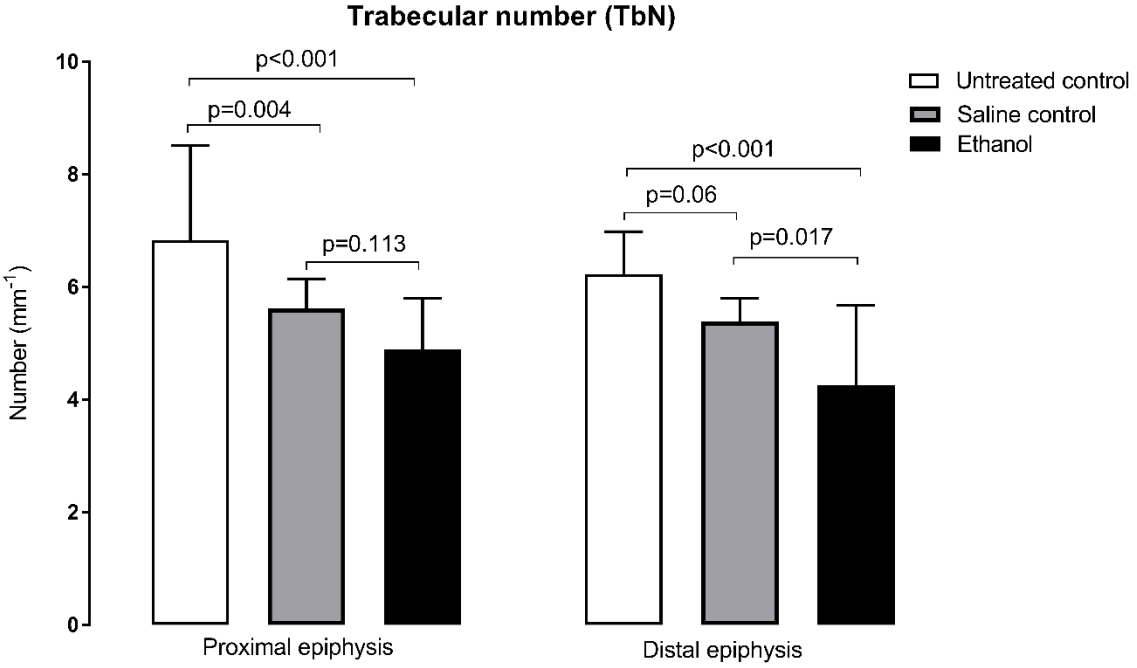


Figure 3.6: Humerus trabecular thickness (TbN) at 3 weeks of age. The mean TbN values are given for the untreated, saline controls and the ethanol group in the proximal and distal epiphysis. Error bars represent standard deviation.

Humerus trabecular spacing (TbSp)

Both epiphyseal ends exhibited a similar pattern in the trabecular spacing (TbSp) when stratified by study grouping. In the proximal epiphysis, trabecular spacing was significantly greater in the ethanol group (mean = 0.049mm ±0.01) compared to saline controls (mean = 0.046mm ±0.02) and untreated group (mean = 0.04mm ±0.01). This difference was significant for the ethanol compared to the untreated controls ($p<0.001$). (Figs. 3.7 and 3.8 a, b, c). Regarding the controls, the saline group trabecular spacing was significantly greater than in the untreated controls ($p=0.035$). In the distal epiphysis, trabecular spacing was significantly greater than in the ethanol group (mean = 0.053mm ±0.01) compared to saline controls (mean = 0.051mm ±0.02) and untreated group (mean = 0.043mm ±0.01) (Figs. 3.7 and 3.8 d, e, f). This difference was significant for the ethanol compared to the untreated controls ($p=0.001$). Regarding the controls, the saline group trabecular spacing was significantly greater than in the untreated controls ($p=0.005$) (Fig.3.7).

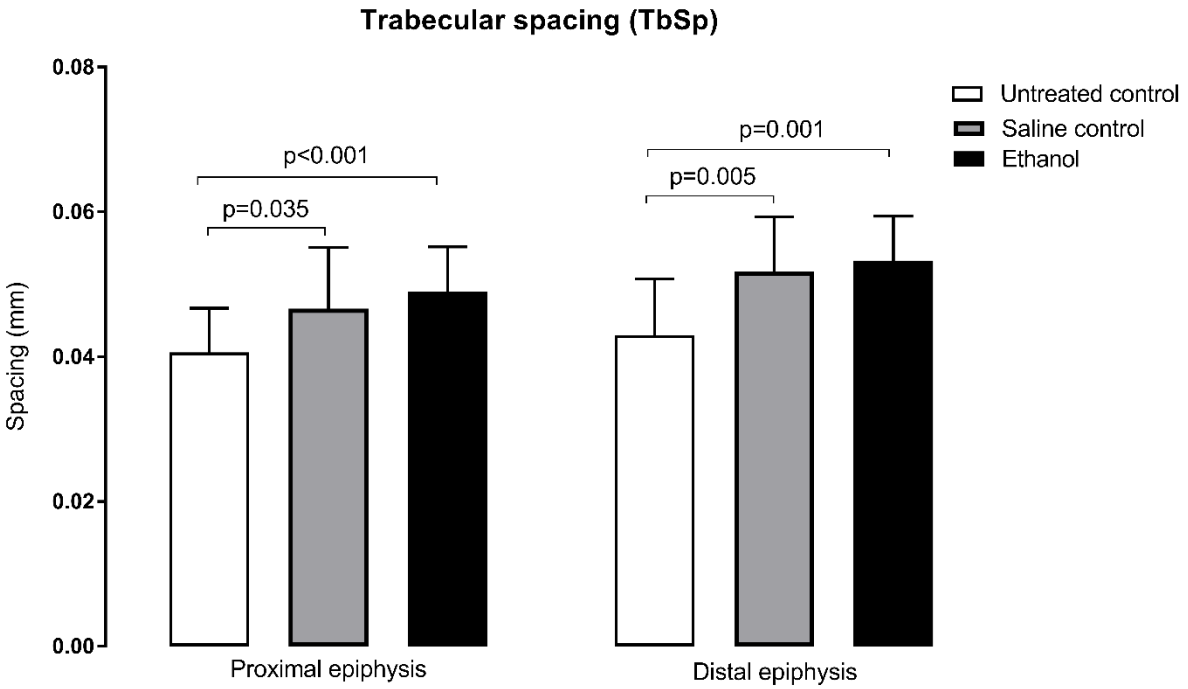


Figure 3.7: Humerus trabecular spacing (TbSp) at 3 weeks of age. The means are given for the proximal and distal epiphysis in the untreated controls, saline controls and the ethanol group. Error bars indicate standard deviation.

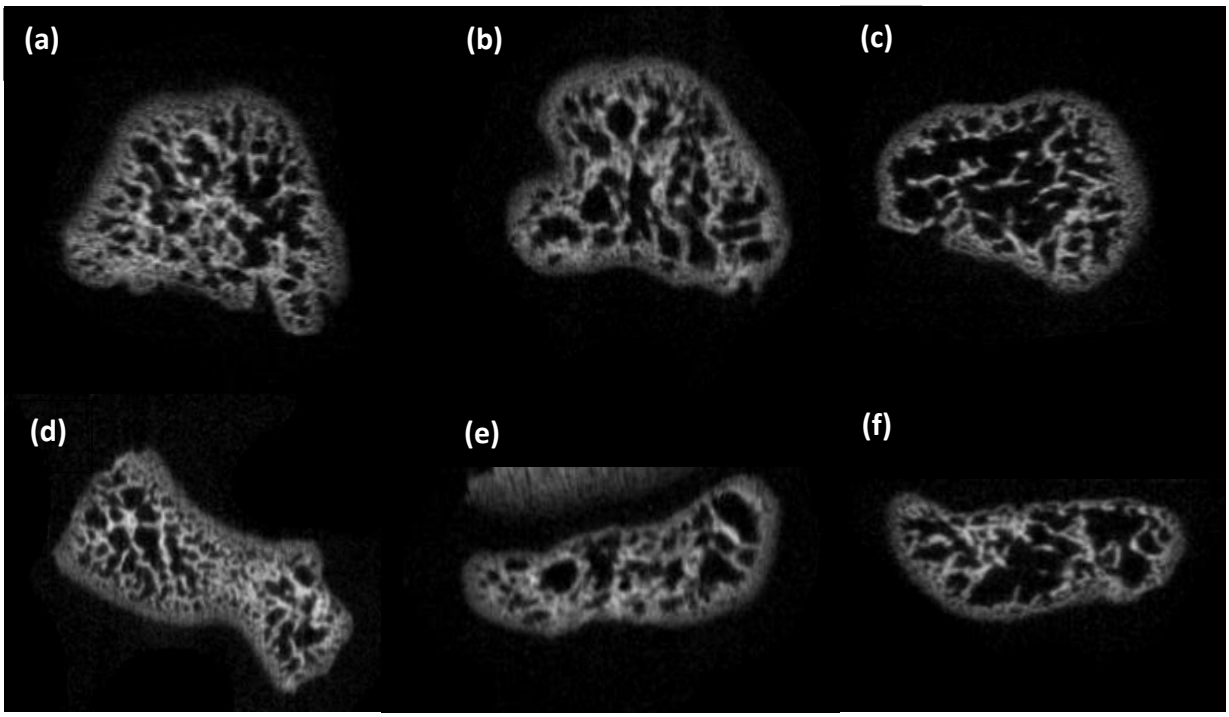


Figure 3.8: Trabecular morphology in the humerus at 3 weeks of age. Representative slices of (a), proximal end in an untreated control showing more trabeculae and less spacing; (b), proximal end in a saline control showing moderate trabeculae and spacing; (c), proximal end of the ethanol group showing fewer trabeculae and wider spacing); (d), distal end of an untreated control showing more trabeculae and less spacing; (e), distal end of saline control showing moderate trabeculae and spacing; (f), distal end of the ethanol group showing fewer trabeculae and wider spacing.

3.3.3 Humerus cross-sectional area, cortical area (thickness) and medullary canal area at 3 weeks of age

Proximal (25th percentile mark)

The proximal cross-sectional area was marginally higher in the untreated (mean = 5.09mm^2 ±1.13) than the saline controls (mean = 4.57mm^2 ±1.43) and ethanol group (mean = 4.79mm^2 ±0.95). There were no statistical group differences detected (p=0.568) (Fig. 3.9). Similarly, medullary canal area was similar for both controls (untreated mean = 2.66mm^2 ± 0.5; saline mean = 2.19 mm^2 ±1.19) and the ethanol group (2.55 mm^2± 1.03) (p=0.43) (Fig. 3.9). Again, group similarities occurred regarding the cortical area (thickness) with the untreated controls (mean = 2.42mm^2 ± 0.77) only showing a marginally higher value, closely followed by the saline (mean =2.38mm^2 ± 0.71) and the ethanol group (mean = 2.24 mm^2 ± 0.28) (p=0.66) (Fig. 3.9).

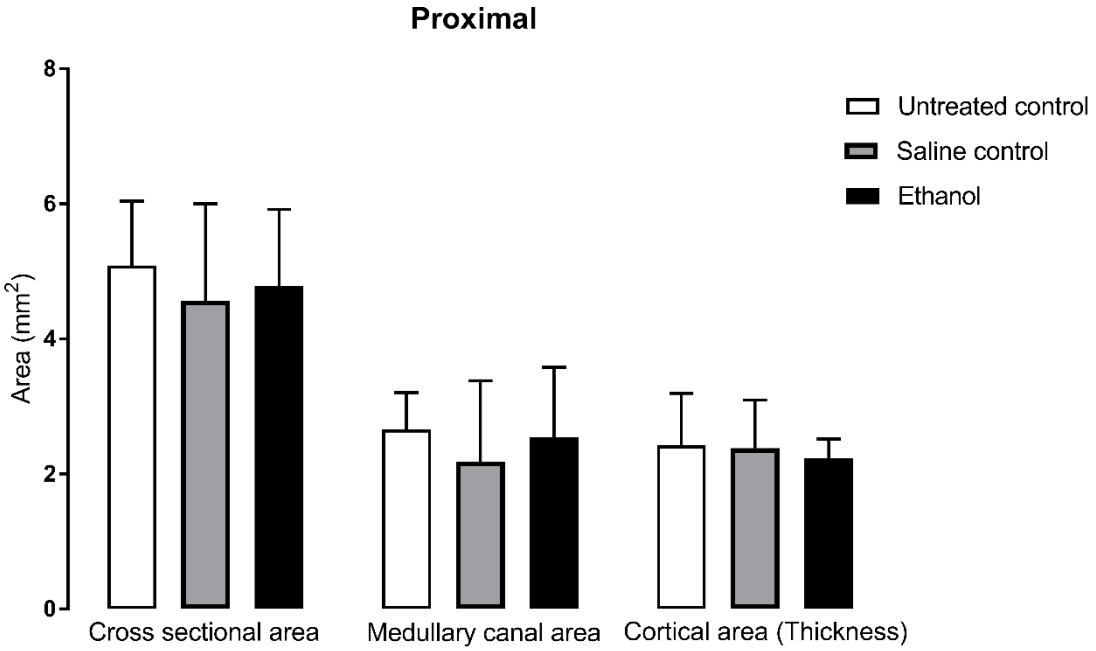


Figure 3.9: Humerus proximal cross-sectional area, medullary area and cortical thickness at 3 weeks of age. The means at the 25th percentile mark given for the three groups studied. Error bars represent standard deviation.

Midshaft (50th percentile mark)

The midshaft cross-sectional area was similar in all three groups studied. The ethanol group had mean of 3.51mm^2 ±0.56, the saline and untreated groups had a mean of 3.34 mm^2 ±0.80 and 3.51mm^2 ±0.53, respectively (p=0.701) (Fig. 3.10). Although the untreated groups (1.63mm^2 ±0.48) seemed to have a larger medullary canal area than the saline controls (mean = 1.58mm^2 ±0.53) and the ethanol group (mean = 1.53mm^2 ±0.27), no significant differences were detected (p=0.86) (Fig. 3.10). Regarding cortical area (thickness) in this bone region, no significant differences occurred between the groups. The untreated controls (mean = 1.89mm^2 ±0.45) appeared to be greater than the saline (mean = 1.76mm^2 ±0.37 and ethanol groups (mean = 1.97 mm^2 ±0.43) (p=0.31) (Fig. 3.10).

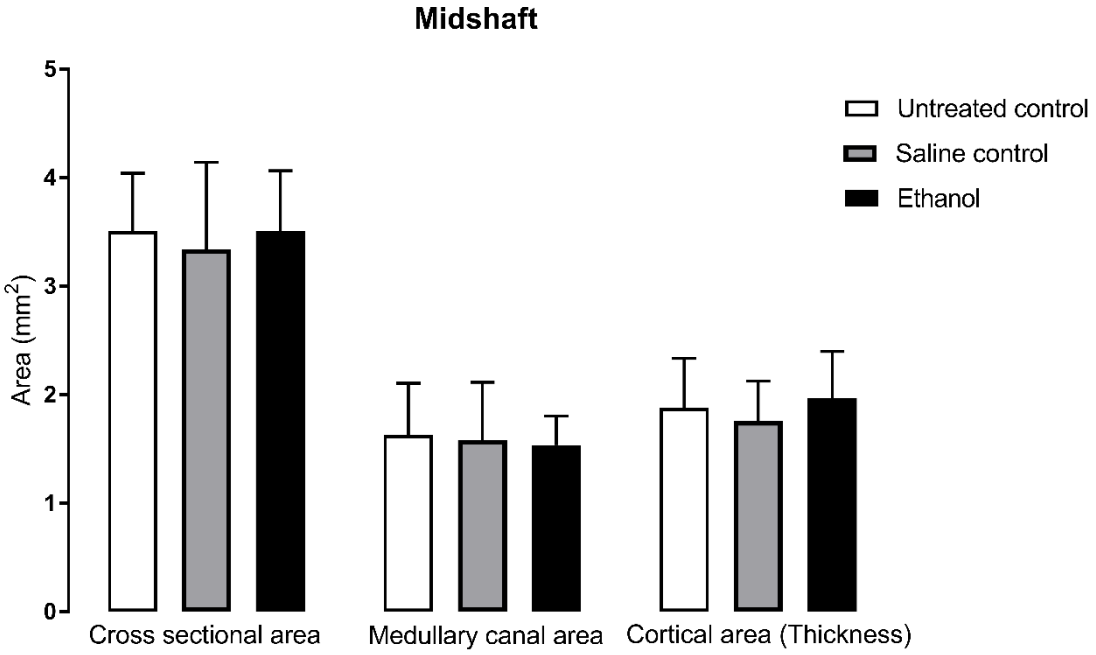


Figure 3.10: Humerus midshaft cross-sectional area, medullary area and cortical thickness at 3 weeks of age. The means at the 50th percentile mark given for the three groups studied. Error bars represent standard deviation.

Distal (75th percentile mark)

The distal cross-sectional area was largest in the saline (mean = 4.98mm^2 ±0.83) compared to the untreated controls (mean = 4.04 mm^2 ±0.67) and the ethanol group (mean = 3.83 mm^2 ±0.64) (p=0.002, p<0.001), respectively) (Fig. 3.11). Similarly, the distal medullary canal was largest in the saline (mean = 2.76mm^2 ±0.51) compared to the untreated controls (mean = 1.73 mm^2 ±0.34) and the ethanol group (mean = 1.75mm^2 ±0.41) (p<0.001 for both comparisons) (Fig. 3.11). With respect to the cortical area (thickness) in this bone region, the ethanol group (mean = 2.07mm^2 ±0.49) exhibited a marginally lower value compared to the saline and untreated controls (mean = 2.22mm^2 ±0.48 and 2.31mm^2 ±0.51, respectively). However, no significant group differences were detected (p=0.41) (Fig. 3.11).

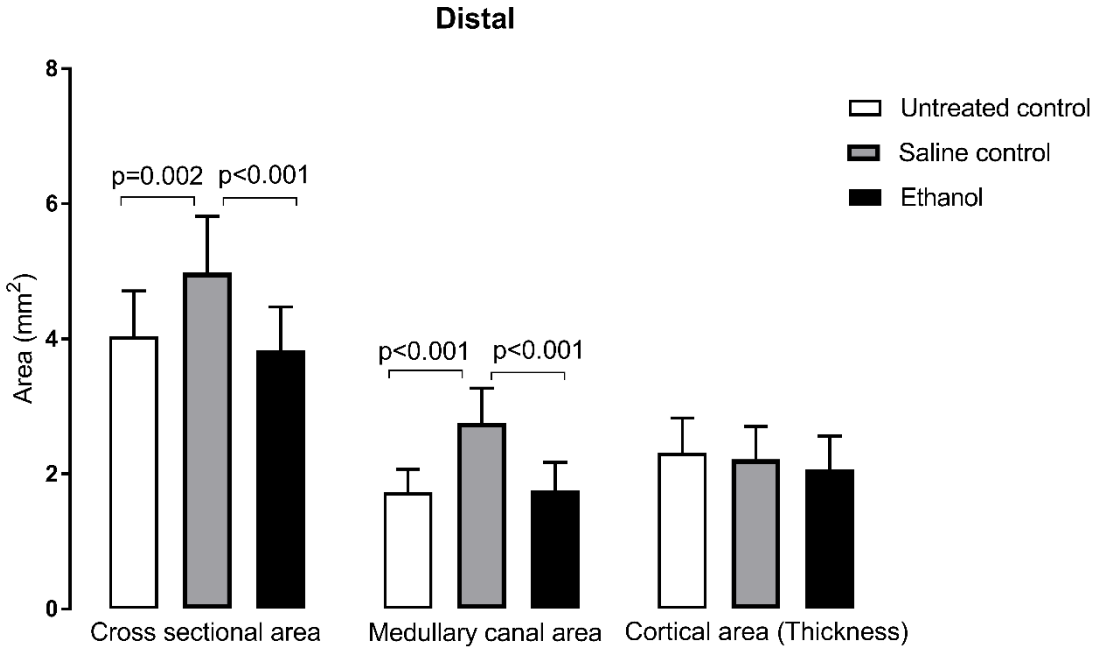


Figure 3.11: Humerus distal cross-sectional area, medullary area and cortical thickness. The means at the 75th percentile mark given for the three groups studied. Error bars represent standard deviation.

3.3.4 Histological characterization at 3 weeks

Humerus epiphyseal growth plate surface area

The epiphyseal plate surface area exhibited regional differences as the proximal aspect had chondrocyte number similarity per group. In contrast, the untreated group had the most chondrocytes in the distal epiphysis**.** In the proximal region, the epiphyseal plate surface area showed no significant groups differences when comparing the untreated (mean = 22.02mm^2 ±0.90), saline controls (mean = 20.80mm^2 ±1.54) and the ethanol group (mean = 20.34mm^2 ±2.09) (p=0.195) (Fig. 3.12). In the distal aspect, the epiphyseal plate surface area was greater in the untreated (mean = 21.17mm^2 ±0.40) than the saline controls (mean = 18.55 ±0.44) and the ethanol group (mean = 18.61mm^2 ±0.52) and had a larger surface area than the ethanol group and saline controls. (p<0.001 for both comparisons) (Fig. 3.12).

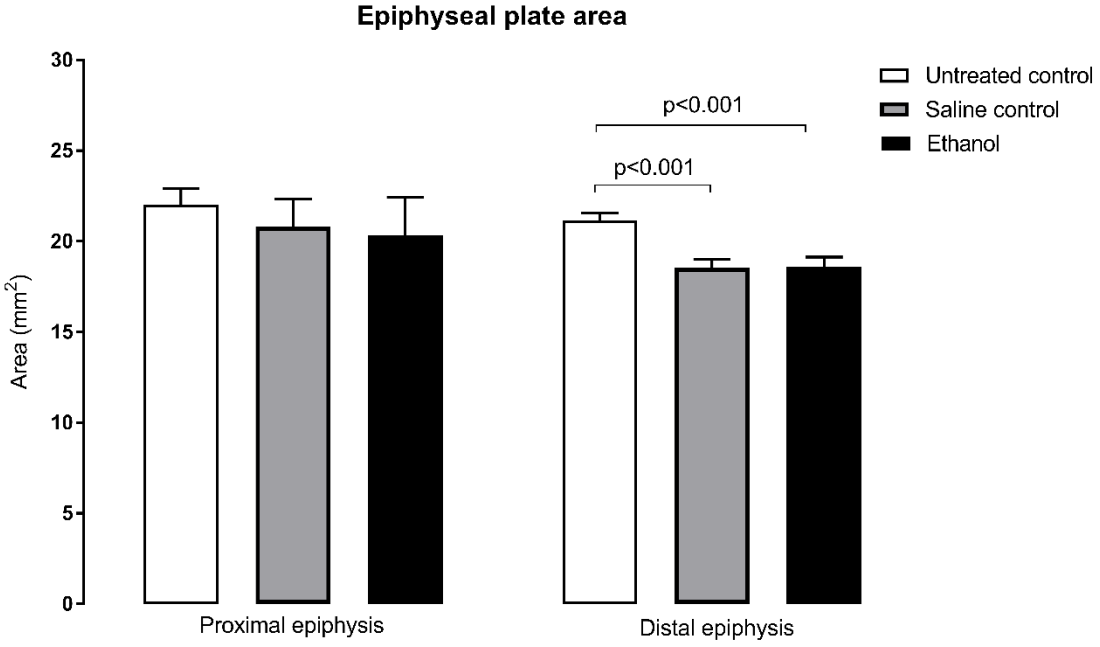


Figure 3.12: Histomorphometry of the epiphyseal growth plate surface area in the humerus at 3 weeks of age. The mean values for the epiphyseal growth plate surface area are given for the untreated, saline controls and the ethanol group. Error bars represent standard deviation.

Cellular morphology of the humerus

The proliferative zone of both epiphyseal ends (proximal and distal), showed a partly similar group comparison. The untreated group had more chondrocytes which were tightly packed in prominent rows than the saline controls and ethanol group (Fig. 3.13) The controls showed the chondrocytes to be evenly distributed with a few gaps, while in the ethanol group the chondrocyctes were loosely packed, with areas with huge gaps (Fig. 3.13). This pattern continued in the distal region (Fig. 3.13).

The hypertrophic zone of the epiphyseal plate showed similar morphology among all the groups in the proximal and distal region with no obvious abnormalities (Fig. 3.13).

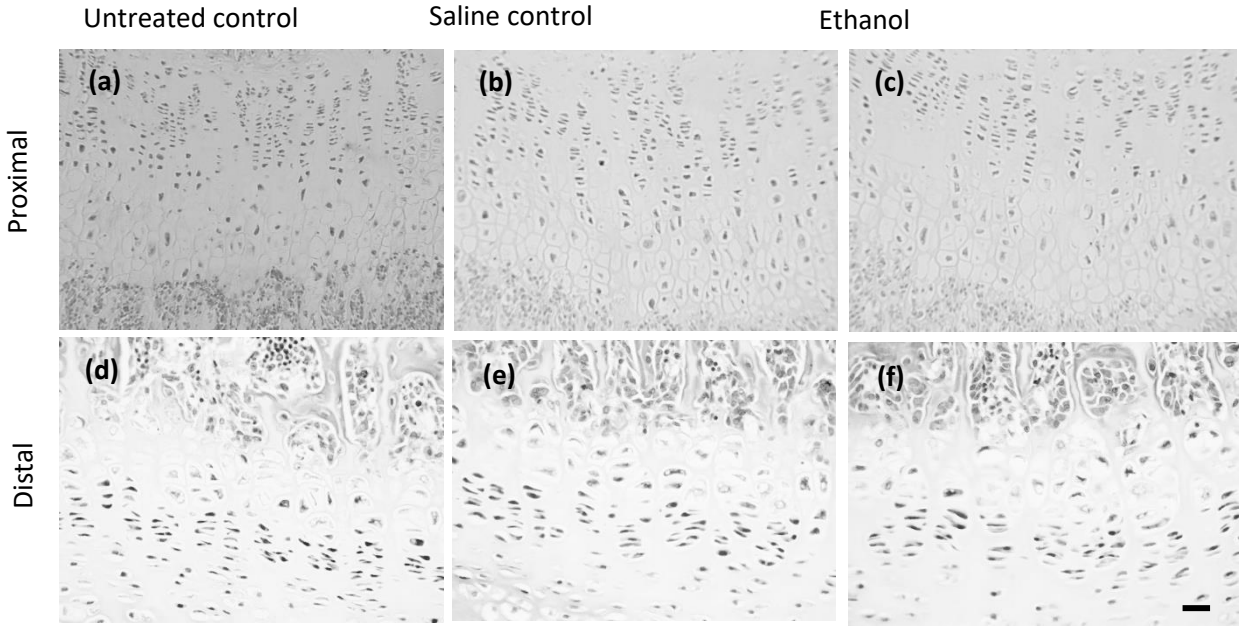


Figure 3.13: Representative photomicrographs of Haematoxylin and Eosin stained sections of the epiphyseal growth plate of the humerus. The photomicrographs show the proximal and distal epiphyseal growth plate for the three groups studied. Scale bar = 20 microns and applies to all images.

Chondrocyte number in the proliferative zone of the humerus

In both epiphyseal growth plates, the untreated group had the most chondrocytes. In the proximal epiphysis, the untreated controls (mean = 1016.83 ±33.96) had significantly more chondrocytes that the saline (mean = 1181.39 ±24.82) and ethanol group (mean = 996.40 ±27.33) which exhibited fewer chondrocytes ($p<0.001$ for both comparisons). The ethanol group and saline controls were similar ($p= 0.21$). (Fig. 3.14). Similarly, the distal epiphysis showed more chondrocytes in untreated group (mean = 866.47 ±22.71) although closely followed by the ethanol and group (mean = 865.00 ±31.71 and ($p=0.93$). The least number of chondrocytes was in the saline controls (mean = 826.99 ±34.43) ($p=0.03$ for saline compared to the other 2 groups) (Fig. 3.14)

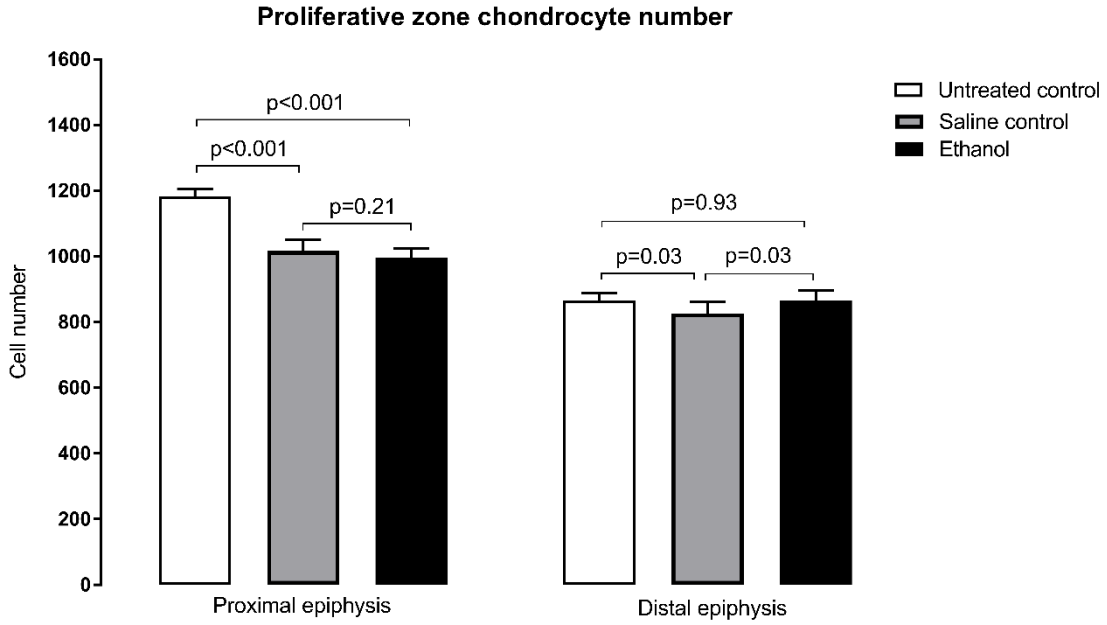


Figure 3.14: Epiphyseal growth plate proliferative zone number of chondrocytes in the humerus. The cell number is given as means for the proliferative zone in the proximal and distal epiphyseal growth plate given for the untreated, saline controls and the ethanol group. Error bars represent standard deviation.

Chondrocyte number in the hypertrophic zone of the humerus

The two epiphyseal ends showed a partly similar group comparison pattern in that the untreated group had the most chondrocytes in the proximal and distal epiphyseal plate hypertrophic zone. In the proximal epiphysis hypertrophic zone, chondrocytes were fewer in the ethanol and saline group, (mean=762.67 ±44.37 and mean = 752 ±35.80, respectively) compared to the untreated group (mean = 881.94 ±28.89) ($p<0.001$ for both comparisons) (Fig. 3.15). In the distal epiphysis hypertrophic zone, untreated group (708,05 ±20.42) had more chondrocytes than the ethanol group (mean = 684.95 ±50.07) and the saline controls (mean = 662.55 ±21.38). However, significant differences were only observed when comparing the untreated with the saline control group ($p=0.029$) (Fig. 3.15).

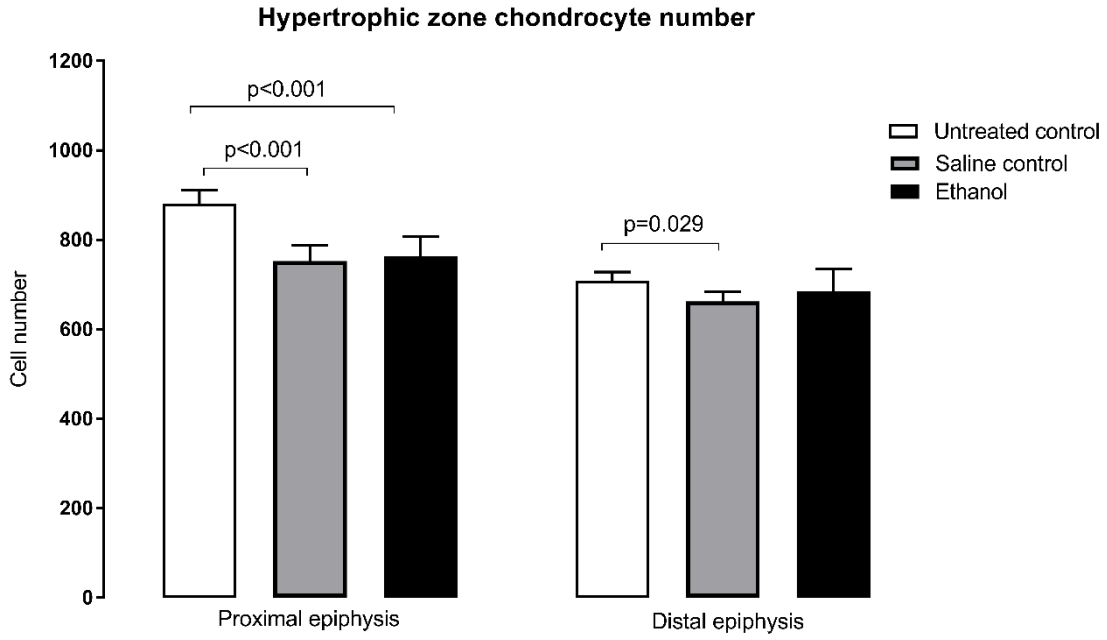


Figure 3.15: Epiphyseal growth plate hypertrophic zone number of chondrocytes in the humerus. The mean values are shown for the hypertrophic zone in the proximal and distal epiphyseal growth plate given for the untreated, saline controls and the ethanol group. Error bars represent standard deviation.

Immunohistochemical characterizations at 3 weeks

Humerus proliferative zone Ki-67 immuno-positive chondrocytes

The proximal and distal epiphysis were similar in that the untreated group had the most chondrocytes in both the proximal and distal epiphyseal plate proliferative zone. In the proximal epiphyseal plate proliferative zone, more Ki-67 labelled chondrocytes were found in the untreated group (mean=906.54 ±15.96) than saline controls (mean = 847.99 ±53.01) and ethanol group (mean = 814.85 ±78.72) (Fig. 3.16 and Figure 3.17 a, b, c). However, statistical significance was only observed between the ethanol and the untreated group (p=0.011) (Fig. 3.14). In the distal region, more Ki-67 positive cells were found in the untreated group (mean = 803.99 ±13.96) compared to the saline controls (mean = 692.06 ±14.61) and ethanol group (mean = 685.15 ±38.63) which had similar numbers (p<0.001 for both comparisons) (Fig. 3.16 and Fig 3.17 d, e, f).

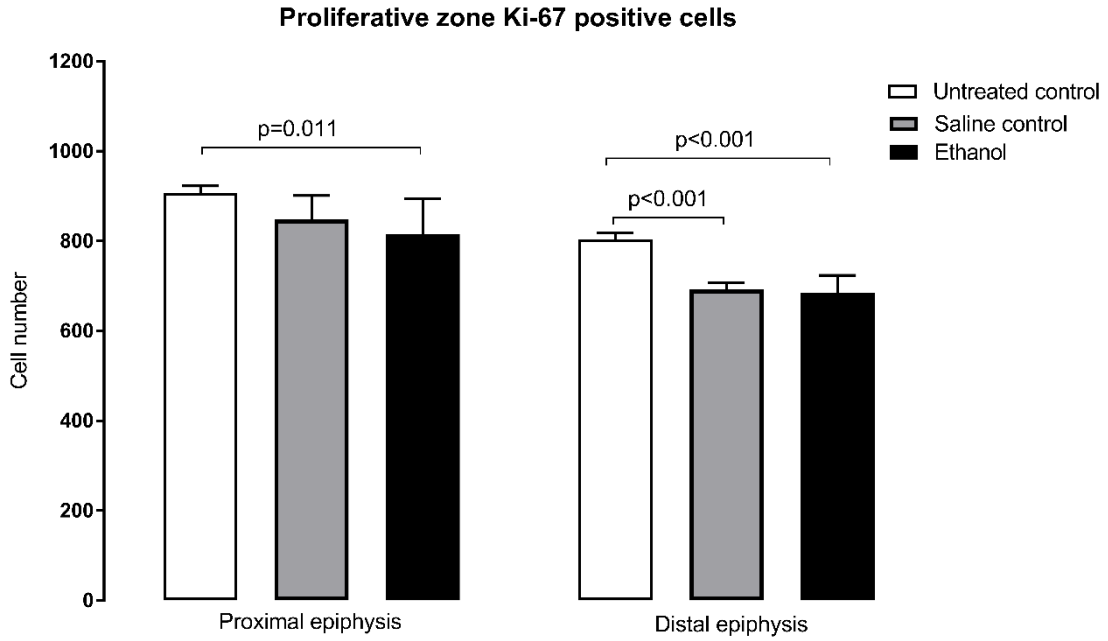


Figure 3.16: Ki-67 immuno-positive proliferative chondrocytes of the humerus. The mean number of Ki-67 immuno-positive proliferative chondrocytes are shown for the proliferative zone in the proximal and distal epiphyseal growth plate for the three groups studied. Error bars represent standard deviation.

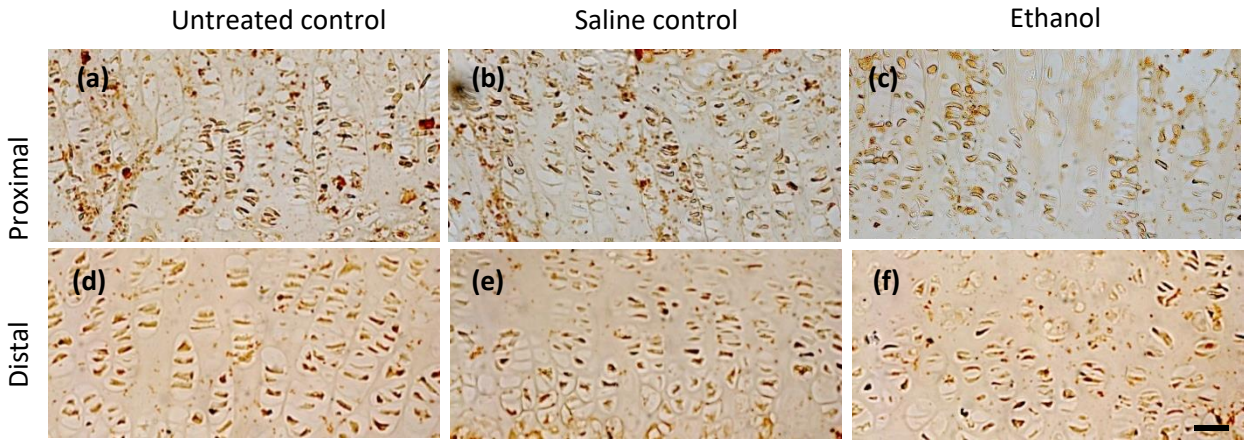


Figure 3.17: Photomicrograph of humerus proliferative zone chondrocytes immunolabeled with the anti-Ki-67 antibody. Representative micrographs of the proximal and distal epiphyseal growth plate for the three groups studied. Scale bar = 20 microns and applies to all images.

Humerus hypertrophic zone Ki-67 immuno-positive cells

The pattern of the untreated group having the most chondrocytes in both the proximal and distal epiphyseal plate proliferative zone was also observed in the hypertrophic zone. In the proximal epiphyseal plate hypertrophic zone, more Ki-67 labelled chondrocytes were found in the untreated control group (mean = 611.04 ±36.08) than the saline controls (mean = 548,31 ±62,28) and the ethanol group which had similar values (mean = 550.38 ±23.19) (Fig. 3.18 and Fig. 3.19 a, b, c). Significance was detected when comparing the untreated group with the saline (p=0.022) or ethanol group (p=0.021) (Fig. 3.18). In the distal region, more Ki-67 labelled chondrocytes were found in the untreated group (mean = 631.81 ±34.21) than the saline controls (mean = 586.50 ±22.08) and ethanol group (mean = 547.81 ±51.18). However, these differences were significant only between the ethanol and the untreated group (p=0.001) (Fig. 3.18 and Fig. 3.19 d, e, f).

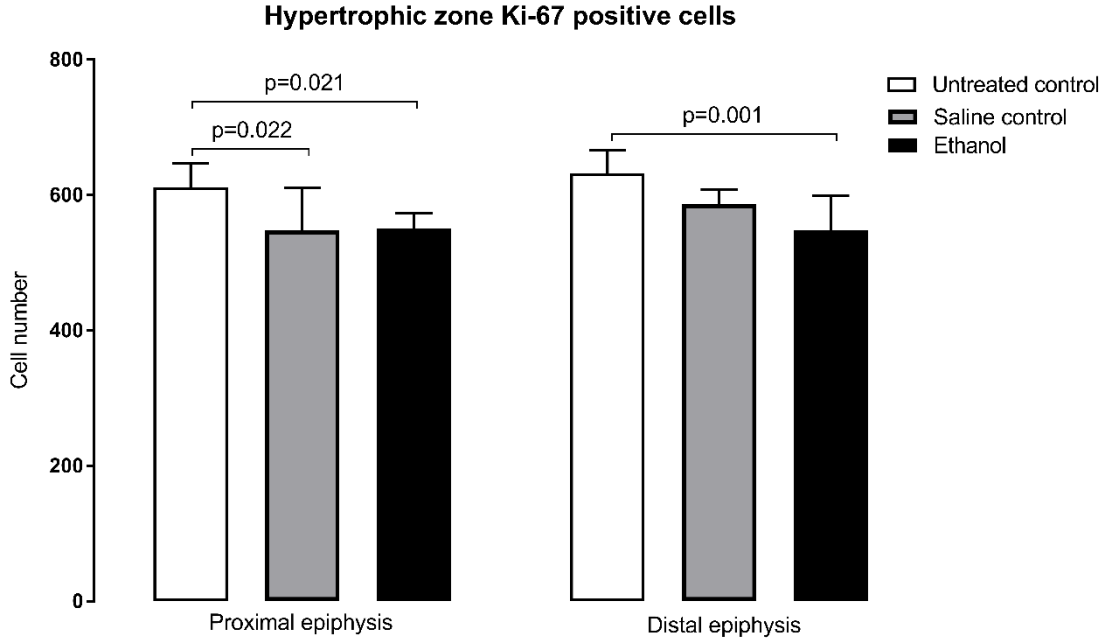


Figure 3.18: Ki-67 immuno-positive hypertrophic chondrocytes of the humerus. The mean number of Ki-67 immuno-positive hypertrophic chondrocytes are shown for the hypertrophic zone in the proximal and distal epiphyseal growth plate for the three groups studied. Error bars represent standard deviation.

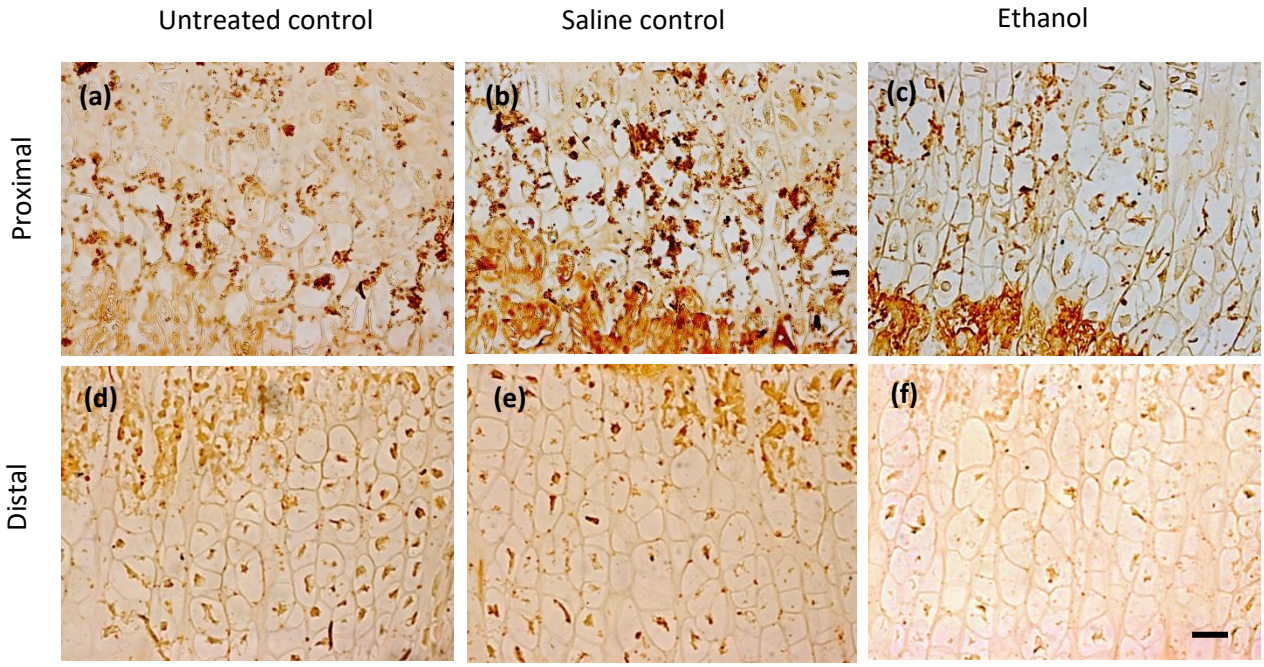


Figure 3.19: Photomicrograph of humerus hypertrophic zone chondrocytes immunolabeled with the anti-Ki-67 antibody. Representative micrographs of the proximal and distal epiphyseal growth plate for the three groups studied. Scale bar = 20 microns and applies to all images.

Humerus proliferative zone TGFβ-1 immuno-positive cells

The proximal and distal epiphyses were similar in that the untreated group had the most chondrocytes in both the proximal and distal epiphyseal plate proliferative zone. The proximal plate proliferative zone showed more TGFβ-1 labelled chondrocytes in the untreated group (mean = 740.72 ±21.47) than the saline controls (mean = 725.53 ±7.88) and ethanol group (mean = 694.05 ±40.53). However, these cell numbers were only significantly different between the ethanol and the untreated group (p=0.011) (Fig. 3.20 and Fig. 3.21 a, b, c). In the distal epiphysis, TGFβ-1 labelled cells were more in the untreated group (mean = 656.78 ±43.40) compared to saline controls (mean = 623.22 ±42.77) and the ethanol group (mean = 595.81 ±26.28) This difference was significant only for the untreated controls compared to ethanol (p=0.01) (Fig. 3.20 1nd Fig 3.21 d, e, f).

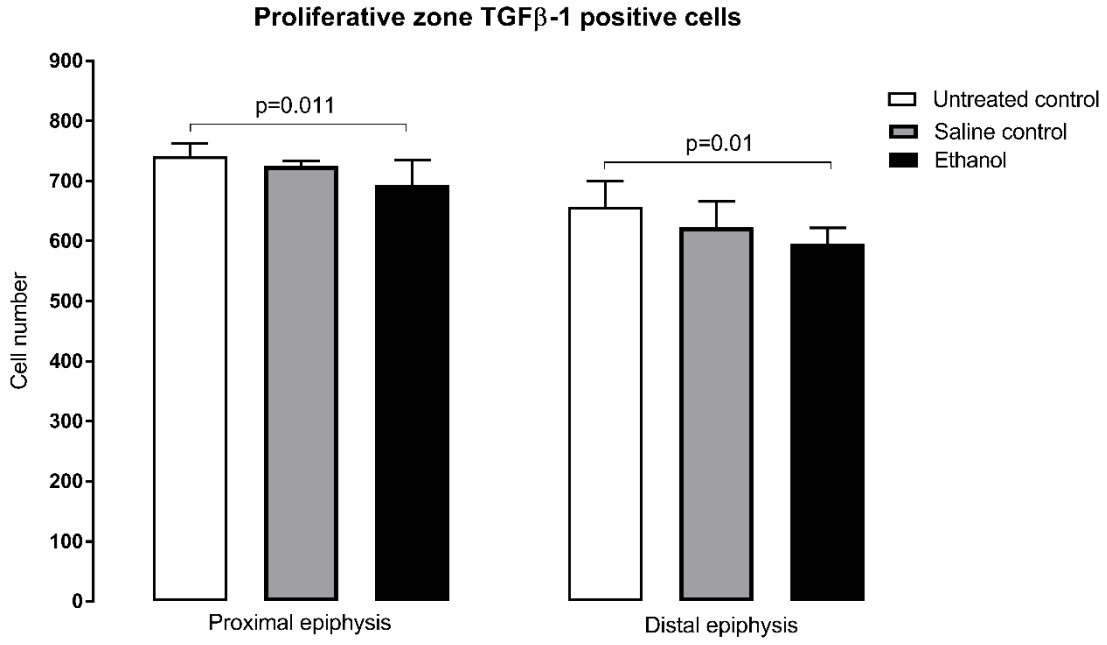


Figure 3.20: TGFβ-1 immuno-positive proliferative chondrocytes in the epiphyseal growth plate of the humerus. The mean values of TGFβ-1 immuno-positive chondrocytes are shown for the proliferative zone in the proximal and distal epiphyseal growth plate. Error bars represent the standard deviation.

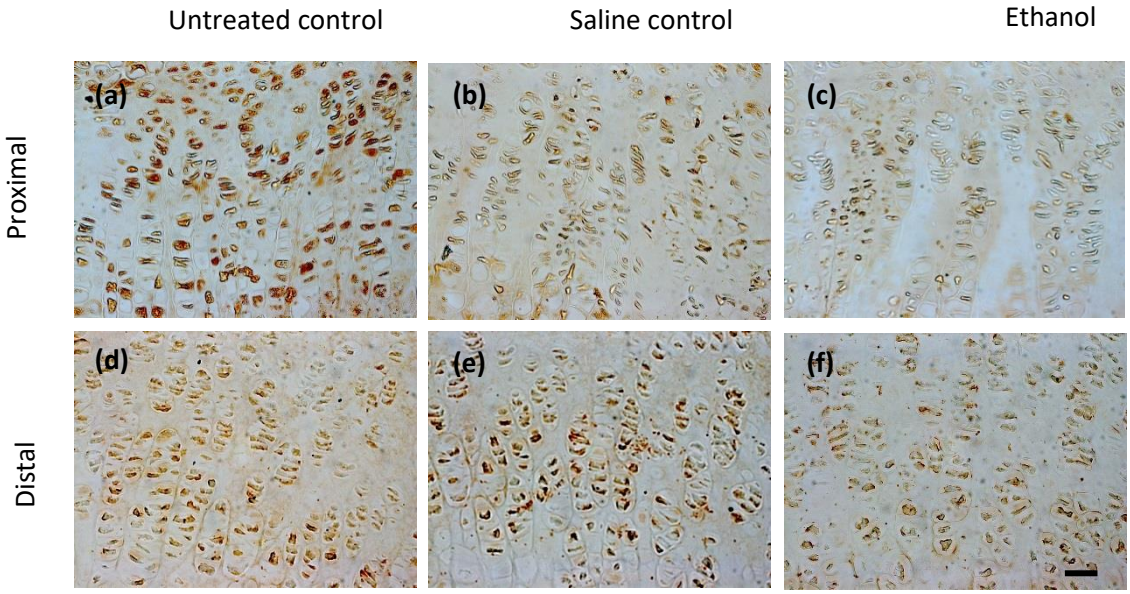


Figure 3.21: Photomicrograph of humerus proliferative zone chondrocytes immunolabeled with the anti-TGFβ1 antibody. Representative micrographs of the proximal and distal epiphyseal growth plate for the three groups studied. Scale bar = 20 microns and applies to all images.

Humerus hypertrophic zone TGFβ-1 immuno-positive cells

No group differences were detected in the hypertrophic zone of the proximal aspect whereas the untreated group had the most chondrocytes in the distal epiphysis. In the proximal epiphysis, the untreated controls (mean = 525.00 ±46.81) appeared to show more TGFβ-1 labelled chondrocytes compared to the saline (mean = 473.33 ±62.23) and ethanol group (mean = 456.67 ±96.57) although no significant differences were detected among the groups (p=0.267) (Fig. 3.22 and Fig. 3.23a, b, c). Similarly, the distal epiphysis showed that the untreated controls (mean = 471.33 ±26.54) compared to the saline (mean = 425.17 ±30.17) and ethanol group had fewer TGFβ-1 labelled cells (mean = 377.33 ±43.51). This difference was significant for the ethanol compared to the saline controls (p=0.025) or untreated group (p<0.001) (Fig. 3.22 and Fig 3.23d, e, f).

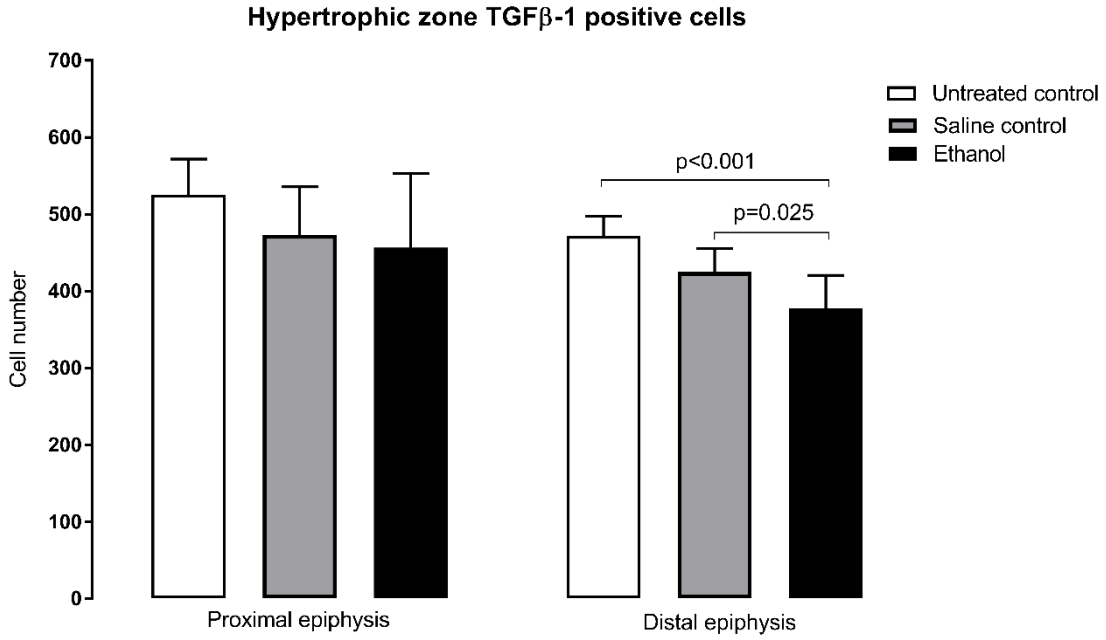


Figure 3.22: TGFβ-1 immuno-positive hypertrophic chondrocytes in the epiphyseal growth plate of the humerus. The mean values of TGFβ-1 immuno-positive chondrocytes are shown for the proliferative zone in the proximal and distal epiphyseal growth plate. Error bars represent the standard deviation.

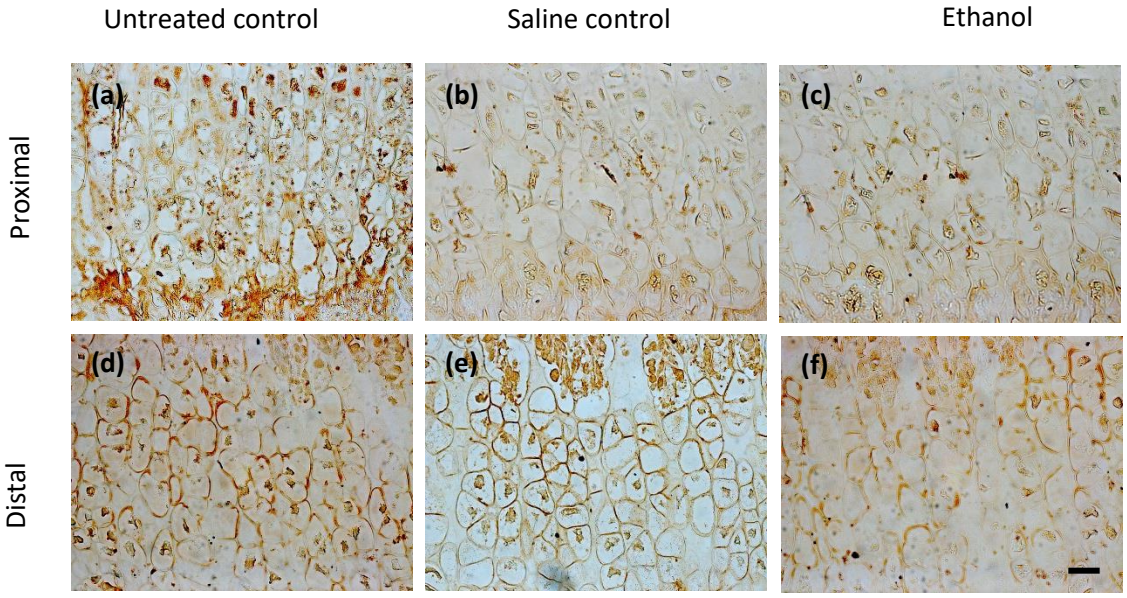


Figure 3.23: Photomicrograph of humerus hypertrophic zone chondrocytes immunolabeled with the anti-TGFβ1 antibody. Representative micrographs of the proximal and distal epiphyseal growth plate for the three groups studied. Scale bar = 20 microns and applies to all images.

3.3.5 Humerus (3 weeks) trabecular morphometric parameters most affected by gestational ethanol

Proximal humerus

The effect of gestational ethanol on bone volume to total volume ratio, trabecular thickness, number and separation was assessed using binary logistic regression in the ethanol and saline control groups. The parameters used could reliably distinguish between the two groups (Table 3.4). A test of the full model against a constant only model was statistically significant, indicating that the predictors as a set, reliably distinguished between ethanol or saline control group membership (Chi-square = 43.716, $p < 0.001$ with df = 6). Nagelkerke's R^2 of 0.899 indicated a very strong relationship between prediction and grouping. The Wald criterion demonstrated that no specific variable predicted membership (Table 3.4). Prediction success overall was 94.9% (94.7% for the ethanol group and 95.0% saline controls) (Table 3.5)

Table 3.4: Humerus osteometric and proximal epiphysis trabecular morphometric parameters in the equation. BV/TV, bone volume to total volume; TbTh trabecular thickness; TbN, trabecular number; TbSp, trabecular spacing.

Variables in the Equation

	B	S.E.	Wald	df	Sig.	Exp(B)
Osteometric parameters						
Length	2.872	2.457	1.366	1	.243	17.668
Epiphyseal volume	-1.525	1.529	.995	1	.319	.218
Proximal epiphysis trabecular morphometric parameters						
BV/TV	315.108	221.434	2.025	1	.155	7.073
TbTh	89.278	127.429	.491	1	.484	5.926
TbN	19.419	11.361	2.922	1	.087	27.3
TbSp	2903.768	1644.761	3.117	1	.077	.2
Constant	-525.136	312.276	2.828	1	.093	.000

Table 3.5: Group membership classification from humerus osteometric and proximal epiphysis trabecular morphometric parameters.

Classification Table

Observed		Predicted		
		Group		Percentage Correct
		Ethanol	Saline Control	
Group	Ethanol	18	1	94.7
	Saline Control	1	19	95
Overall Percentage				94.9

Distal humerus

The effect of gestational ethanol on bone volume to total volume ratio, trabecular thickness, number and separation was assessed using binary logistic regression in the ethanol and saline control groups. The parameters used could reliably distinguish between the two groups. A test of the full model against a constant only model was statistically significant, indicating that the predictors as a set, reliably distinguished between ethanol or saline control group membership (Chi-square = 30.793, $p < 0.001$ with df = 6). Nagelkerke's R^2 of 0.740 indicated a very strong relationship between prediction and grouping. The Wald criterion demonstrated that only the bone volume to total volume ratio (BVTV) trabecular number (TbN) predicted membership (Table 3.6). Prediction success overall was 78.6% (84.2% for the ethanol group and 73.9% saline controls) (Table 3.7)

Table 3.6: Humerus osteometric and distal epiphysis trabecular morphometric parameters in the equation. BV/TV, bone volume to total volume; TbTh trabecular thickness; TbN, Trabecular number; TbSp, Trabecular spacing.

Variables in the Equation

	B	S.E.	Wald	df	Sig.	Exp(B)
Osteometric parameters						
Length	-.383	1.239	.096	1	.757	.682
Epiphyseal volume	.353	.753	.219	1	.640	1.423
Distal epiphysis trabecular morphometric parameters						
BV/TV	87.847	39.006	5.072	1	.024	1.418
TbTh	-24.851	33.818	.540	1	.462	.001
TbN	3.917	1.739	5.072	1	.024	50.233
TbSp	363.523	223.000	2.657	1	.103	7.517
Constant	-97.313	44.921	4.693	1	.030	.000

Table 3.7: Group membership classification from humerus osteometric and distal epiphysis trabecular morphometric parameters.

Classification Table

Observed		**Predicted**		
		Group		**Percentage Correct**
		Ethanol	Saline Control	
Group	Ethanol	17	2	89.5
	Saline Control	4	15	78.9
Overall Percentage				84.2

3.4 DISCUSSION

We sought to understand whether binge intrauterine alcohol exposure would affect the rat humerus epiphyseal growth plate and diaphysis dimensions. Gestational alcohol exposure resulted in a smaller epiphyseal growth plate with fewer proliferating chondrocytes and reduced TGFβ1 expression. Use of three-dimensional micro-focus X-ray computed tomography (3D- μCT) to assess trabeculae volume, thickness, number and spacing in the proximal and distal epiphysis of the humerus showed altered trabecular parameters in the alcohol-exposed group. The diaphyseal cortical and medullary cavity proportions were also affected.

Bone osteometry and epiphyseal trabecular morphometric parameters

In the present study, there were no significant differences in bone length among the three groups. Other studies (Nwaogu, 2002; Simpson et al., 2005; Snow and Keiver, 2007) found the length to be reduced in the alcohol group. The difference in the findings could be related to the dosage of alcohol administered to the dams. In the present study, we used 25.2% ethanol whereas other studies used a higher ethanol concentration of 30 and 36% in their studies (Nwaogu, 2002; Simpson et al., 2005; Snow and Keiver, 2007). The effects of prenatal ethanol exposure on bone are dose-dependent as Snow and Keiver (2007) and Simpson et al. (2005) showed that 36% ethanol causes more adverse effects than 15% and 25% ethanol administered in gestation. A possibility exists that we could have found a shorter length in the ethanol group had we used a higher concentration such as 36%.

Since length is a linear measurement in a single dimension, size information from other aspects in three-dimensional space tends to be excluded. The present study addressed this problem by incorporating volume estimates. We calculated the proximal and distal epiphyseal volumes. The ethanol group had a lower epiphysis volume in both extremities compared to the controls. We could not find comparable studies that investigated this parameter. Also, the bone volume to total volume (BV/TV) was lower in the ethanol group in both extremities compared to the controls, only in the proximal epiphysis leaving the distal end unaffected. This could be attributed to the higher bone activity in the proximal

than the distal end (Payton, 1933). We could not find BV/TV literature that investigated gestational alcohol exposure prior to the current study. However, literature exists about postnatal alcohol consumption in animals showing alteration of BV/TV (Diamond et al., 1989; Wezeman et al., 1999; Turner et al., 2001; Maddalozzo et al., 2009). Our study indicates that prenatal alcohol exposure effects may persist up to 3-weeks postnatally. Therefore, alcohol affects BV/TV despite stoppage after birth, with similar effects on BV/TV when alcohol is taken in postnatal life.

Thinnest and fewer trabeculae with larger spacings were observed in the ethanol group in both extremities. Since trabeculae are a proxy for collagen deposition, thinner and fewer trabeculae in the present study suggest that fewer collagen fibres were deposited in the ethanol group. Postnatal alcohol use is known to impair osteoblast function (Martin and Correa, 2010; Mikosch, 2014) and has a negative effect on trabecular number (Turner, 2000; Maurel et al., 2012a; Mikosch, 2014). This is similar to our findings in gestational alcohol exposure. Thinner trabeculae suggest that osteoblasts which produce collagen may have been adversely affected by alcohol. A possibility exists that intrauterine alcohol exposure may increase osteoclast activity, resorbing collagen fibres while also decreasing osteoblast activity to impede collagen synthesis. This phenomenon occurred in our study although the alcohol was only administered during gestation.

The thinner and fewer trabeculae, with larger spaces in the ethanol group in both extremities, may be linked to bone weakness. Studies of postnatal alcohol intake report increased trabecular spacing (Maurel et al., 2012b; Mikosch, 2014). This is thought to be due to an osteoclastic phase of bone loss contributing to ethanol-mediated osteoporosis. Children exposed to gestational alcohol during pregnancy, particularly those with FAS are at risk of osteoporosis and have a high bone fracture rate. Our findings of thinner and fewer trabeculae with larger spacings in the ethanol group support the phenomenon of weak bones prone to osteoporosis and fracture.

We observed a smaller cross-sectional and medullary canal area in the ethanol group in the distal shaft only. This may indicate that the development of the proximal and distal region of the bone occurs differently in that the proximal diaphysis elongates faster (Payton, 1933). This inherent faster elongation rate that occurs proximally may have had a role in protecting the ethanol group at the ethanol dosage given in the present study. A smaller cortical thickness with a smaller medullary cavity significantly weakens bone (Maurel et al., 2012a) this phenomenon may explain the weaker bones reported in FAS children.

The role of TGFB1 in maintaining the epiphyseal growth plate and its cellular components

The epiphyseal plate surface area was smaller for the ethanol group in the distal epiphysis whereas no differences were found in the proximal region. The lack of significant differences in the proximal epiphyseal plate surface area observed in the present study suggests that this area could have compensated for growth in length resulting in similar lengths across the groups. In the same manner, the similarities in the proximal cross-sectional area could be attributed to the proximal epiphyseal plates that seemed unaffected by ethanol. A viable epiphyseal plate would be expected to lead to better diaphyseal dimensions as the diaphyseal development is dependent on epiphyseal plate integrity.

The ethanol group had a significantly lower chondrocyte number, as well as fewer actively dividing cells (Ki-67 immuno-positive). The fewer chondrocytes observed in our study is a similar finding to that of Miralles-Flores and Delgado-Baeza (1992) who found that both the proliferative and hypertrophic zone had fewer chondrocytes. The authors of this study attributed this to alteration in mitochondrial function that could affect extracellular matrix synthesis and maturation of the proliferative chondrocytes. They also suggested that calcification in the bottom of the hypertrophic zone is unaffected resulting in a reduced hypertrophic zone height.

However, the information about markers of cell proliferation was not in the scope of their study (Miralles-Flores and Delgado-Baeza, 1992). We found fewer proliferating cells (Ki-67 immuno-positive) together with fewer cells expressing TGFβ1 in the ethanol group. This suggests that alcohol may interfere with TGFβ1 signalling pathway for cell proliferation in the growth plate resulting in fewer dividing cells.

Parameters most affected by prenatal ethanol exposure

Employing a binary logistic regression showed that the distal BV/TV and trabecular number were the main parameters that determined group membership into either ethanol or saline control. This means that these two parameters (distal BV/TV and trabecular number) are affected the most in gestational alcohol exposure. Distal bone parameters varied more between the groups. This may explain why none of the samples was misclassified. It is important to note no proximal trabecular parameters could be singled out as crucial for correct group membership assignment into ethanol or saline. This means that group variations were minimal with respect to the proximal bone parameters.

3.4.1 Conclusion

Gestational alcohol affects the bone internal morphology through inhibiting cell proliferation and disturbing TGFβ1 expression in both extremities of the humerus. Alcohol affected some of the trabecular parameters in the same way in both extremities of the humerus whereas some were affected differently. This is shown by the fewer trabeculae that were widely spaced both in the proximal and distal epiphysis. On the other hand, the bone to total volume ratio (BV/TV) and trabecular thickness (TbTh) was the smallest in the ethanol group only for the proximal region whereas the distal was unaffected. Although this is the case we conclude from our binary logistic regression findings that gestational alcohol exerts its adverse effects on the rat humerus by altering the trabecular number and BV/TV in the distal region.

Chapter 4

Intrauterine alcohol exposure delays growth and disturbs trabecular morphology through inhibiting epiphyseal plate chondrocyte Transforming Growth Factor Beta-1 (TGFβ1) expression in 3-week-old Sprague Dawley rat femur

Table of Contents

4.1 INTRODUCTION 83
4.2 MATERIALS AND METHODS 84
4.2.1 Sample 84
Skeletal harvesting 84
4.2.2 Three-dimensional Micro-focus X-ray Computed Tomography (3D- µCT) 84
4.2.3 Tissue processing for histological and immunohistochemical techniques 86
Immunohistochemistry for Ki-67 and TGFβ1 in the femur epiphyseal growth plate 86
Photography and quantification of chondrocytes 87
4.2.4 Data analysis 87
4.3 RESULTS 89
4.3.1 Osteometry and trabecular morphometry of the femur 3 weeks of age 89
Femoral length 89
Femoral shaft volume 90
Femoral bicondylar breadth 91
Femoral proximal and distal epiphysis volume 92
Femoral bone to total volume ratio (BV/TV) 93
Femoral trabecular thickness (TbTh) 94
Femoral Trabecular number (TbN) 95
Femoral Trabecular spacing (TbSp) 96
4.3.2 Femoral cross-sectional area, cortical area (thickness) and medullary canal area at 3 weeks of age 97
Proximal (25th percentile mark) 97
Midshaft (50th percentile mark) 98
Distal (75th percentile mark) 99
4.3.3 Femoral epiphyseal growth plate histological and immunohistochemical characterization at 3 weeks of age 100
Femoral epiphyseal plate surface area 100
Femoral proliferative zone chondrocyte number 101
Femoral hypertrophic zone chondrocyte number 104
Femoral proliferative zone Ki-67 immuno-positive chondrocytes 105
Femoral hypertrophic zone Ki-67 immuno-positive chondrocytes 107
Femoral proliferative zone TGFβ-1 immuno-positive chondrocytes 109
4.3.4 Femur (3 weeks) trabecular morphometric parameters most affected by gestational ethanol 113

4.4 DISCUSSION.....116
4.4.1 Conclusions.....119

4.1 INTRODUCTION

Features of growth retardation occur in children born to mothers who drink alcohol during pregnancy (Snow and Keiver, 2007; Simpson et al., 2005). This may be attributed to the disruption of growth plate chondrocyte activity, and trabecular architecture (Turner, 2000; Maurel et al., 2011; Mikosch, 2014). The literature on bone postnatal development in prenatal alcohol exposure has received relatively minimal attention (Keiver and Weinberg, 2003; Simpson et al., 2005; Snow and Keiver, 2007). Most of the existing literature is based on *in utero* skeletal investigation of gestational alcohol exposure (Keiver and Weinberg, 2003; Simpson et al., 2005; Snow and Keiver, 2007) and few (Miralles-Flores and Delgado-Baeza, 1992; Ertem et al., 2006) studies on the postnatal effects. However, markers of cell proliferation and apoptosis have not been used to establish the number of proliferating cells in the respective zones. Therefore, this knowledge gap needs further investigation.

Transforming Growth Factor β1 (TGFβ1), the most abundant growth factor found in the osseous tissue (Chen et al., 2012) is involved in embryogenesis and in postnatal life (Kanaan and A Kanaan, 2006). It regulates cell proliferation, differentiation, motility and apoptosis (Wu et al., 2016) and controls the migration of cells to the site of further skeletogenesis in fetal development (Kanaan and A Kanaan, 2006). Driver et al. (2015) established that ethanol is inhibitory to osteopontin mediated TGFβ1 expression. It is not known if this effect persists throughout life or that the effects may be reversed when alcohol is withdrawn.

We sought to determine whether gestational ethanol interrupts trabecular morphology through inhibiting epiphyseal plate chondrocyte TGFβ1 expression. The growth plate and epiphysis were studied in both the proximal and distal aspects as well as osteometric parameters. The study used histological means for assessing general morphology and immunohistochemistry for determination of proliferating cells (Ki-67) and quantification of chondrocytes expressing TGFβ1. The internal architecture was assessed from data obtained through the use of micro focus X ray computed tomography.

4.2 MATERIALS AND METHODS

4.2.1 Sample

Twelve dams treated as in section 2.1.1 were used to obtain 30 pups allocated into the ethanol (n=12), saline-treated (n=12) and untreated controls (n=6). These pups remained with their respective dams till 3 weeks of age.

Skeletal harvesting

The rats were terminated by a lethal pentobarbital intraperitoneal injection. The entire animal was then immediately immersed in 10% buffered formalin after an abdominal incision was made to allow for the penetration of the fixative. To expose the femur, skin incisions were made on the respective limbs and muscles were meticulously teased away. The skeletal samples were then individually immersed and stored in 10% buffered formalin to continue fixation until further processing. The left side bones were used for histological and immunohistochemistry. The bilateral femur was used for 3D- microtomography.

4.2.2 Three-dimensional Micro-focus X-ray Computed Tomography (3D- µCT)

Bilateral 3-week old femora were examined by 3D- µCT. A Nikon XTH 225/320 LC X-ray microtomograph was used for computed tomography scanning. To keep the samples steady during scanning, the bones were placed in plastic tubes and mounted in low density Styrofoam, while allowing the X-rays to get to the sample with negligible absorption. The plastic container with the sample inside was then positioned on a rotating manipulator in the scanning chamber for the scanning. The scanning parameters used as in section 3.2.2

Parts of the femora and trabecular morphometry parameters studied

Following reconstruction, VG studio Max ®3.2 was used for data analysis as previously described (Bouxsein et al., 2010). The VG studio software built in calliper was used to determine the femoral osteometric parameters. The full bone length and bicondylar length and bicondylar breadth were measured from the femur (Fig. 4.1 and Table 4.1). The trabecular morphometric parameters were studied in the proximal and distal epiphysis of the bone. The following parameters were determined the trabecular number, thickness,

spaces and volume (see table 3.3 in section 3.2.2). A cross-sectional slice from each percentile mark was then saved for further analysis on Fiji image J. From these slices, the cross-sectional area, cortical area and medullary canal area of the shaft were measured at 3 positions; 25th (proximal), 50th (midshaft) and 75th (distal) percentile marks (Fig. 4.1 and Table 4.1).

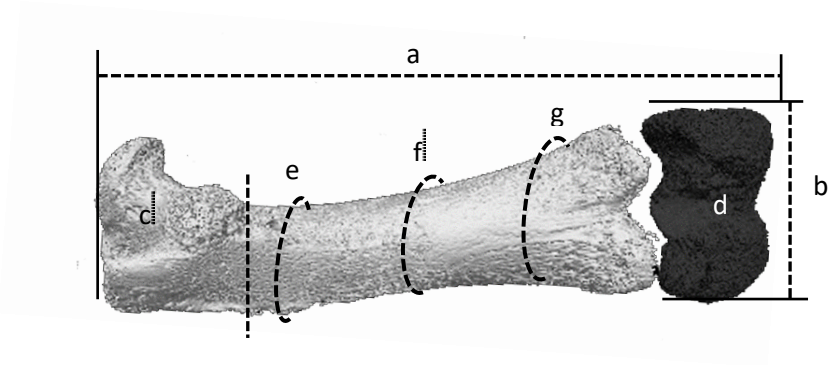


Figure 4.1: Three-dimensional reconstruction of a 12-week old femur showing the parts that were investigated. (a), full femur length; (b), bicondylar breadth; (c) and (d), proximal and distal epiphysis. (e), (f), (g), 25th (proximal); 50th (midshaft) and 75th (distal) percentile marks, respectively; (Image courtesy of R. Ndou and D Pillay).

Table 4.1: Osteometric parameter descriptions

Parameter	Description
Full femur length	The maximum length measured between the top of the greater trochanter and the bottom of the farthest condyle
Bicondylar breadth	the distance between the medial most and lateral most points on the epicondyles
Proximal epiphysis	The part of the bone above the proximal epiphyseal growth plate
Distal epiphysis	The part of the bone below the distal epiphyseal growth plate

Cross-sectional area	the area of a slice taken from the outer margins encompassing the shaft at the 25th, 50th and 75th percentile marks
Medullary cavity area	the area of a slice taken from the outer margins encompassing the medullary canal at the 25th, 50th and 75th percentile marks
Cortical thickness	the difference between the cross-sectional area and the medullary cavity area at the shaft 25th, 50th and 75th percentile marks.

4.2.3 Tissue processing for histological and immunohistochemical techniques

Bone samples were removed and fixed in 10% buffered formalin for a minimum of 14 days. They were then decalcified in 14% w/v ethylenediaminetetraacetic acid (EDTA, pH 7.4) for 10 days in an incubator with regular gentle shaking at 45˚C. The bones were then rinsed and divided into proximal and distal samples and immersed in 10% buffered formalin for 24 hours. An automatic processor (Citadel 2000, Thermo Fischer Scientific) was then used to take the samples through ascending grades of ethanol prior to embedding in paraffin wax. When embedding, care was taken to ensure that the bone samples were orientated longitudinally to minimise differences in the sectioning angle. Bone sections were cut at 5µm thickness using a microtome (Leica RM2125 RTS, Leica Biosystems, USA) and placed on silane-coated glass slides. Sections in a sequence of 1 in 3 were stained with Haematoxylin and Eosin (H&E) to assess epiphyseal growth plate morphology and chondrocytes or immunolocalization of the Ki-67 protein (cell proliferation maker) or Transforming Growth Factor Beta 1 (TGFβ1) (See Appendix).

Immunohistochemistry for Ki-67 and TGFβ1 in the femur epiphyseal growth plate

Immunolocalization of epiphyseal growth plate chondrocytes expressing the Ki-67 protein and TGFβ1 was performed using an anti-Ki-67 antibody (ab66155) or anti-TGFβ1 antibody (ab215715). Both antibodies were sourced from Abcam. In summary, sections were deparaffinized, rehydrated and subsequently, immersed with citrate buffer solution (pH=6) kept in a water bath set at a temperature of 60^0C overnight. The next morning, tissue sections were allowed to cool to room temperature for 20 minutes and then washed in phosphate buffer solution (PBS) (pH=7.4) for 5 minutes. Endogenous peroxidase was blocked with 1% hydrogen peroxide (H_2O_2), washed with PBS for 3 x 5 minutes, incubated

with normal goat serum for 10 minutes, incubated with primary antibody (anti-Ki-67 in 1:1200 or TGFB1 in 1:250 dilution factor) overnight at 4^0C. On the 3rd third day, sections were allowed to reach room temperature, washed in PBS for 3 x 5 minutes. A biotinylated secondary antibody (Biotinylated Goat Anti-Rabbit IgG (H+L) (ab64256) was applied for 10 minutes and then washed in PBS for 3 x 5 minutes. To reduce nonspecific staining background while enhancing antibody binding, sections were incubated with streptavidin HRP for 10 minutes (ab64269) and washed in PBS for 3 x 5 minutes. For visualisation under a light microscope, sections were then incubated with 3-3' di-aminobenzidine (DAB) working solution for 5 minutes, rinsed in running tap water for 5 minutes. Finally, the sections were dehydrated through alcohol grades, cleared in xylene and eventually mounted in entellen(See Appendix).

Photography and quantification of chondrocytes

A light microscope (Zeiss Axioscope 2 plus) fitted with an axiocam HRC digital camera was used to take photomicrographs of the stained slides. These were taken under ×10 magnification. Photomicrographs were imported into Fiji Image-J software and the parameters measured were delineated based on cell morphology. The proliferative zone was delineated by the first flattened chondrocyte on the epiphyseal end and the first hypertrophic chondrocyte on the metaphyseal side. The hypertrophic zone was delineated by the first hypertrophic chondrocyte from the epiphyseal side and by the last transverse septum on the metaphyseal side.

The built image J tool for estimation of area was used to estimate the area of the respective epiphyseal growth plate zones. For quantification of chondrocytes, the manual counting method from the images was employed (See Appendix).

4.2.4 Data analysis

The data were managed in Microsoft Excel 2016 (Microsoft Corporation) and analysed using SPSS® version 25 (IBM®). ANOVA with LSD post-hoc was used for multiple group comparisons of means. Statistical analyses were performed with SPSS® version 25 (IBM®).

Binary logistic regression was used to predict group membership into either the ethanol or saline control group. Significance level was set at $p < 0.05$.

4.3 RESULTS

4.3.1 Osteometry and trabecular morphometry of the femur 3 weeks of age

Femoral length

All three groups in the study exhibited mean differences in femoral bone length. The ethanol group had the shortest femora (mean =1 5.65mm ±0.84) compared to the saline (mean = 16.01mm ±0.74) and untreated controls (mean = 17.16 ±0.85) (Fig. 4.2). However, femora belonging to the ethanol group were only significantly shorter when compared to the untreated controls but not the saline group ($p<0.001$ and $p=0.140$, respectively). The saline controls were also significantly shorter than the untreated group ($p<0.001$).



Figure 4.2: Femur length at 3 weeks of age. The mean values for the bone length are given for the untreated, saline controls and the ethanol group. Error bars indicate standard deviation.

Femoral shaft volume

The phenomenon of lowest values in the ethanol group was also observed regarding shaft volume as it was lowest in the ethanol group (mean = 36.62mm ±6.30). It was significantly lower than the saline (mean = 44.29mm ±6.90 control) and untreated controls (mean = 46.90 ±6.28) ($p<0.001$ for ethanol compared to both controls). No significant differences were detected between the control groups ($p=0.286$) (Fig. 4.3).

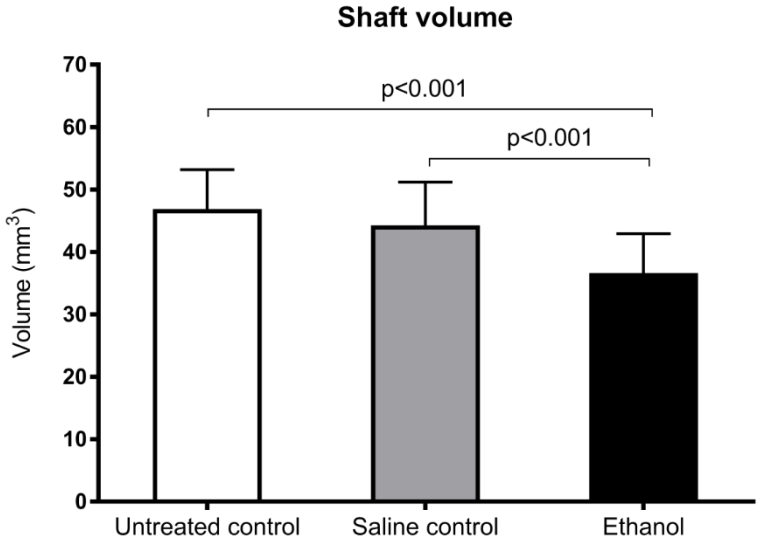


Figure 4.3: Femoral shaft volume at 3 weeks of age. The mean values for the shaft volume are given for the untreated, saline controls and the ethanol group. Error bars indicate standard deviation.

Femoral bicondylar breadth

The mediolateral dimension varied between the groups investigated with the ethanol group (mean = 3.88mm ±0.68) showing a significantly lower bicondylar breadth in comparison to both the controls (saline; mean = 4.34mm ±0.41 and untreated mean = 4.45 ±0.42) (p=0.006 for both comparisons). No significant differences were detected between the control groups (p=0.59) (Fig 4.4).

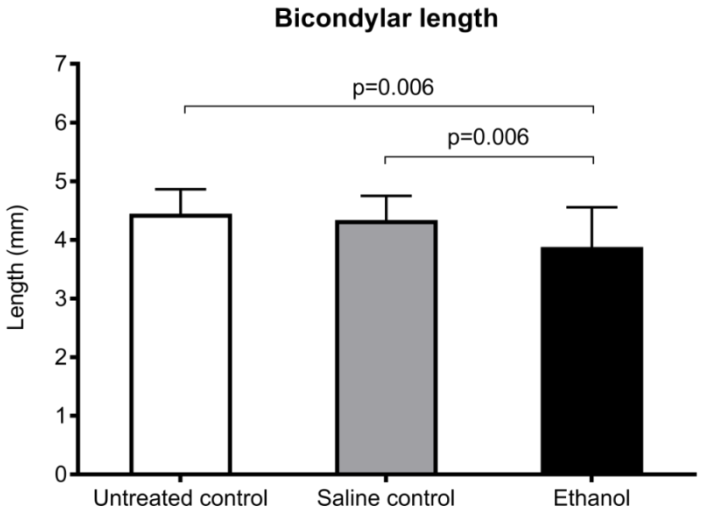


Figure 4.4: Femoral bicondylar length at 3 weeks of age. The mean values for the bicondylar length are given for the untreated, saline controls and the ethanol group. Error bars indicate standard deviation.

Femoral proximal and distal epiphysis volume

The size of the epiphysis showed regional similarities in the proximal and distal epiphysis among the study groupings. The proximal epiphysis had a marginally larger volume in the untreated controls (mean = 20.75mm^3 ±1.24) compared to the saline (mean = 18.73mm^3 ±3.39) and in the ethanol group (mean = 18.66mm^3 ±2.86). However, no significance was observed among the three groups (p=0.113). In the distal epiphysis, a greater volume in the untreated controls (mean = 23.75mm^3 ±3.06) compared to the saline (mean = 20.57mm^3 ±3.91) and ethanol group (mean = 19.83mm^3 ±2.90) was found (p=0.013 and p=0.002, respectively) (Fig. 4.5).

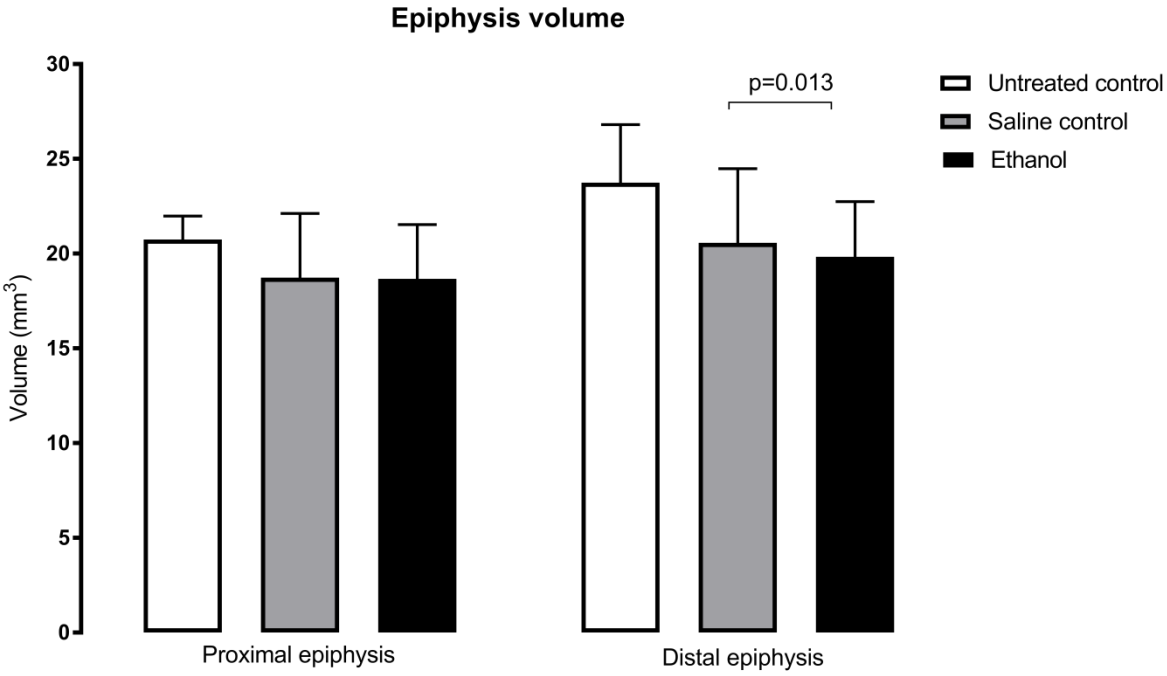


Figure 4.5: Femoral epiphysis volume at 3 weeks of age. The mean values are given for the proximal and distal epiphysis in the untreated, saline controls and the ethanol group. Error bars indicate standard deviation.

Femoral bone to total volume ratio (BV/TV)

Regarding the proximal region, BV/TV was highest in the untreated controls (mean = 69.75% ±4.91) compared to the saline controls (mean = 67.18% ±11.33) and the ethanol group (mean = 62.02% ±10.65) (Fig. 4.6). This difference was significant for the ethanol and untreated controls (p=0.041), with controls showing no significant differences (p=0.195). In distal region, the saline (mean = 69.78% ±11.95) and untreated controls (mean = 57.43 % ±3.27) had more BV/TV than the ethanol group (mean = 52.53% ±12.30) (p=0.004 and p<0.001, respectively) (Fig. 4.6).

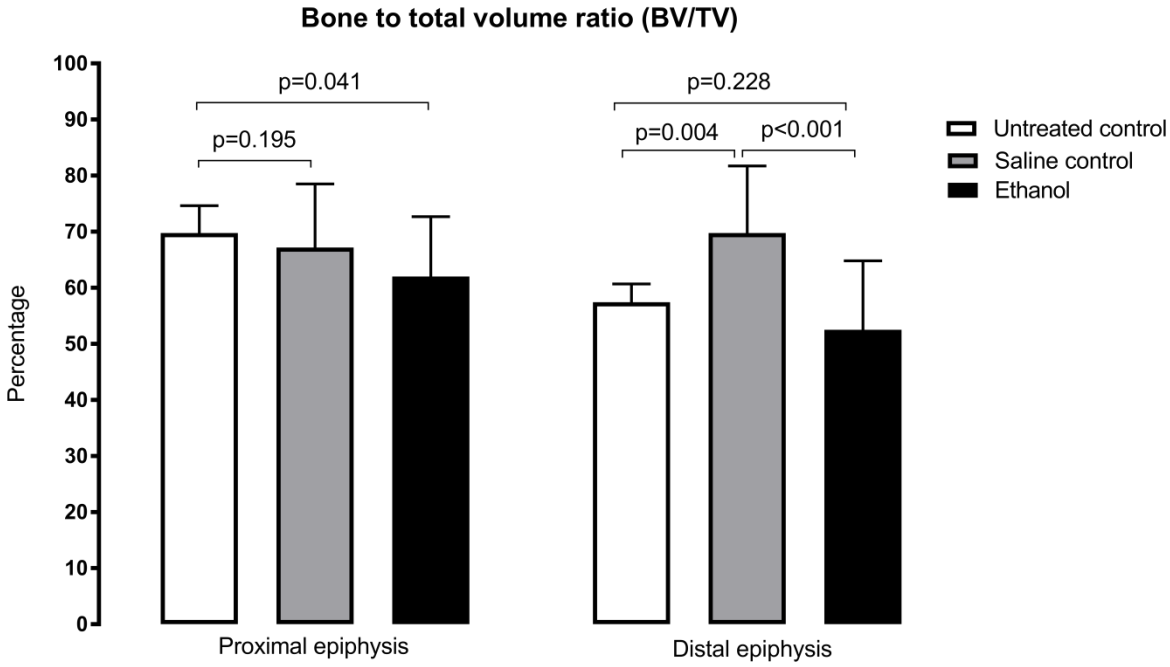


Figure 4.6: Femoral bone to total volume ratio (BV/TV) at 3 weeks of age. The mean values are given for the proximal and distal epiphysis in the untreated, saline controls and the ethanol group. Error bars indicate standard deviation.

Femoral trabecular thickness (TbTh)

Regional differences were observed in the trabecular thickness among the three groups. In the proximal region, all three groups had similarities in trabecular thickness (ethanol group; mean = 0.11mm ±0.05, saline controls; mean = 0.13mm ±0.07 and untreated controls; mean = 0.11mm ±0.03) (p=0.313) (Fig. 4.7). Conversely, the distal region revealed that the ethanol group (mean = 0.08mm ±0.04) had thinner trabeculae (TbTh) than the saline controls (mean = 0.15mm ±0.07) although similar to the untreated controls (mean=0.08mm ±0.02) (p< 0.001 for ethanol and saline controls) (Fig. 4.7).

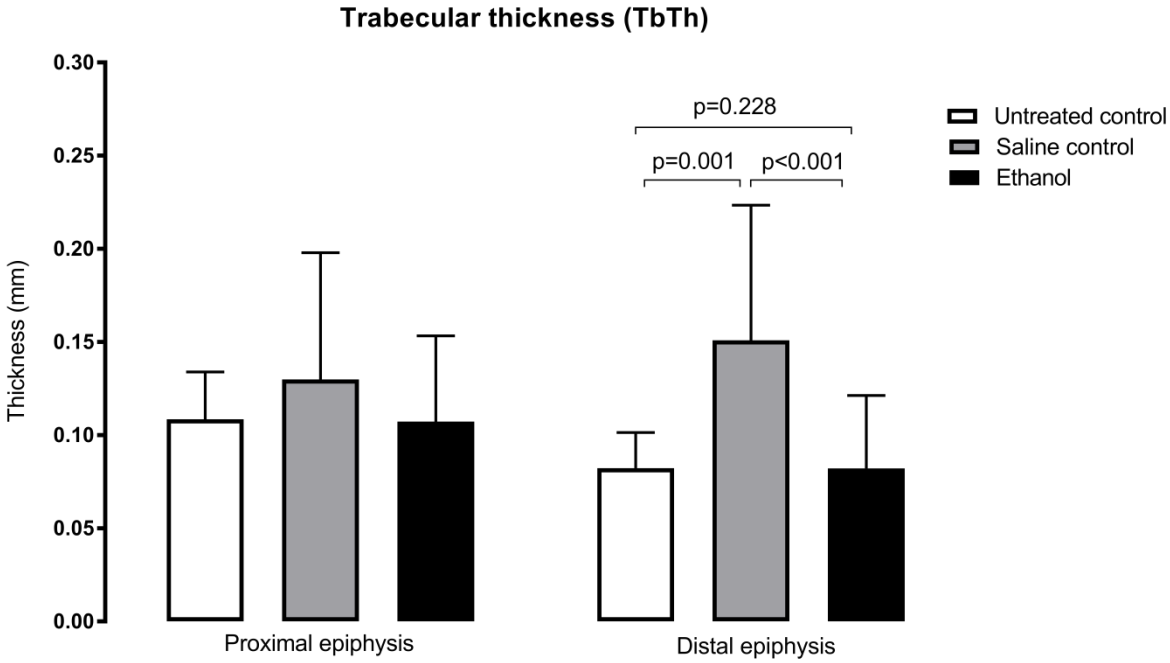


Figure 4.7: Femoral trabecular thickness (TbTh) at 3 weeks of age. The mean values are given for the proximal and distal epiphysis in the untreated, saline controls and the ethanol group. Error bars indicate standard deviation.

Femoral Trabecular number (TbN)

Trabecular distribution by study group showed a varied pattern when stratified by epiphyseal region. The number of trabecular (TbN) in the proximal region was greatest in untreated controls (mean = 6.26 mm^{-1} ± 1.00) followed by the saline (mean = 5.76 mm^{-1} ±1.24) and the ethanol group (mean = 5.10mm^{-1} ±1.22) (Fig. 4.8). However, these differences were only significant between the ethanol and untreated controls (p=0.009).

In the distal region, the untreated controls (mean = 7.41 mm^{-1} ±1.17) had more trabeculae than the saline (mean = 5.50 mm^{-1} ±1.21) and ethanol groups (mean = 6.38 mm^{-1} ±1.68) (p=0.001 and p=0.05, respectively) (Fig. 4.8).

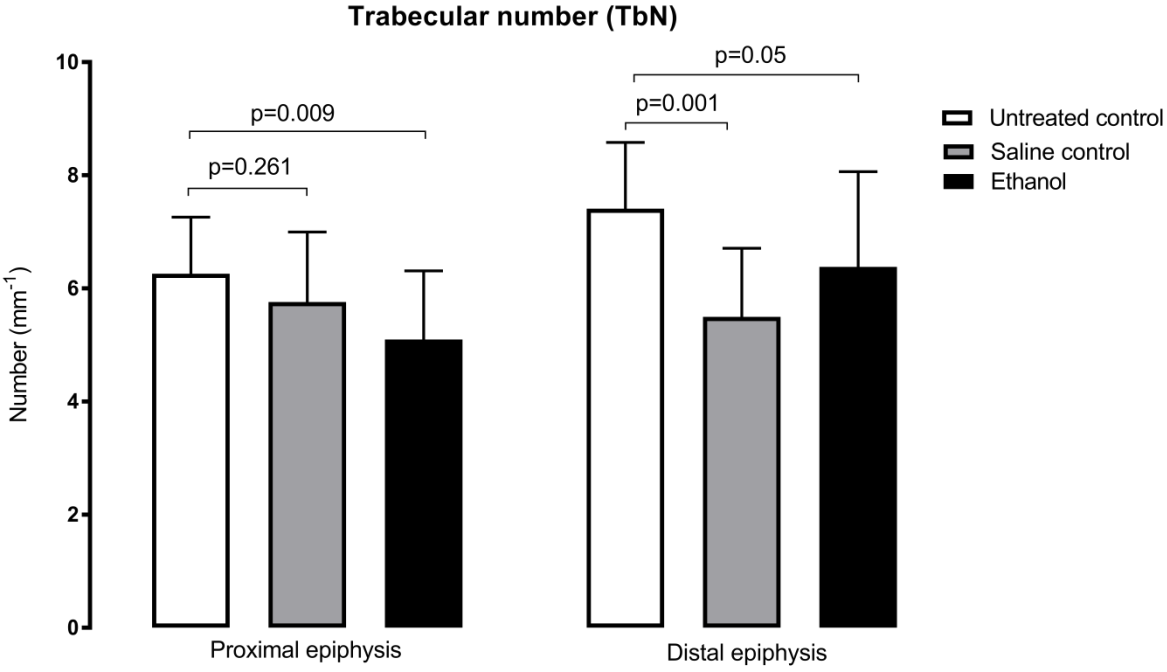


Figure 4.8: Femoral trabecular number (TbN) at 3 weeks of age. The mean values are given for the proximal and distal epiphysis in the untreated, saline controls and the ethanol group. Error bars indicate standard deviation.

Femoral Trabecular spacing (TbSp)

Unlike the other trabecular morphometric parameters, trabeculae spacing (TbSp) showed similarities among the groups in both the proximal and distal epiphyseal regions. In the proximal region, the saline and untreated groups had a mean of 0.056mm (±0.01) whereas the ethanol group (mean = 0.06mm ±0.012) had marginally wider trabeculae spacings (p=0.160 among the three groups) (Fig. 4.9). In the distal region, all three groups had identical mean trabeculae spacing (TbSp) (untreated and saline control mean = 0.06mm ±0.007), although the ethanol group had a different standard deviation despite equal means (ethanol; mean = 0.06 ±0.009) (p=0.97 among the three groups) (Fig. 4.9).

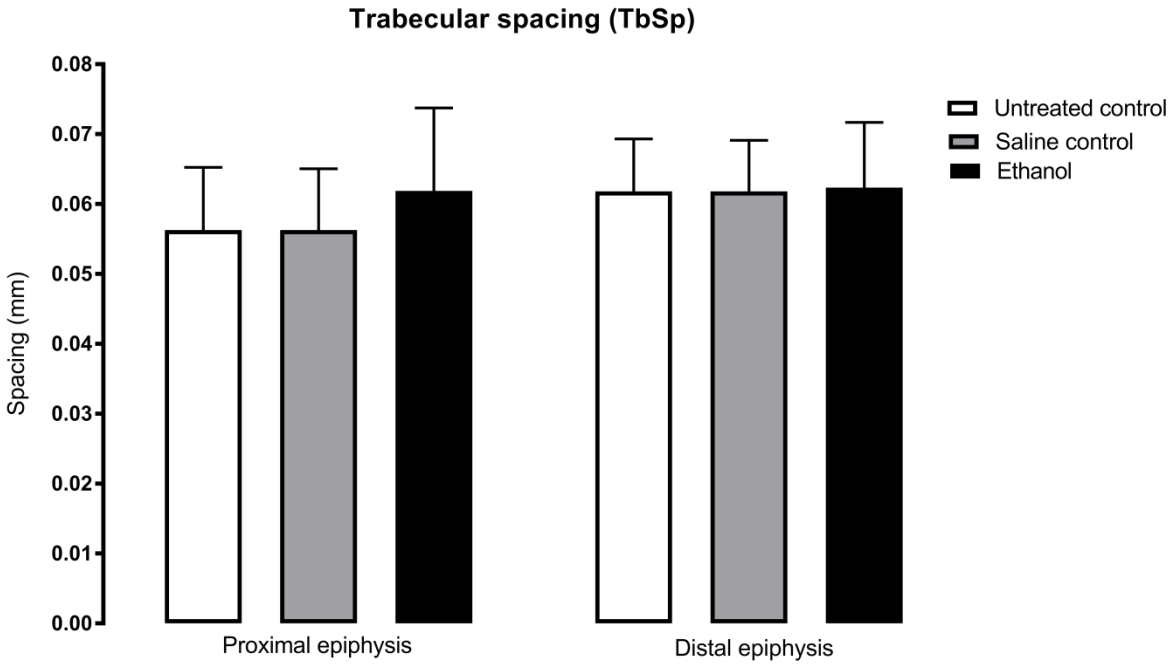


Figure 4.9: Femoral trabecular spacing (TbSp) at 3 weeks of age. The mean values are given for the proximal and distal epiphysis in the untreated, saline controls and the ethanol group. Error bars indicate standard deviation.

4.3.2 Femoral cross-sectional area, cortical area (thickness) and medullary canal area at 3 weeks of age

Proximal (25th percentile mark)

The proximal cross-sectional areas were similar in all three groups (ethanol group; mean = 4.52mm^2 ±0.89, saline controls; mean = 4.68mm^2 ±0.89 and untreated controls; mean = 4.62mm^2± 0.72) (p=0.822) (Fig. 4.10). Also, the medullary canal area was similar in all three groups as the ethanol group had a mean of 2.21mm^2 (±0.52) and the saline controls had a mean of 2.21mm^2 (±0.40) and untreated controls had a mean of 2.14 mm^2 (±0.68) (p=0.913) (Fig. 4.10). With respect to cortical area (thickness) in this region, the ethanol group (mean = 2.31mm^2 ±1.07) exhibited a marginally lower value compared to the saline (mean = 2.47mm^2 ±0.96) and the untreated controls (mean = 2.48mm^2 ±0.54). No significance was detected among the three groups (p=0.812) (Fig. 4.10).

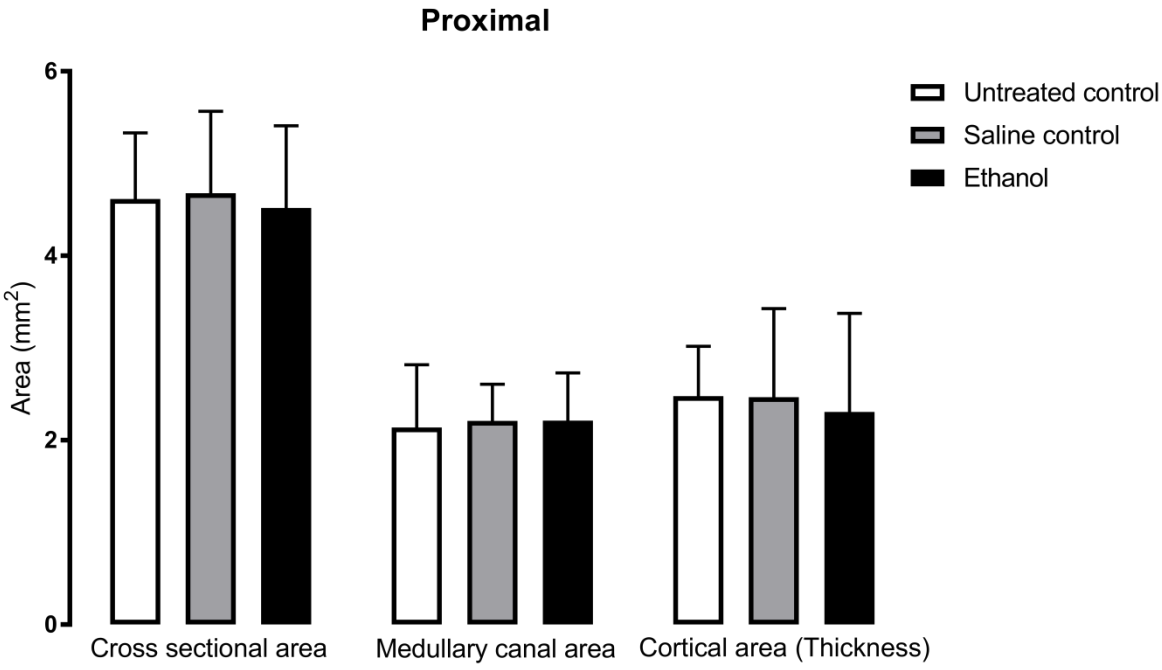


Figure 4.10: Proximal (25th percentile mark) dimensions of the femur at 3 weeks of age. The mean cross-sectional area, medullary canal area and cortical thickness are given for the three groups studied. Error bars represent standard deviation.

Midshaft (50th percentile mark)

The midshaft cross-sectional area was similar in all three groups studied with the untreated groups having a mean of 4.69mm^2 (±0.82), saline mean = 4.66mm^2 (±0.92) and the ethanol with 4.58mm^2 (±0.68) (p=0.923) (Fig. 4.11). The medullary canal area was the same in the controls (untreated and saline; mean of 2.34 mm^2 ±0.42 and 2.34mm^2 ±0.43, respectively). The ethanol group (mean = 2.81 ±0.74) had the largest medullary canal area with significant differences detected when compared to the untreated and saline controls (p=0.031 and p=0.008, respectively) (Fig. 4.11). Regarding cortical area (thickness) in this region, the untreated (mean = 2.35mm^2 ±1.00) and saline controls (mean=2.32mm^2 ±1.03) had similar values. The ethanol group (mean=1.78mm^2 ±0.69) exhibited lower values compared to untreated and saline controls. However, significance was only detected between the ethanol and saline controls (p=0.044) (Fig. 4.11).

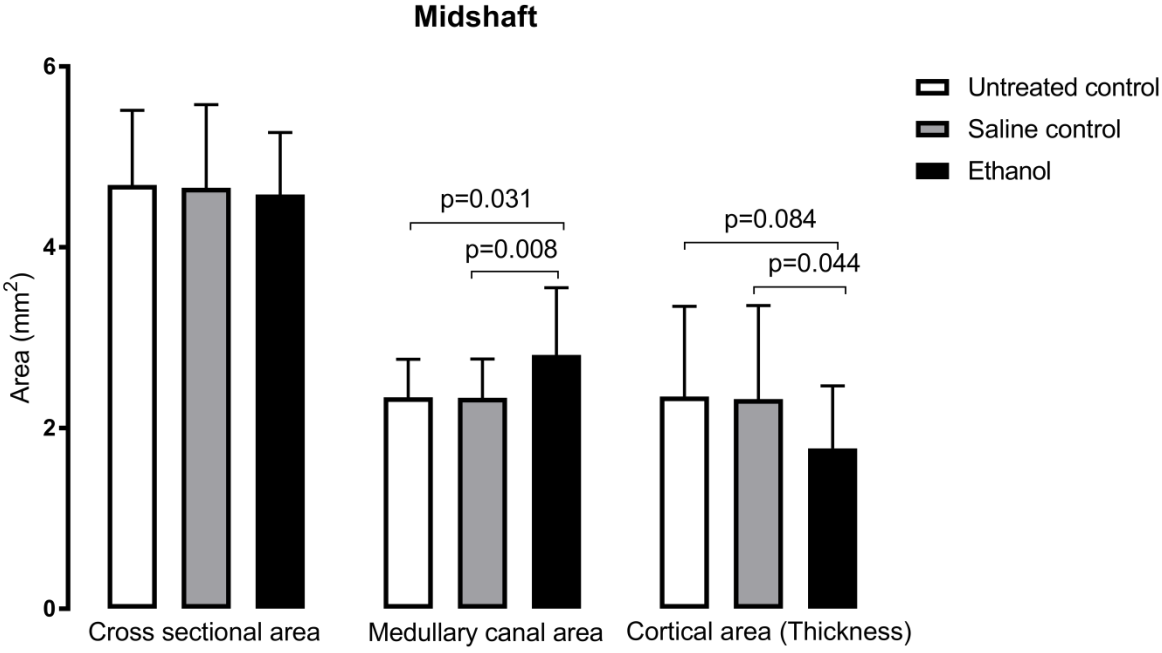


Figure 4.11: Midshaft (50th percentile mark) dimensions of the femur at 3 weeks of age. The mean cross-sectional area, medullary canal area and cortical thickness are given for the three groups studied. Error bars represent standard deviation.

Distal (75th percentile mark)

The distal cross-sectional area was marginally smaller in the ethanol group (mean = 5.52 mm^2 ±0.97) compared to the saline and untreated controls (mean = 5.90mm^2 ±0.97 and 5.96mm^2 ±0.62, respectively). However, no significant differences were observed among the three groups (p=0.26) (Fig. 4.12). The medullary canal area was marginally smaller in the ethanol group (mean = 3.89 mm^2 ±0.71) compared to the saline and untreated controls (mean = 3.93mm^2 ±0.62 and 3.98mm^2 ±0.93, respectively). No significant differences were observed among the three groups (p=0.95) (Fig. 4.12). With respect to cortical area (thickness) in this region, the ethanol group (mean = 1.62 mm^2 ±0.45) exhibited a marginally lower value compared to the saline controls (mean = 1.96 mm^2 ±0.90) and the untreated controls (mean = 1.98mm^2 ±0.60) although no significant differences were detected among the three groups p=0.19) (Fig. 4.12).

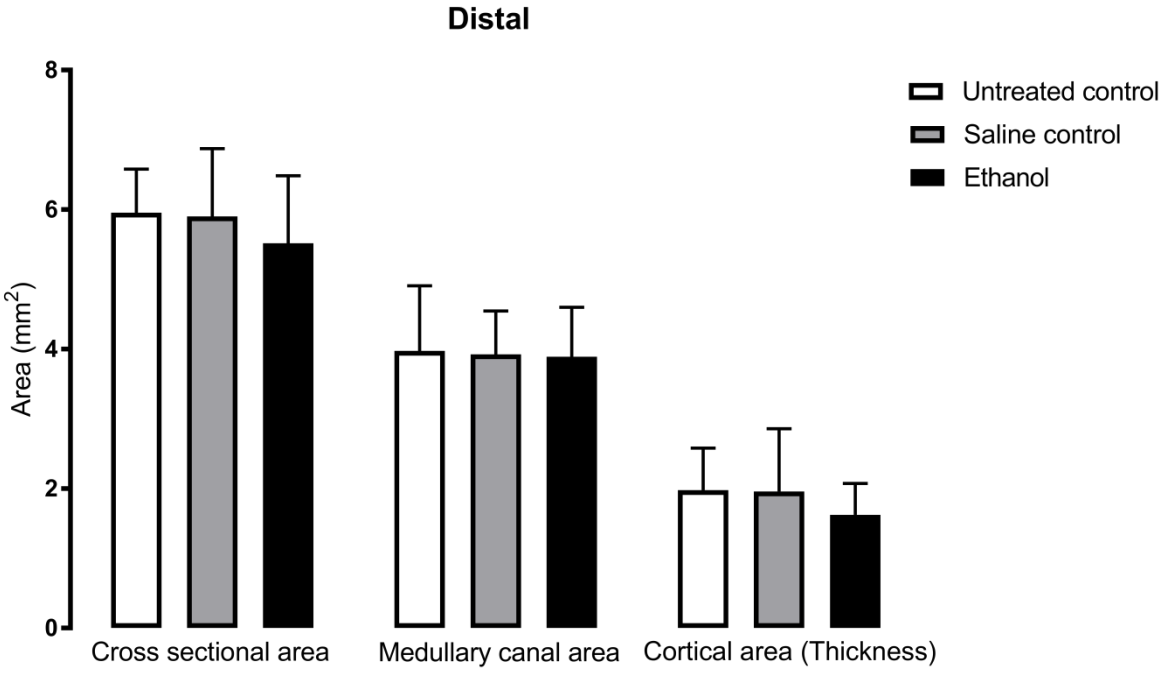


Figure 4.12: Distal (75th percentile mark) dimensions of the femur at 3 weeks of age. The mean cross-sectional area, medullary canal area and cortical thickness are given for the three groups studied. Error bars represent standard deviation.

4.3.3 Femoral epiphyseal growth plate histological and immunohistochemical characterization at 3 weeks

Femoral epiphyseal plate surface area

The two epiphyseal ends showed a partly similar group comparison in that the untreated controls had the greatest surface area, followed by the saline and ethanol group in both the proximal and distal epiphysis**.** In the proximal region, the epiphyseal plate surface area was significantly greater for the untreated (mean = 0.70mm^2 ±0.09) and saline controls (mean = 0.64mm^2 ±0.11) compared to the ethanol group (mean = 0.54mm^2 ±0.02) (p=0.007 and p=0.05, respectively). No significant differences were detected for the controls (p=0.270) (Fig. 4.13). In the distal aspect, the epiphyseal plate surface area was significantly greater for the untreated (mean = 1.00mm^2 ±0.04) and saline controls (mean = 0.93 ±0.04) compared to the ethanol group (mean = 0.88mm^2 ±0.03) which had the least surface area (p<0.001 and p=0.019, respectively). Between the controls, the untreated group displayed a significantly greater surface area than saline controls (p=0.006). (Fig. 4.13).

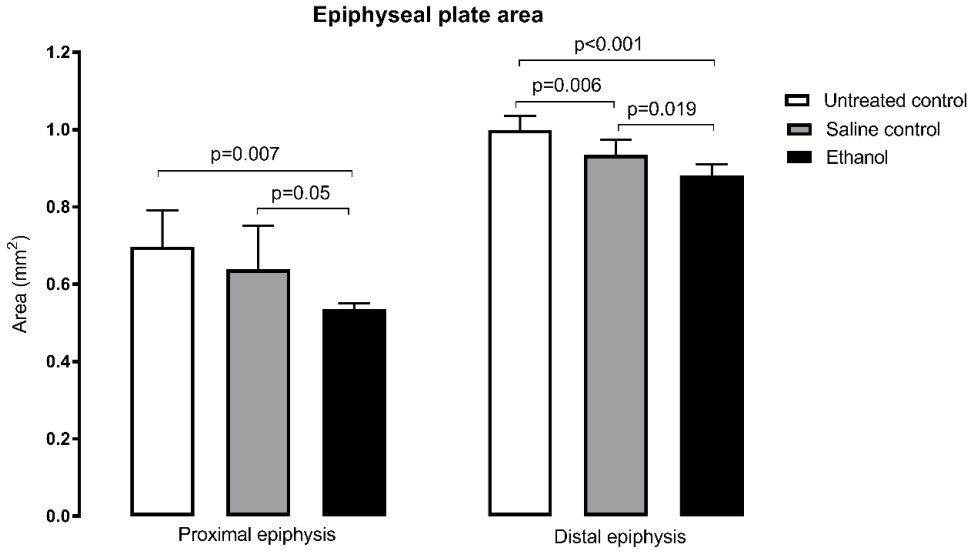


Figure 4.13: Histomorphometry of the epiphyseal growth plate surface area in the femur at 3 weeks of age. The mean values for the epiphyseal growth plate surface area are given for the untreated, saline controls and the ethanol group. Error bars represent standard deviation.

Cellular morphology of the femur epiphyseal growth plate

The proximal and distal region of the proliferative zone showed a similar group comparison where the untreated group had more chondrocytes which were tightly packed in prominent rows than the saline controls and ethanol group (Fig. 4.14). The saline controls the chondrocytes were evenly distributed with a few gaps, while in the ethanol group the chondrocyctes were loosely packed, with areas with huge gaps (Fig. 4.14). This pattern continued in the distal region (Fig. 4.14).

The two epiphyseal ends showed a partly similar group comparison with respect to the hypertrophic zone. The untreated group showed gradual cellular enlargment, the chondrocyctes and the lacunae increasing in size, with no empty lacunae. However, in the saline controls, we observed the pyknotic chondroblasts had a few empty lacunae that presented with diffuse distribution. The ethanol group had a large number of empty lacunae that presented with diffuse distribution (Fig. 4.14).

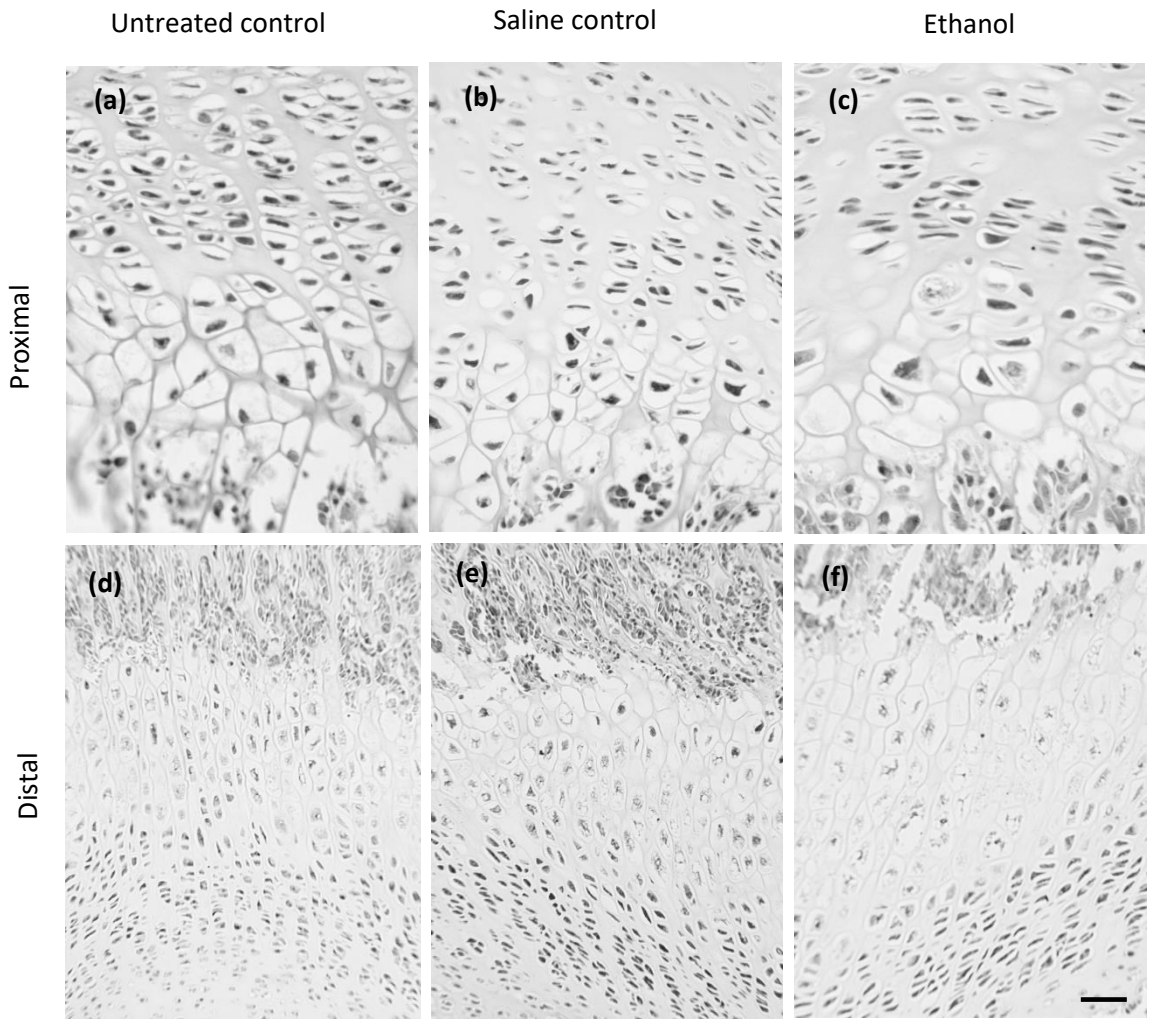


Figure 4.14: Prepresantative photomicrographs of Haematoxylin and Eosin stained epiphyseal growth plate of the femur sections. Photomicrographs of the proximal and distal epiphyseal growth plate for the three groups studied are shown. Scale bar = 20 microns and applies to all images.

Femoral proliferative zone chondrocyte number

Regional similarities were observed in that the untreated group had the most chondrocytes, closely followed by the saline and ethanol groups in both epiphyseal growth plates. In the proximal region, the epiphyseal growth plate had more chondrocytes in the untreated and saline controls (mean = 1212.80 ±49.39 and 1149.67 ±67.35, respectively) compared to the ethanol group (mean = 1012.58 ±73.86) which had fewer chondrocytes. These cells were significantly fewer between the ethanol and the untreated and saline group ($p<0.001$ and $p=0.003$, respectively) (Fig. 4.15). No significant differences were detected between the control groups ($p=0.133$). In the distal epiphysis proliferative zone of the growth plate, the untreated (mean = 1793.83 ±62.09) and saline controls (mean = 1730.58 ±30.24) exhibited more chondrocytes than the ethanol group (mean = 1632.92 ±63.83) ($p<0.001$ and $p=0.007$, respectively). Similar, to the proximal region, no significant differences were detected between the control groups ($p=0.062$) (Fig. 4.15).

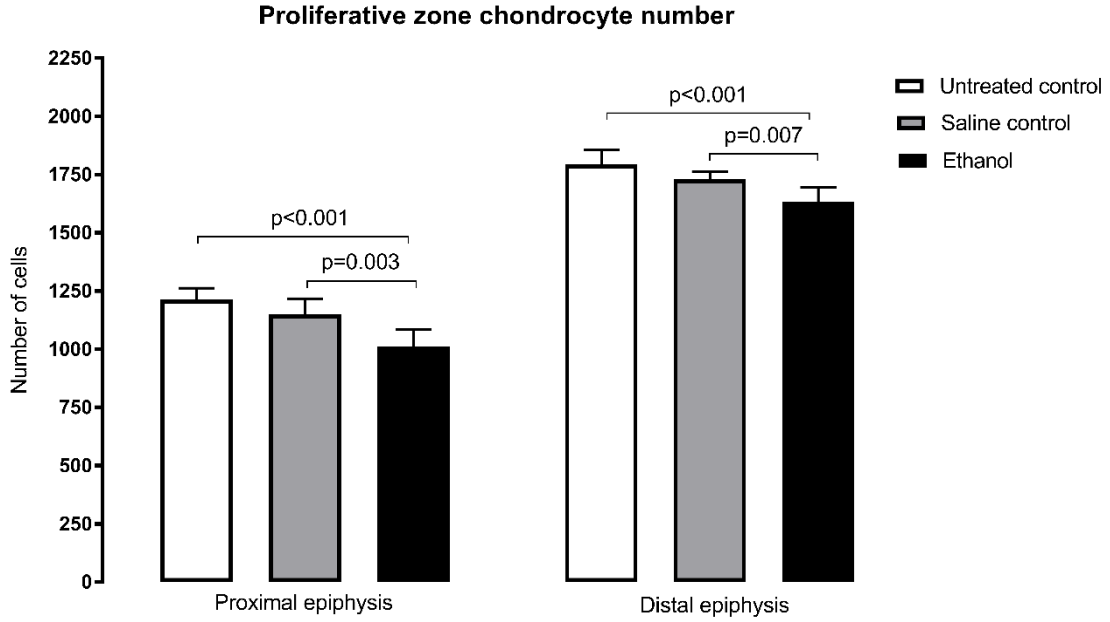


Figure 4.15: Epiphyseal growth plate proliferative zone number of chondrocytes in the femur. The mean values are shown for the proliferative zone in the proximal and distal epiphyseal growth plate given for the untreated, saline controls and the ethanol group. Error bars represent standard deviation.

Femoral hypertrophic zone chondrocyte number

In the proximal epiphysis hypertrophic zone, the saline control group (mean = 966.25 ±79.18 had the least number of chondrocytes. These cells were significantly fewer compared to the ethanol (mean = 1046.33 ±25.72) and untreated group (mean = 1104.60 ±19.81) (p=0.016; p=0.001, respectively) (Fig. 4.16). In contrast, a similar number of chondrocytes were recorded for the ethanol and untreated group (p=0.079). In the distal epiphysis hypertrophic zone, a similar cell quantity in the ethanol and saline groups was recorded (mean = 1650.167 ±42.85 and 1665.67 ±35.67, respectively). The number of chondrocytes in these groups was significantly lower than the untreated controls (mean=1788.58 ±32.51) (p<0.001 for both comparisons) (Fig. 4.16).

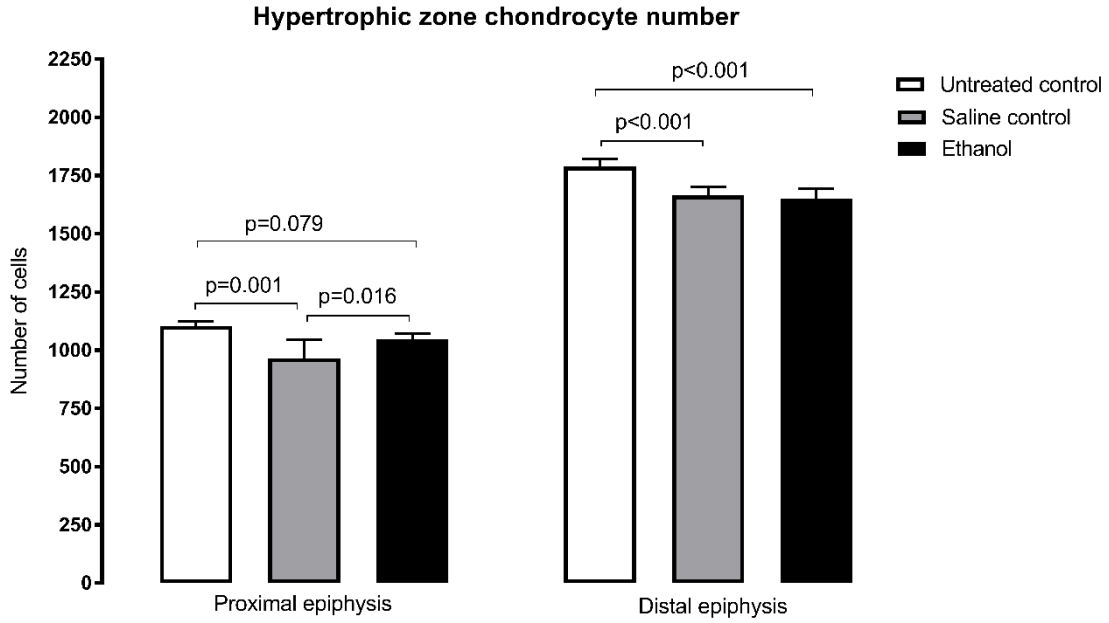


Figure 4.16: Epiphyseal growth plate hypertrophic zone number of chondrocytes in the femur. The mean values are shown for the hypertrophic zone in the proximal and distal epiphyseal growth plate given for the untreated, saline controls and the ethanol group. Error bars represent standard deviation

Femoral proliferative zone Ki-67 immuno-positive chondrocytes

Group comparisons in the proximal and distal epiphyses were similar in that the untreated controls had the most chondrocytes in both epiphyseal plate proliferative zones. In the proximal epiphyseal plate proliferative zone, fewer Ki-67 labelled cells were found in the ethanol group (mean = 841.44 ±30.76) than the saline controls (mean = 959.39 ±19.82) and untreated group (mean = 1001.75 ±57.71) ($p<0.001$ both comparisons to the ethanol group). Although the saline controls appeared to have fewer Ki-67 immuno-positive cells than the untreated group, these differences were not significant ($p=0.090$) (Fig. 4.17 and Fig. 4.18). In the distal region, fewer Ki-67 positive cells were found in the ethanol group (mean = 923.00 ±16.21) compared to the saline controls (mean = 942.75 ±67.63) and untreated group (mean=1014.75 ±39.70). However, significance was only detected between the ethanol and untreated group in this comparison ($p=0.004$). When comparing the controls, the saline group had significantly fewer cells recorded ($p=0.017$) in this region. (Fig. 4.17 and Fig. 4.18).

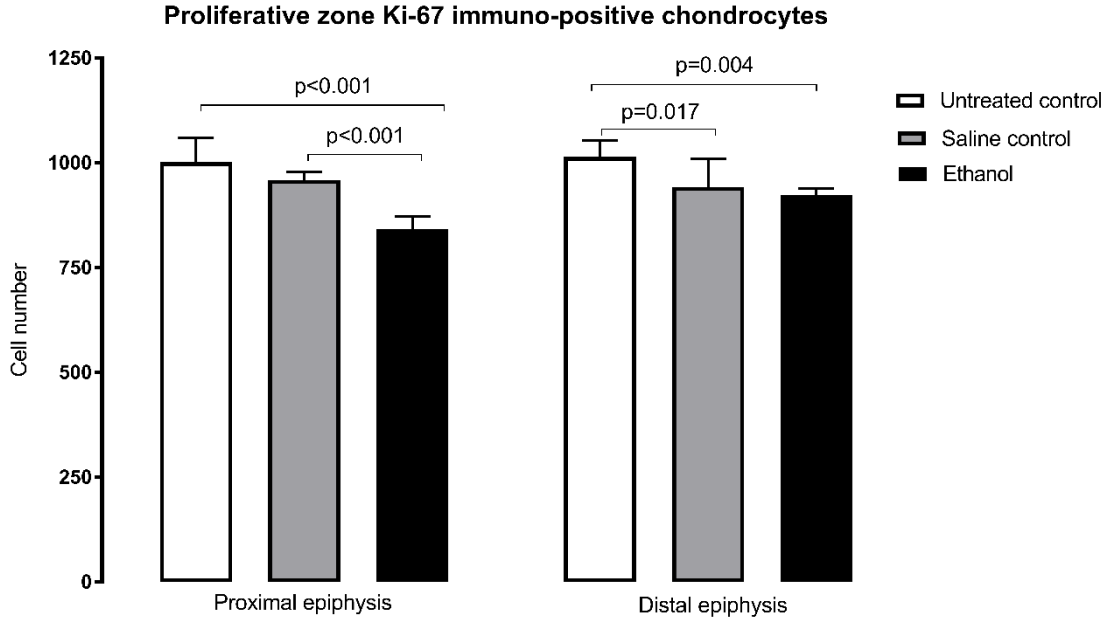


Figure 4.17: Ki-67 immuno-positive proliferative chondrocytes of the femur. The mean number of Ki-67 immuno-positive proliferative chondrocytes are shown for the proliferative zone in the proximal and distal epiphyseal growth plate for the three groups studied. Error bars represent standard deviation.

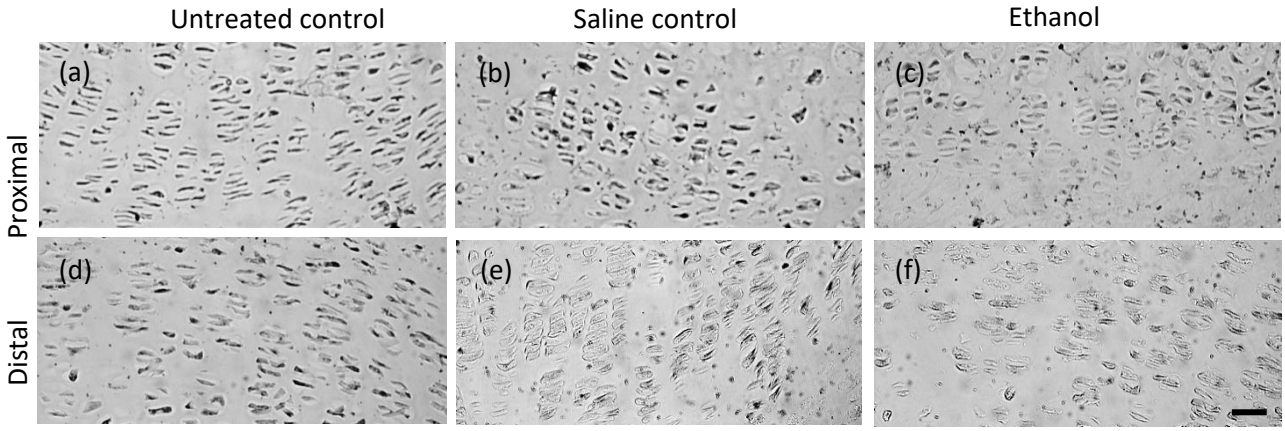


Figure 4.18: Photomicrograph of femur proliferative zone chondrocytes immunolabeled with the anti-Ki-67 antibody. Representative micrographs of the proximal and distal epiphyseal growth plate for the three groups studied. Scale bar = 20 microns and applies to all images.

Femoral hypertrophic zone Ki-67 immuno-positive chondrocytes

In the proximal epiphyseal plate hypertrophic zone, the saline controls (mean = 909.58 ±50.92) exhibited more Ki-67 labelled cells than the ethanol group (mean = 815.75 ±40.95) and untreated controls (mean = 788.33 ±26.03) ($p=0.002$ and $p<0.001$, respectively). The ethanol group and untreated controls were not significantly different ($p=0.335$). In the distal region, marginally fewer Ki-67 labelled cells were recorded for the ethanol group (mean = 863.67 ±46.61) than the saline controls (mean = 892.41 ±55.48) and untreated group (mean = 901.75 ±13.04)(Fig. 4.19 and Figure 4.20).

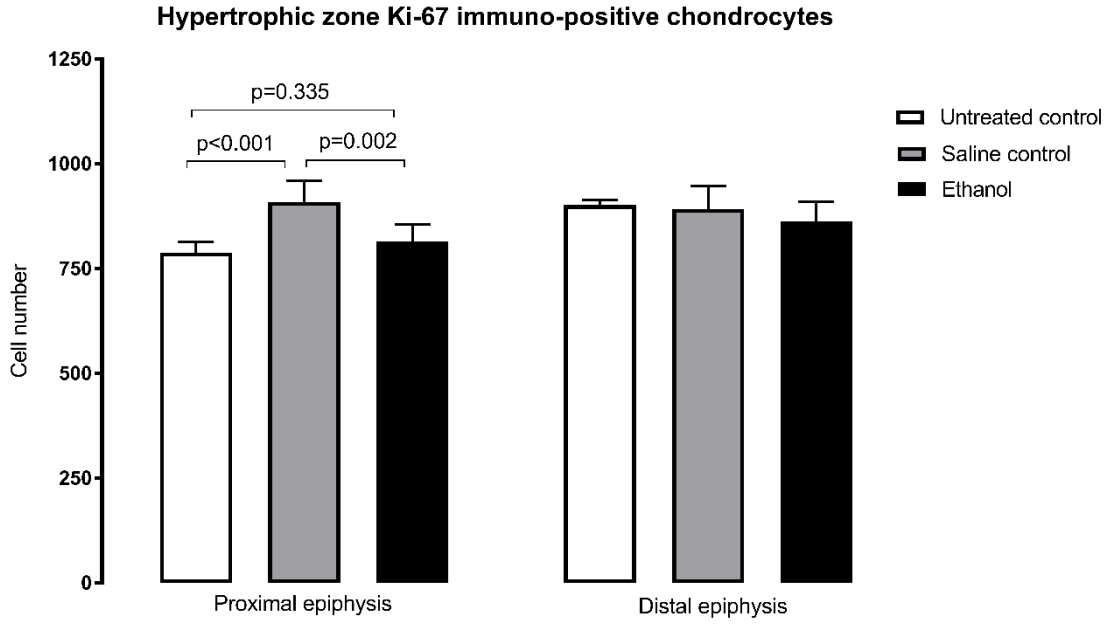


Figure 4.19: Ki-67 immuno-positive hypertrophic chondrocytes of the femur. The mean number of Ki-67 immuno-positive hypertrophic chondrocytes are shown for the hypertrophic zone in the proximal and distal epiphyseal growth plate for the three groups studied. Error bars represent standard deviation.

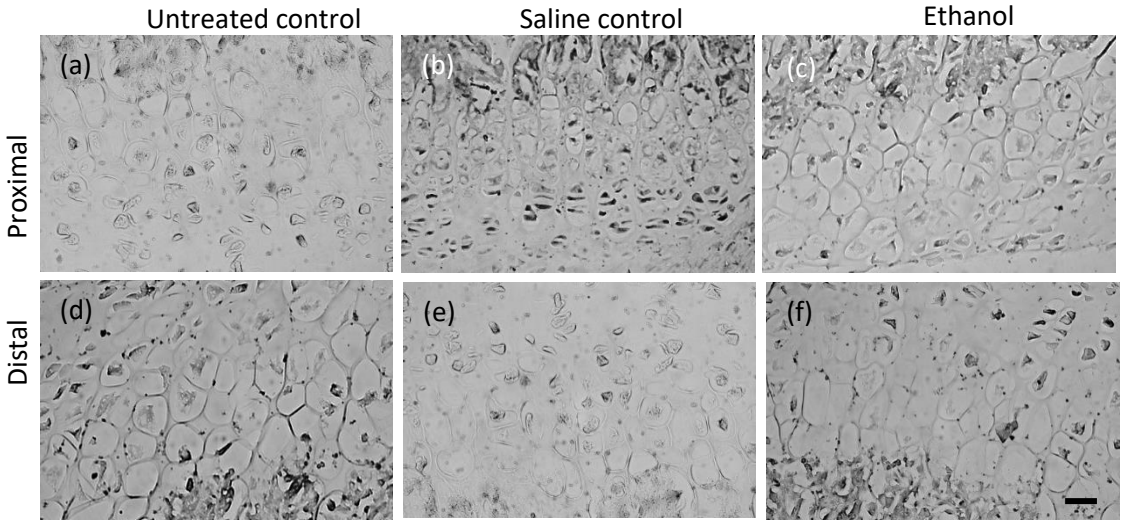


Figure 4.20: Photomicrograph of femur hypertrophic zone chondrocytes immunolabeled with the anti-Ki-67 antibody. Representative micrographs of the proximal and distal epiphyseal growth plate for the three groups studied. Scale bar = 20 microns and applies to all images.

Femoral proliferative zone TGFβ-1 immuno-positive chondrocytes

Regional similarities in the distribution of TGFβ-1 positive cells occurred with the untreated group exhibiting most chondrocytes in both the proximal and distal epiphyseal plate proliferative zone. The proximal epiphyseal plate proliferative zone showed more TGFβ-1 labelled chondrocytes in the untreated group (mean = 976.300 ±36.60) than the saline controls (mean = 911.33 ±21.02) and ethanol group (mean = 867.25 ±28.92) ($p<0.001$ and $p=0.002$. respectively). The ethanol group also showed significantly fewer TGFβ-1 positive cells than the saline controls ($p=0.02$). Similarly, in the distal epiphysis, TGFβ-1 labelled cells were most abundant in the untreated group (mean = 970.25 ±20.76) than saline controls (mean=907.75 ±15.91) and the ethanol group (mean = 886.90 ±23.09) ($p<0.001$ for both comparisons). The ethanol and saline had no significant differences detected ($p=0.106$) (Fig. 4. 21 and Fig. 4.22).

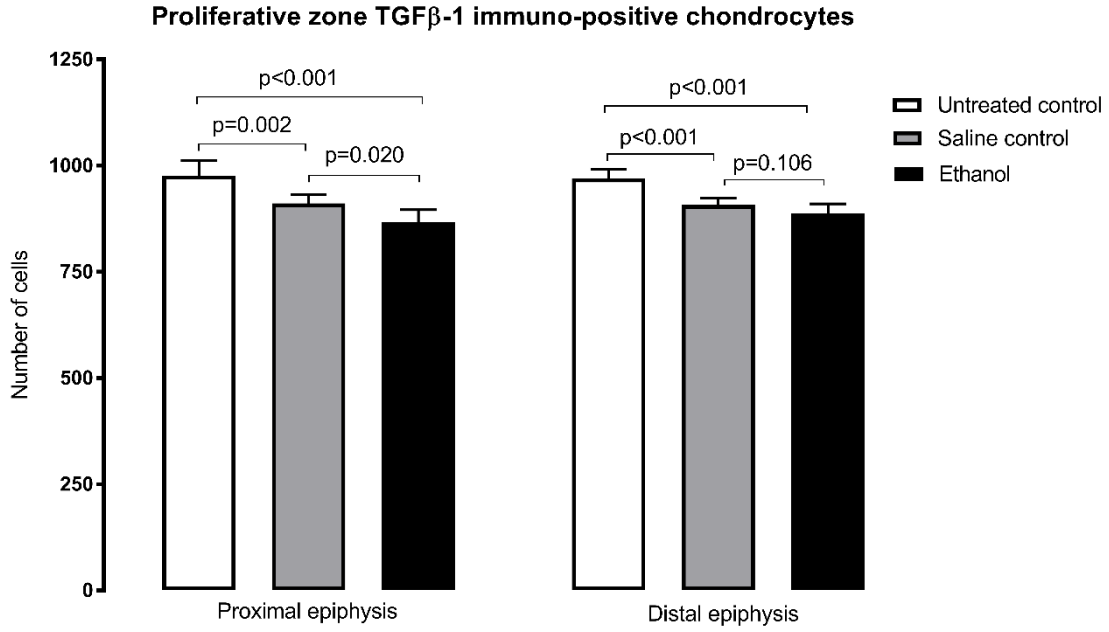


Figure 4.21: TGFβ-1 immuno-positive proliferative chondrocytes in the epiphyseal growth plate of the femur. The mean values of TGFβ-1 immuno-positive chondrocytes are shown for the proliferative zone in the proximal and distal epiphyseal growth plate. Error bars represent the standard deviation.

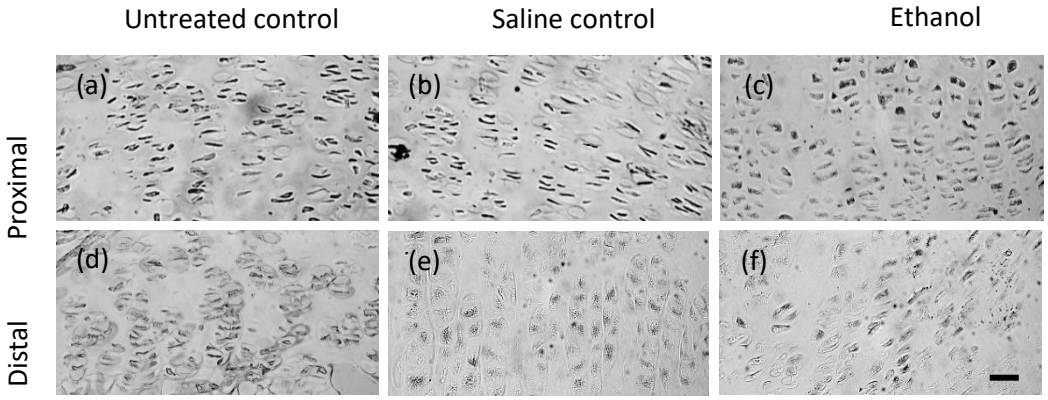


Figure 4.22 Photomicrograph of femur proliferative zone chondrocytes immunolabeled with the anti-TGFB1 antibody. Representative micrographs of the proximal and distal epiphyseal growth plate for the three groups studied. Scale bar = 20 microns and applies to all images.

Femoral hypertrophic zone TGFβ-1 immuno-positive chondrocytes

The hypertrophic zone displayed a similar pattern to that of the proliferative zone with regional similarities in the distribution of TGFβ-1 positive cells. The proximal and distal epiphyseal plate hypertrophic zone revealed more TGFβ-1 positive chondrocytes in the untreated group in both the proximal and distal epiphyseal plate. In the proximal epiphyseal plate, the untreated group had a mean of 996.80 ±75.48 which was significantly more than the saline controls (mean = 909.83 ±29.68) and ethanol group (mean = 844.67 ±17.08) ($p=0.006$ and $p<0.001$, respectively). The ethanol group also showed significantly fewer TGFβ-1 positive cells than the saline controls ($p=0.027$). In the distal epiphysis, TGFβ-1 labelled cells were significantly less than in the ethanol group (mean = 886.20 ±23.93) compared to saline controls (mean = 913.92 ±31.35) and untreated group (mean = 987.67 ±41.93). This difference was significant for the ethanol compared to the untreated controls ($p<0.001$). A comparison of the control groups showed the saline controls to have significantly fewer cells ($p= 0.002$) (Fig. 4.23 and Fig. 4.24).

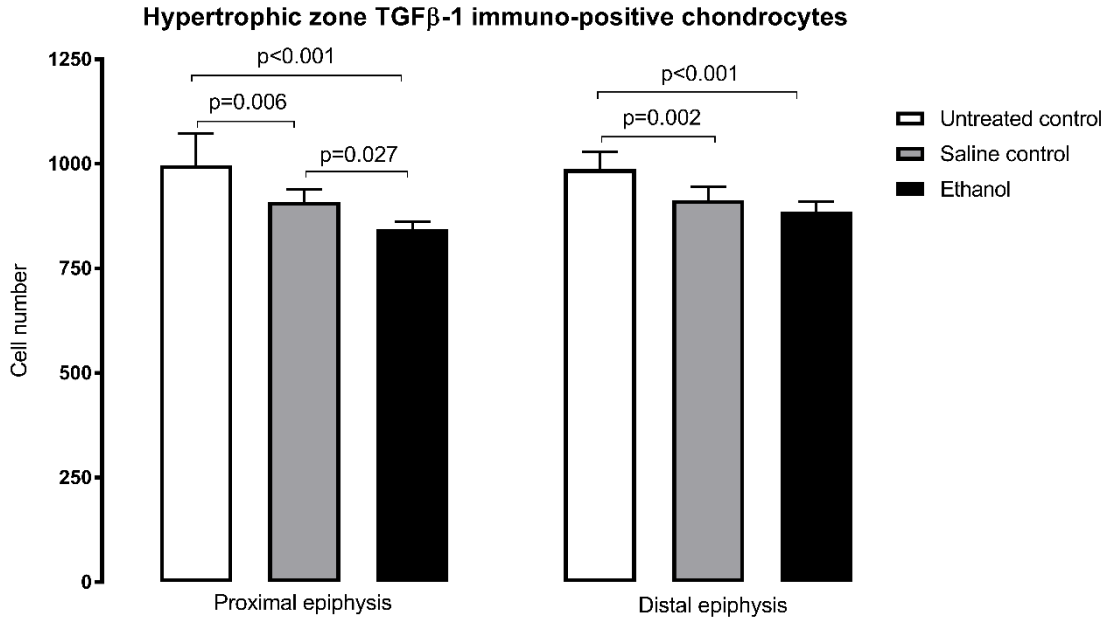


Figure 4.23: TGFβ-1 immuno-positive hypertrophic chondrocytes in the epiphyseal growth plate of the femur. The mean number of TGFβ-1 immuno-positive chondrocytes are shown for the hypertrophic zone in the proximal and distal epiphyseal growth plate. Error bars represent the standard deviation.

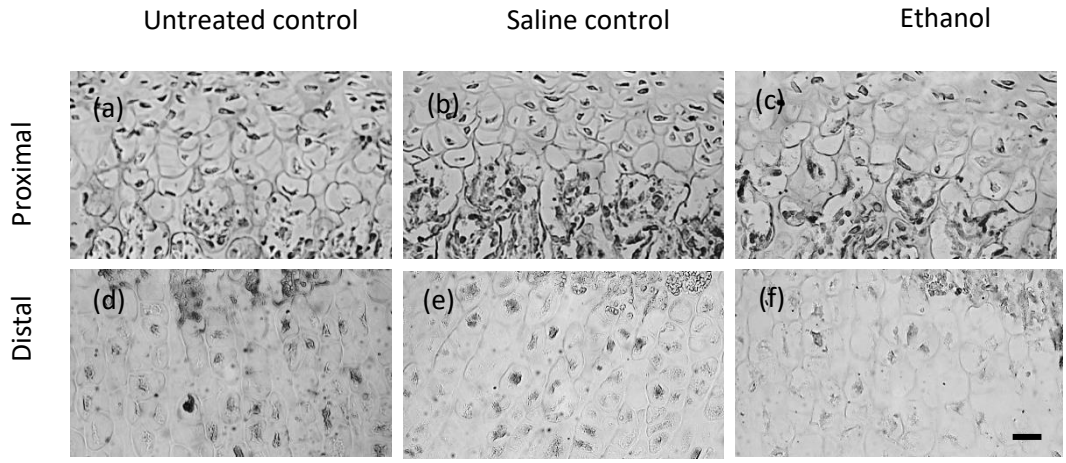


Figure 4.24: Photomicrograph of femur hypertrophic zone chondrocytes immunolabeled with the anti-TGFβ1 antibody. Representative micrographs of the proximal and distal epiphyseal growth plate for the three groups studied. Scale bar = 20 microns and applies to all images.

4.3.4 Femur (3 weeks) trabecular morphometric parameters most affected by gestational ethanol

Proximal femur at age 3 weeks

The effect of gestational ethanol on length, shaft volume, proximal bone volume to total volume (BV/TV), proximal trabecular thickness (TbTh), proximal trabecular number (TbN), proximal trabecular spacing (TbSp), proximal volume, proximal cortical thickness, midshaft cortical thickness were assessed using binary logistic regression in the ethanol and saline control groups (Table 4.2). The parameters used could reliably distinguish between the two groups. A test of the full model against a constant only model was statistically significant, indicating that the predictors as a set, reliably distinguished between ethanol or saline control group membership (Chi-square = 24.443, p =0.004 with df = 9). Nagelkerke's R^2 of 0.550 indicated a moderately strong relationship between prediction and grouping. The Wald criterion demonstrated that no specific variable predicted membership (Table 4.3). Prediction success overall was 78.3% (75.0% for the ethanol group and 81.8% saline controls).

Table 4.2: Femur osteometric and proximal epiphysis trabecular and cortical morphometric parameters in the equation. BV/TV, bone volume to total volume; TbTh trabecular thickness; TbN, Trabecular number; TbSp, Trabecular spacing.

Variables in the Equation

	B	S.E.	Wald	df	Sig.	Exp(B)
Osteometric parameters						
Length	.463	.671	.477	1	.490	1.589
Shaft Volume	-.206	.077	7.069	1	.008	.814
Epiphyseal Volume	.053	.190	.077	1	.782	1.054
Proximal epiphysis trabecular and cortical morphometric parameters						
BV/TV	-.084	.069	1.492	1	.222	.919
TbTh	-4.486	14.408	.097	1	.756	.011
TbN	-.555	.427	1.690	1	.194	.574
TbSp	-64.12	41.116	2.432	1	.119	.000
Proximal Cortical Thickness	.270	.685	.156	1	.693	1.311
Midschaft Cortical Thickness	-.533	.638	.698	1	.404	.587
Constant	13.704	11.928	1.320	1	.251	894545.791

Table 4.3: Group membership classification from osteometric and proximal epiphysis trabecular morphometric parameters of the femur.

Classification Table

Observed		Predicted		
		Group		Percentage Correct
		Ethanol	Saline Control	
Group	Ethanol	18	4	81.8
	Saline Control	6	18	75.0
Overall Percentage				78.3

Distal femur at age 3 weeks

The effect of gestational ethanol on length, shaft volume, midshaft cortical thickness, distal bone volume to total volume (BV/TV), distal trabecular thickness (TbTh), distal trabecular number (TbN) , distal trabecular spacing (TbSp) , distal volume, distal mediolateral (ML), distal cortical thickness were assessed using binary logistic regression in the ethanol and saline control groups (Table 4.4). The parameters used could reliably distinguish between the two groups. A test of the full model against a constant only model was statistically significant, indicating that the predictors as a set, reliably distinguished between ethanol or saline control group membership (Chi-square = 36.004, p <0.001 with df = 10). Nagelkerke's R^2 of 0.724 indicated a very strong relationship between prediction and grouping. The Wald criterion demonstrated that no specific variable predicted membership (Table 4.5). Prediction success overall was 91.3% (95.8% for the ethanol group and 86.4% saline controls).

Table 4.4: Femur osteometric and distal epiphysis trabecular and cortical morphometric parameters in the equation. BV/TV, bone volume to total volume; TbTh trabecular thickness; TbN, Trabecular number; TbSp, Trabecular spacing.

Variables in the Equation

	B	S.E.	Wald	df	Sig.	Exp(B)
Osteometric parameters						
Length	3.226	1.679	3.690	1	.050	25.178
Bicondylar length	.248	1.547	.026	1	.873	1.281
Shaft Volume	-.291	.148	3.861	1	.049	.748
Epiphyseal Volume	-.176	.277	.403	1	.525	.839
Distal epiphysis trabecular and cortical morphometric parameters						
BV/TV	-.350	.234	2.246	1	.134	.704
TbTh	-13.144	42.873	.094	1	.759	.000
TbN	-1.492	.984	2.302	1	.129	.225
TbSp	-188.693	137.911	1.872	1	.171	.000
Proximal Cortical Thickness	-2.746	1.325	4.291	1	.038	.064
Midschaft Cortical Thickness	-1.228	.903	1.847	1	.174	.293
Constant	12.851	16.041	.642	1	.423	381250.305

Table 4.5: Group membership classification from osteometric and distal epiphysis trabecular morphometric parameters of the femur.

Classification Table

Observed		**Predicted**		
		Group		**Percentage Correct**
		Ethanol	Saline Control	
Group	Ethanol	19	3	86.4
	Saline Control	1	23	95.8
Overall Percentage				91.3

4.4 Discussion

The main aim was to test the hypothesis that gestational ethanol interrupts trabecular morphology through inhibiting epiphyseal plate chondrocyte transforming growth factor-beta-1 (TGFβ1) expression in a binge alcohol drinking rat model. We studied the growth plate and epiphysis in both proximal and distal aspects and measured osteometric parameters in the femur at 3 weeks postnatal age. Histological and immunohistochemical techniques were employed to assess general morphology and to quantify proliferating chondrocytes (Ki-67) and those expressing TGFβ1. The group exposed to alcohol during gestation showed smaller epiphyseal plate surfaces area and significantly shorter bones with smaller bicondylar breadths. This group also had fewer chondrocytes and Ki-67 immunolabelling showed impaired chondrocyte proliferative rate in the proliferative and hypertrophic zones. These observations occurred for both the proximal and distal epiphyseal growth plates in most cases. The exception was that Ki-67 positive chondrocytes were similar in number for the hypertrophic zone in the distal epiphysial plate. The internal architecture was assessed from the data obtained through the use of micro focus X ray computed tomography. We found altered trabecular parameters in the alcohol exposed group. The diaphyseal cortical and medullary cavity proportions were also affected, particularly in the midshaft.

One of the major impacts of drinking alcohol in pregnancy is children considered small for age (O'Leary, 2004; Olivier et al., 2016). Bone growth and development impact bone size and ultimately lead to short stature as observed in children of mothers who admit to drinking alcohol during pregnancy (Lemoine et al., 2003; Katwan et al., 2011). Therefore, understanding bone size in research related to the effects of alcohol consumption during pregnancy is crucial. In the present study, we used micro CT data to determine the shaft volume, epiphyseal volume, length and bicondylar length. We could not find comparable studies with respect to the shaft and epiphyseal plate volume as well as bicondylar breadth. However, numerous studies report on full bone length (Nwaogu, 2002; Simpson et al., 2005; Snow and Keiver, 2007). We were concerned that length alone as a single linear

measurement would not be adequate to use as a proxy for bone size. Having used micro-computed tomography data, we were able to quantify the bone size in the form of volume in a manner that best or reliably estimates the true bone sizes.

Limb bone elongation takes place through endochondral ossification, which is entirely dependent on the existence and viability of the epiphyseal growth plate (Lui et al., 2011). It has been proposed that alcohol exposure during intrauterine life could result in shorter bone due to disturbances in chondrocyte number and differentiation rate as well as the size of the epiphyseal growth plate (Miralles-Flores and Delgado-Baeza, 1992; Snow and Keiver, 2007). Researchers (Pan et al., 2016) have used length (height) measurements of the growth plate and its various zones for use as a proxy of epiphyseal growth plate size. Since this measurement would be in the vertical direction, size information with respect to the horizontal aspects of the growth plate would not be captured. Also, the vertical measurements of the growth plate and its various zones differ in each part of the growth plate when assessed from the mediolateral aspect. This means that the height depends on where the researcher measures and is prone to difficulties in reproducibility. To overcome this problem, we used measurements of surface area to gain a better estimate of the sizes of the growth plate and its zones.

In the present study, the group exposed to alcohol during gestation showed smaller epiphyseal plate surface areas, together with smaller proliferative and hypertrophic zones. We speculate that gestational alcohol exposure would inhibit longitudinal bone growth through alterations in the proliferative cells of the growth plate. These findings are similar to the reports of Snow and Keiver (2007) in fetuses as well as Miralles-Flores and Delgado-Baeza (1992). The present study differs with those of (Miralles-Flores and Delgado-Baeza, 1992; Snow and Keiver, 2007) that used a higher dosage of 36% ethanol. These researchers also employed unrestricted access to a diet containing ethanol unlike a single daily dose as in simulating binge drinking. Therefore, this study design differs from the present study which was binge drinking based and administering a lower alcohol concentration of 25.2%.

Despite the differences in the alcohol dosage, our findings support the proposition that no amount of alcohol intake during pregnancy is safe for the offspring (Popova et al., 2017).

One of the distinguishing features of the present study was the use of the anti-Ki-67 antibody as a proxy for proliferation cells. We found that the ethanol group had fewer proliferating chondrocytes than the controls. This supports the proposition that the stunted growth and short stature seen in children of mothers who drink during pregnancy is due to the teratogenic effects of alcohol on the epiphyseal growth plate (Miralles-Flores and Delgado-Baeza, 1992; Snow and Keiver, 2007).

In the present study, we found fewer TGFβ1 immuno-positive cells in the ethanol group both in the proliferative and hypertrophic zones in both the proximal and distal epiphyseal growth plates. The role of TGFβ1 in chondrocyte differentiation has been extensively reviewed by van der Kraan et al. (2009). TGFβ1 regulates chondrocyte differentiation through the Smad pathway (Kanaan and A Kanaan, 2006; Chen et al., 2012). In this pathway, Smad1/5/8 promotes chondrocyte differentiation whereas Smad2/3 inhibits it. We propose that it is possible *in utero* ethanol results in shorter bones through disturbances of the balance between Smad1/5/8 and Smad2/3.

In general, fewer chondrocytes and multiplying cells in the proliferative and hypertrophic zones in both epiphyseal growth plates were recorded. The exception was that proliferating chondrocytes were similar in number for the hypertrophic zone in the distal epiphysial plate. However, TGFβ1 immuno-positive cells were fewer in the ethanol group in both histological zones studied in both epiphyseal growth plates. This is contrary to our anticipation. We expected TGFβ1 immuno-positive cells to be similar in number for all groups in the distal epiphysial plate hypertrophic zone, to commensurate the number of multiply cells as observed by Ki-67 immunolabeling. This suggests that other growth factors whose role is yet to be determined may be involved in the control of chondrocyte differentiation when exposed to ethanol *in utero*.

We found a lower bone to tissue volume ratio in the ethanol group together with fewer and thinner trabeculae. We could not find applicable literature on gestational alcohol trabecular morphology in the femur of animals exposed to alcohol during intrauterine life. However, numerous studies elucidate the effects of alcohol use on bone strength and trabecular architecture (Diamond et al., 1989; Diez et al., 1997; Wezeman et al., 1999; Maddalozzo et al., 2009). These studies report altered bone to volume ratio, trabecular thinning as well as fewer trabeculae with larger spaces (Turner, 2000; Maurel et al., 2011; Mikosch, 2014). Mean trabecular spacing appeared to be unaffected in our study as there were no group differences.

Employing a binary logistic regression showed that shaft volume, length and proximal cortical thickness were the main parameters that determined group membership into either ethanol or saline control. This means that these three parameters are affected the most in gestational alcohol exposure. When using the proximal trabeculae morphometric parameters more saline control were misclassified as belonging to the ethanol group. This suggests that there was less group variation in these parameters. This, in turn, suggests that that intrauterine ethanol effects in the femur may be minimal for the proximal aspect of the bone.

4.4.1 Conclusions

Gestational alcohol exposure had an adverse impact on bone size at 3 weeks in postnatal life. The smaller bones observed following intrauterine alcohol exposure could be due to a smaller epiphyseal growth plate with fewer actively dividing chondrocytes (Ki-67 immuno-positive) and reduced TGFβ1 expression. This, in turn, led to the altered trabecular parameters and cortical as well as medullary cavity proportions in the femoral midshaft.

Chapter 5

Trabecular morphometry and bone strength in postnatal life (12 weeks) of Sprague Dawley rats exposed to intrauterine alcohol

TABLE OF CONTENTS

5.0 INTRODUCTION 123
5.2 MATERIALS AND METHODS 125
5.2.1 Study sample 125
Skeletal elements harvesting 125
5.2.2 Three-dimensional Micro-focus X-ray Computed Tomography (3D- µCT) 125
Parts of the humeri and femora and trabecular parameters studied 126
5.2.3 Three-point Bending 128
5.2.4 Data analysis 129
5.3 RESULTS 130
5.3.1 Humerus at 12 weeks of age 130
Bone length humerus and epicondylar breadth 130
Humerus bone to total volume ratio (BV/TV) at 12 weeks of age 131
Humerus trabecular thickness (TbTh) at 12 weeks of age 132
Humerus trabecular number (TbN) at 12 weeks of age 133
Humerus trabecular spacing (TbSp) at 12 weeks of age 134
5.3.2 Humerus cross-sectional area, cortical area (thickness) and medullary canal area at 12 weeks of age 136
Proximal (25th percentile mark) 136
Midshaft (50th percentile mark) 137
Distal (75th percentile mark) 138
Tensile strength of the humerus using 3-point bending tests 139
5.3.3 Femur 140
Femur bone length at 12 weeks of age 140
Femur bicondylar breadth at 12 weeks of age 140
Femur bone to total volume ration at 12 weeks of age (BV/TV) 141
Femur trabecular number (TbN) at 12 weeks of age 143
Femur trabecular spacing (TbSp) at 12 weeks of age 144
5.3.4 Femur cross-sectional area, cortical area (thickness) and medullary canal area at 12 weeks of age 146
Proximal (25th percentile mark) 146
Midshaft (50th percentile mark) 147
Distal (75th percentile mark) 148
Tensile strength of the femur using 3-point bending tests 149
5.3.5 Major parameters for the ethanol and saline controls 150

5.4 DISCUSSION 153
5.4.1 Conclusions 155

5.0 INTRODUCTION

The deleterious consequence of gestational alcohol exposure on skeletal elements are acknowledged in the medical literature (Adebsi, 2005; Snow and Keiver, 2007). Several studies (Jones and Dwyer, 2000; Cooper et al., 2001; Godfrey et al., 2001) suggest that low birth weight and impaired bone growth, as well as a decrease in mineralization in utero, may reduce peak bone mass and increase the risk of fractures and osteoporosis later in life.

A reduction in bone mass and disruption of trabecular and compact bone structure, causing a loss of mechanical strength and increased fracture risk are characteristic of osteoporosis (Osterhoff et al., 2016). The ability of the osseous tissue to resist mechanical forces and fractures relies not only on the quantity but the quality of bone tissue. Bone quality is established by the structural and material properties which are influenced by the remodelling rate (Martin and Correa, 2010). Bone remodelling is a continuous process, comprising the renewal of the osseous tissue in which, osteoclasts resorb damaged or old bone, and osteoblasts deposit the new bone (Hadjidakis and Androulakis, 2006). Alcohol is known to affect the balance of bone resorption and deposition, disrupting the cortical and trabecular morphology, which results in diminished bone strength (Schnitzler and Solomon, 1984).

The strength of a bone and its structural properties are determined by shape and size as well as its microarchitecture (Martin and Correa, 2010). The microarchitecture of the osseous tissue is composed of 2 components trabecular and compact bone. Previous reports indicate that alcohol causes a reduction in compact and trabecular bone density and trabecular bone volume in young growing rats (Sampson et al., 1996). Similarly, Chen et al. (2001) found a decrease in trabecular number in the hamster femur following alcohol consumption. This is thought to be due to the decline in osteoblast number and size as previously reported in alcohol-exposed rats (Diez et al., 1997). A study by Ramadoss et al. (2006) found bone strength to be altered by maternal ethanol intake in fetal sheep. As there are no comparable studies on postnatal bone strength in prenatal alcohol-exposed sheep,

it remains unknown whether intrauterine alcohol affects bone function in long-term postnatal life.

Although the efefcts of alcohol on bone quality are affected when consumed during gestation and when used in adult life, it remains unclear as to whether the deleterious effects on bone persist into adolescence and adult life in cases of intrauterine alcohol exposure. We wondered whether gestational alcohol exposure would affect bone strength and trabecular morphological parameters in postnatal life. As such, we investigated this question using the humerus and femur in 12-week-old rats that were subjected to alcohol during gestation.

5.2 MATERIALS AND METHODS

5.2.1 Study sample

Twelve dams treated as in section 2.1.1 were used to obtain 24 pups allocated into the ethanol (n=12) and saline-treated groups (n=12). These pups were weaned at 3 weeks of age and individually housed in cages until termination of experiment at 12 weeks of age. These rats were weighed weekly until termination.

Skeletal elements harvesting

The rats were terminated by a lethal dose of pentobarbital intraperitoneal injection. The entire animal was then immediately immersed in 10% buffered formalin after an abdominal incision was made to allow for the penetration of the fixative. To expose the humeri and femora, skin incisions were made on the respective limbs and muscles were meticulously teased away. The skeletal samples were then individually immersed and stored in 10% buffered formalin to continue fixation until further processing. Bilateral humeri and femora were used for 3D- microtomography. The right-sided bones of the humeri and femora were used for three-point bending tests.

5.2.2 Three-dimensional Micro-focus X-ray Computed Tomography (3D- µCT)

A Nikon XTH 225/320 LC X-ray microtomograph was used to scan the bilateral 12-week old humeri and femora for 3D-µCT examination. To keep the samples steady during scanning, the bones were mounted in low-density Styrofoam, placed in plastic tubes while allowing the X-rays to get to the sample with negligible absorption. The plastic container with the sample inside was then positioned on a rotating manipulator in the scanning chamber for the scanning. The scanning parameters used are shown in table 5.1.

Table 5.1: Scanning parameters of 12-week old bones.

Parameter	Value
X-ray voltage	70kv
X-ray current	400µa
Filter	1mm aluminium
Scanning resolution	20µm
Tomographic rotation	360 degrees
Rotation step	1 degree
Frame averaging	4
Scan duration	8 minutes

Parts of the humeri and femora and trabecular parameters studied

The VG studio software built in calliper was used to determine humeri and femoral osteometric parameters. From the humerus, the full bone length and epicondylar breath were taken, whereas full bone length, biomechanical and bicondylar length were measured from the femur (Figs. 5.1 and 5.2.). The cross-sectional area, cortical area and medullary canal area of the shaft were measured at 3 positions; 25th (proximal), 50th (midshaft) and 75th (distal) percentile marks from both the humerus and femur (Figs. 5.1 and 5.2.). The trabecular morphometric parameters were studied in the proximal and distal aspects in both bones. Following reconstruction, VG studio Max ®3.2 was used for data analysis as previously described (Bouxsein et al., 2010) (see section 3.2.2). The following trabecular parameters were assessed: bone volume to total volume (BV/TV), Trabecular thickness (TbTh) trabecular number (TbN) and trabecular spacing (TbSp) (See section 3.2.2). cross-sectional circumference, cross-sectional area and cortical thickness were determined (see section 3.).

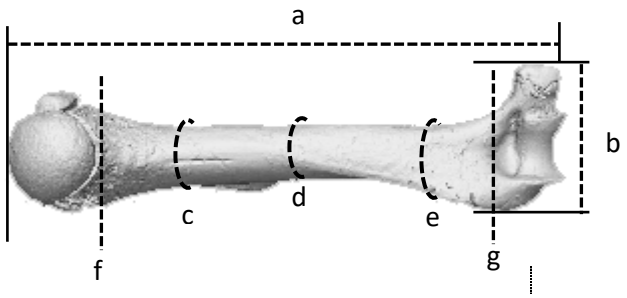


Figure 5.1. Three-dimensional reconstruction of a 12-week old humerus showing the parts that were investigated. (a), full humerus length; (b), epicondylar breadth; (c), (d), (e), 25th (proximal); 50th (midshaft) and 75th (distal) percentile marks, respectively; (f) and (g), proximal and distal ROI for trabeculae morphological assessment. (Image courtesy of R. Ndou and D Pillay).

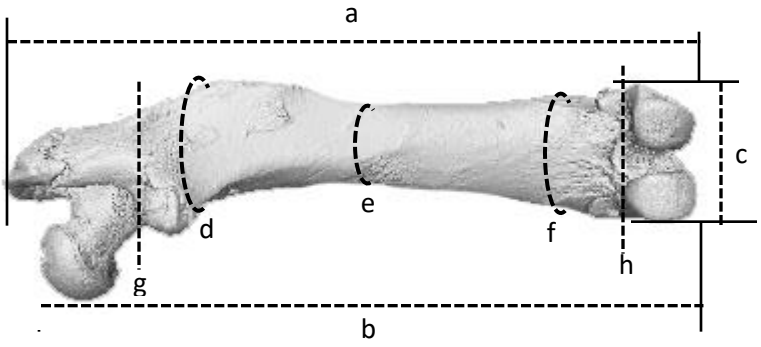


Figure 5.2. Three-dimensional reconstruction of a 12-week old femur showing the parts that were investigated. (a), full femur length; (b), biomechanical length; (c), bicondylar breadth (d), (e), (f), 25th (proximal); 50th (midshaft) and 75th (distal) percentile marks, respectively; (g) and (h), proximal and distal ROI for trabeculae morphological assessment. (Image courtesy of R. Ndou and D Pillay).

Table 5.2: Osteometric parameter descriptions

Parameter	Description
Full humerus length	The maximum length that can be measured between the top of the humeral head and the most distant point on the distal humerus.
Epicondylar breadth	the greatest distance between the medial and lateral epicondyles
Full femur length	The maximum length measured between the top of the greater trochanter and the bottom of the farthest condyle
Biomechanical length	The maximum length measured between the top of the femoral head and the bottom of the farthest condyle.
Bicondylar breadth	the distance between the medial most and lateral most points on the epicondyles

5.2.3 Three-point Bending

The right femora and humeri of each rat were subjected to a three-point bending test. The load was applied at the midshaft, midway between two supports that were 15mm apart for the femur and 13 mm apart for the humerus (Fig. 5.3). Before mechanical testing, various osteometric measurements were taken using a digital calliper. The femora and humeri were positioned so that bending occurred at the anteroposterior plane and mediolateral plane, respectively. Load-displacement curves were recorded at a constant speed of 5mm/min until failure.

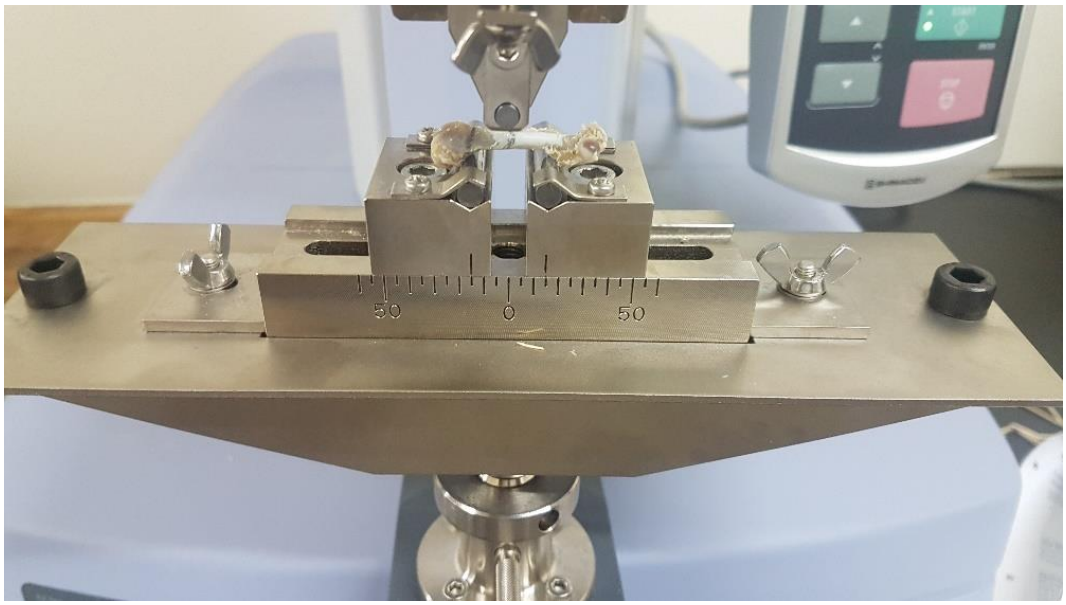


Figure 5.3: Three-point bending test. The load has been applied to the midshaft of the humerus between two supports 15mm part in the mediolateral plane.

5.2.4 Data analysis

The data were managed in Microsoft Excel 2016 (Microsoft Corporation) and analysed using SPSS® version 25 (IBM®). ANOVA with LSD post-hoc was used for multiple group comparisons of means. Principal components analysis was conducted to assess how femur and humerus morphology parameters clustered. Significance level was set at $p < 0.05$.

5.3 RESULTS

5.3.1 Humerus at 12 weeks of age

Bone length humerus and epicondylar breadth

The humerus length was significantly lower in the ethanol group (mean = 25.78mm ±0.93) than the saline controls (mean = 26.06mm ±1.36) although this difference seemed marginal (p=0.008) (Fig. 5.4a). Also, the ethanol group (mean = 6.02mm ±0.51) showed a smaller epicondylar breadth than the saline control (mean = 6.33mm ±0.65) (Fig. 5.4b) (p=0.013).

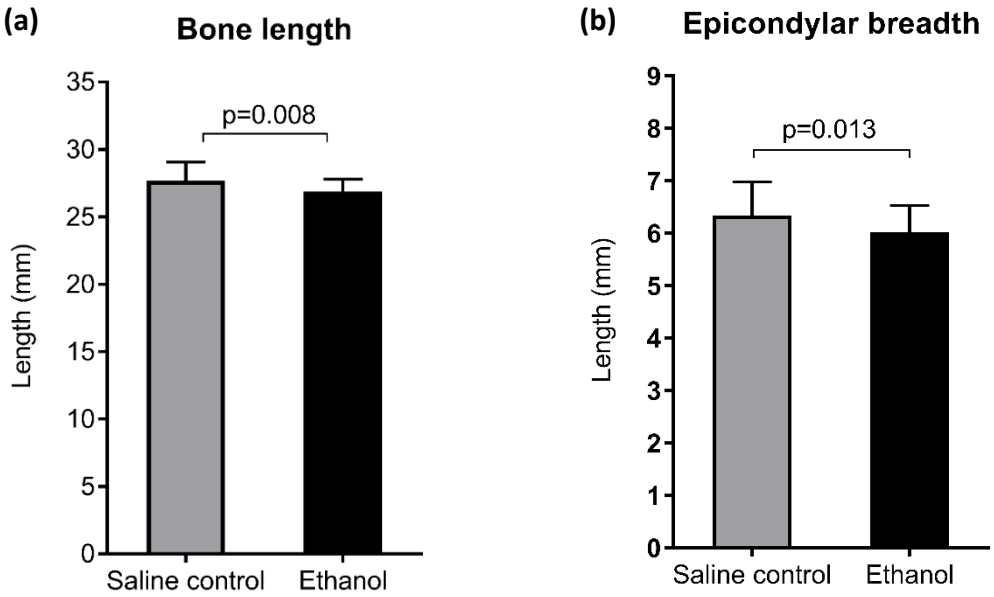


Figure 5.4: Humerus osteometric measurements at 12 weeks of age. (a), full bone length; (b), epicondylar breadth. The lengths are given as means for the saline controls and the ethanol group. Error bars indicate standard deviation.

Humerus bone to total volume ratio (BV/TV) at 12 weeks of age

In the proximal region, bone to total volume ratio (BV/TV) was lower in the ethanol group (mean = 71.92% ±5.68) than the saline controls (mean = 77.44% ±4.23) ($p<0.001$). Similarly, in the distal region, we found a significantly low bone to total volume (BV/TV) in the ethanol group (mean = 71.76% ±6.52) compared to the saline controls (mean = 78.76% ±3.98) ($p<0.001$) (Fig. 5.5).

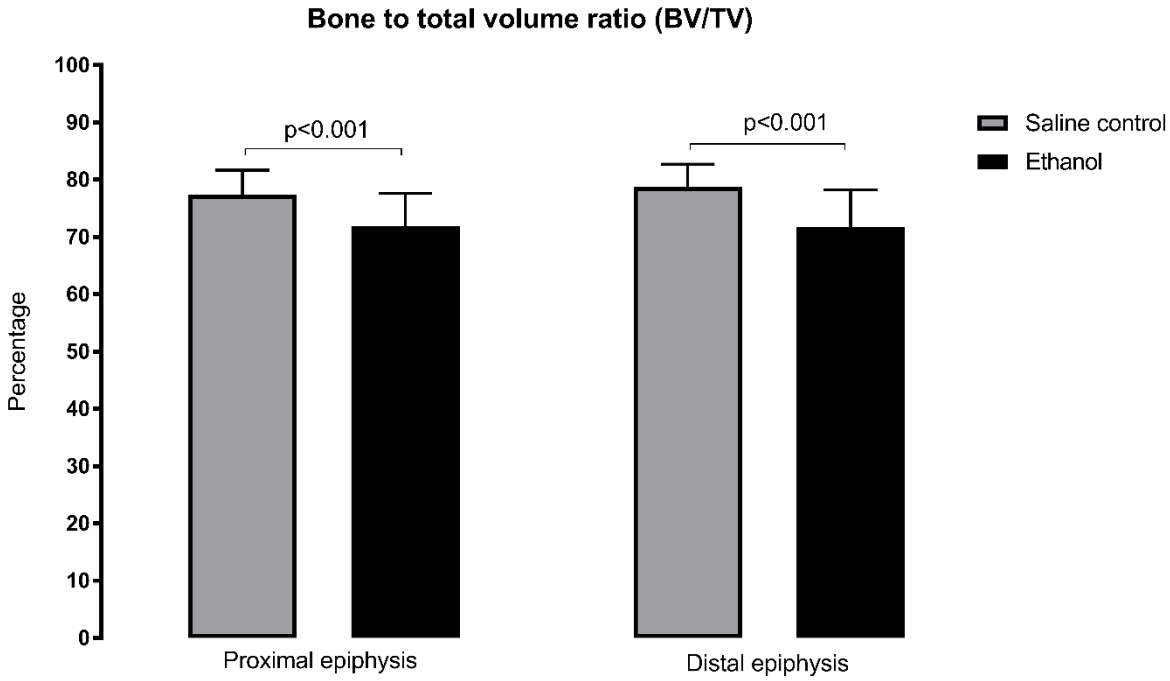


Figure 5.5: Humerus bone to total volume ratio (BV/TV) at 12 weeks of age. The mean percentages are given for the proximal and distal epiphysis in the saline controls and the ethanol group. Error bars indicate standard deviation.

Humerus trabecular thickness (TbTh) at 12 weeks of age

No group differences in trabecular thickness (TbTh) were observed in the proximal and distal extremities of the humerus (Fig. 5.6). In the proximal region, trabecular thickness (TbTh) was marginally lower in the saline (mean = 0.31 ±0.07) compared to the ethanol group (mean = 0.32mm ±0.06) (p=0.41 among the two groups). Again, in the distal region, the trabecular thickness was similar between the two groups (ethanol, mean = 0.40mm ±0.07; saline control, mean = 0.38 ±0.09) (p=0.82 between the two groups).

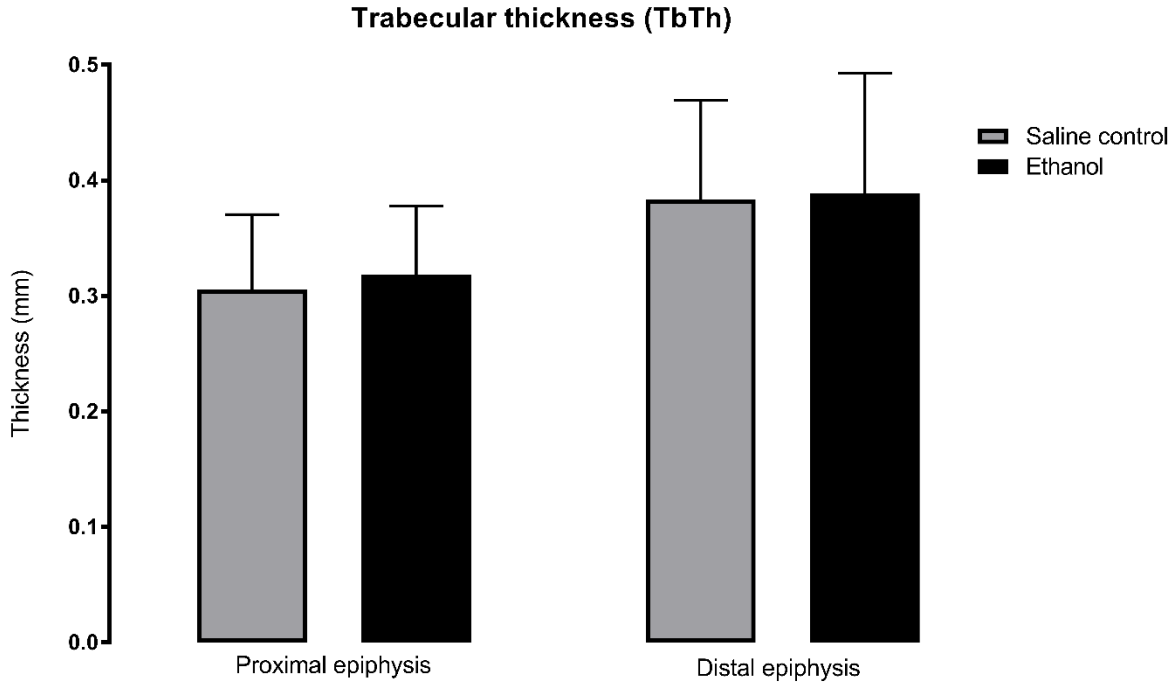


Figure 5.6: Humerus trabecular thickness (TbTh) at 12 weeks of age. The mean values are given for the proximal and distal epiphysis in the saline controls and the ethanol group. Error bars indicate standard deviation.

Humerus trabecular number (TbN) at 12 weeks of age

Trabecular distribution stratified by study group membership showed a similar pattern when arranged by the epiphyseal end (proximal and distal). The proximal region exhibited fewer trabeculae in the ethanol group (mean = 2.24 ±0.39) than the saline (mean = 2.64± 0.53) (p=0.004). This pattern of lower trabecular (TbN) in the ethanol group (mean=2.24 ±0.39) than the saline controls (mean = 2.64±0.53) continued in the distal epiphysis (p=0.003) (Fig. 5.7).

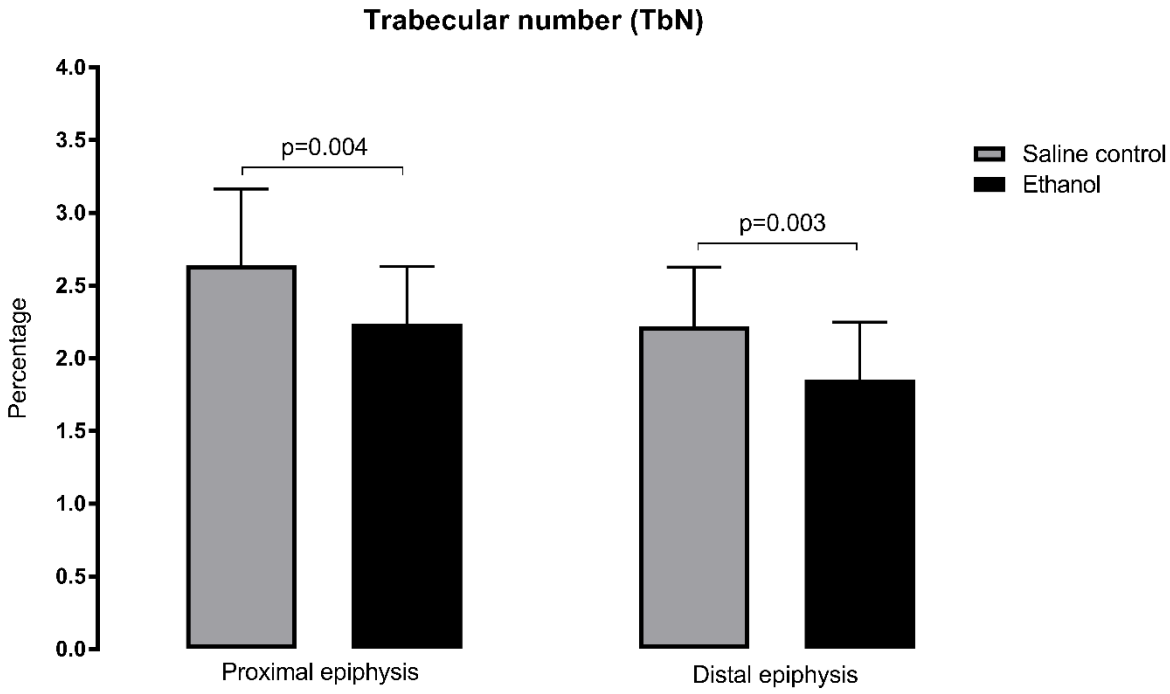


Figure 5.7: Humerus trabecular number (TbN) at 12 weeks of age. The mean values are given for the proximal and distal epiphysis in the saline controls and the ethanol group. Error bars indicate standard deviation.

Humerus trabecular spacing (TbSp) at 12 weeks of age

In the proximal epiphysis, trabecular spacing was wider in the ethanol group (mean = 0.093mm ±0.01) compared to saline controls (mean = 0.085mm ±0.01) (p=0.016). (Figs. 5.8 and 5.9 a and b). Similarly, in the distal epiphysis, trabecular spacing was wider in the ethanol group (mean = 0.094mm ±0.02) compared to saline controls (mean = 0.083mm ±0.01) (p=0.004) (Figs. 5.8 and 5.9 c and d).

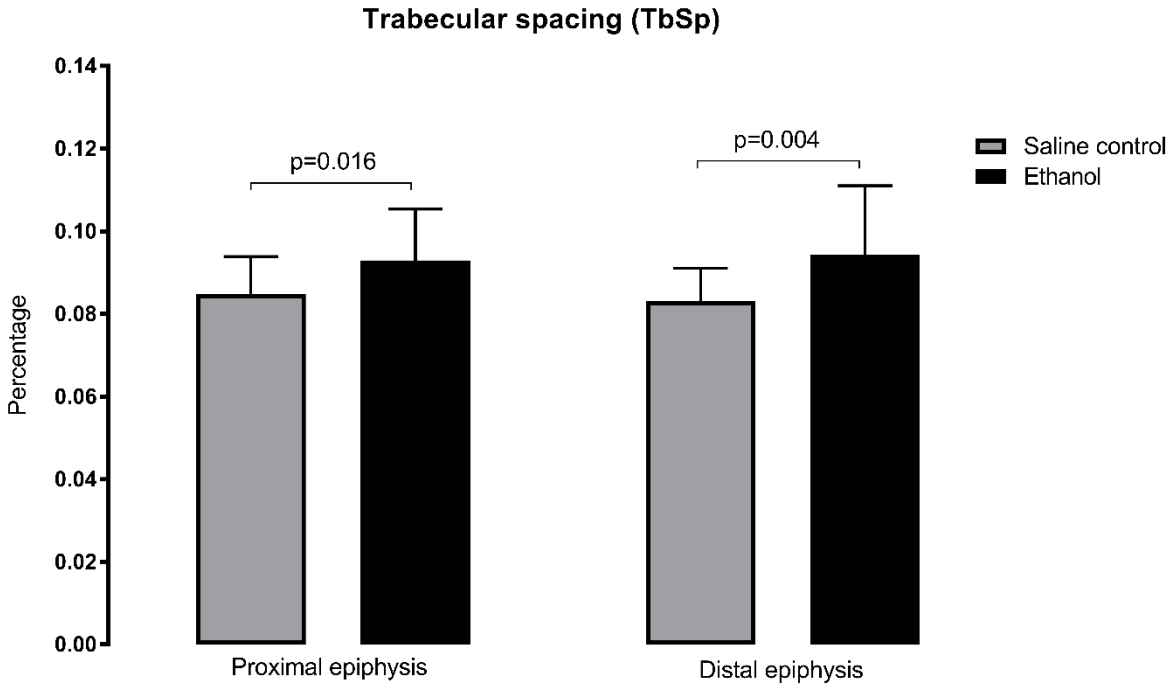


Figure 5.8: Humerus trabecular spacing (TbSp) at 12 weeks of age. The means are given for the proximal and distal epiphysis in the saline controls and the ethanol group. Error bars indicate standard deviation.

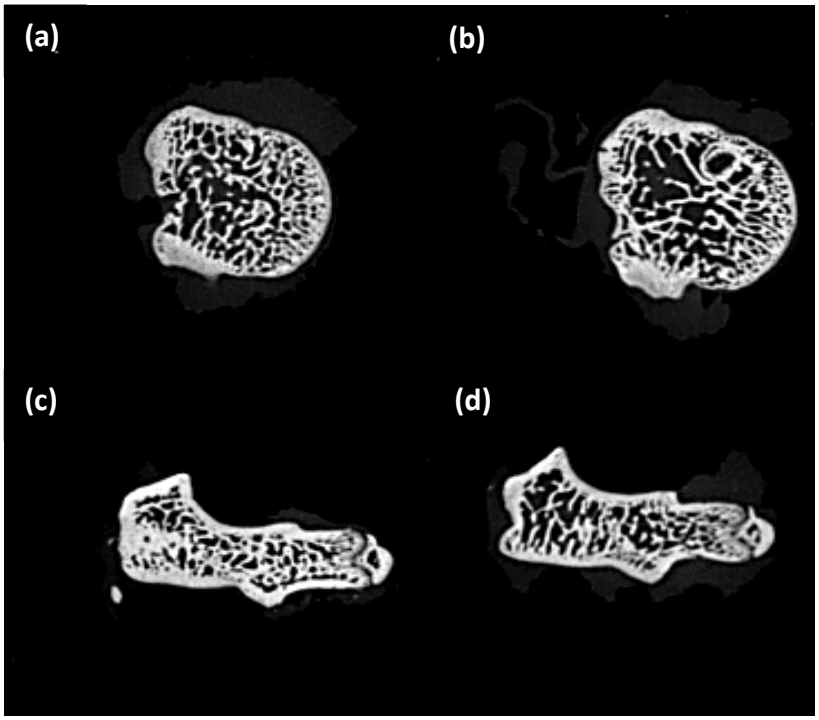


Figure 5.9: Trabecular morphology in the humerus at 12 weeks of age. Representative slices of (a), proximal end in a saline control showing more trabeculae and less spacing; (b), proximal end of the ethanol group showing fewer trabeculae and wider spacing); (c), distal end of saline control showing more trabeculae and less spacing; (d), distal end of the ethanol group showing fewer trabeculae and wider spacing.

5.3.2 Humerus cross-sectional area, cortical area (thickness) and medullary canal area at 12 weeks of age

Proximal (25th percentile mark)

The proximal cross-sectional area was larger in the ethanol group (mean = 9.06mm^2 ± 2.33) compared to the saline controls (mean = 8.611mm^2 ±1.83) although not statistically significant (p=0.93) (Fig. 5.10). Conversely, the medullary canal area appeared to be larger in the ethanol (mean = 5.305 mm^2 ±1.68) than the saline group (mean = 4.66mm^2 ±1.25) although not statistically significant (p=0.13) (Fig. 5.10). With respect to the cortical area (thickness) in this region, the ethanol group (mean = 3.75mm^2± 0.28) exhibited a marginally lower value compared to the saline (mean = 3.95mm^2 ± 1.03) which was not significant (p=0.55).

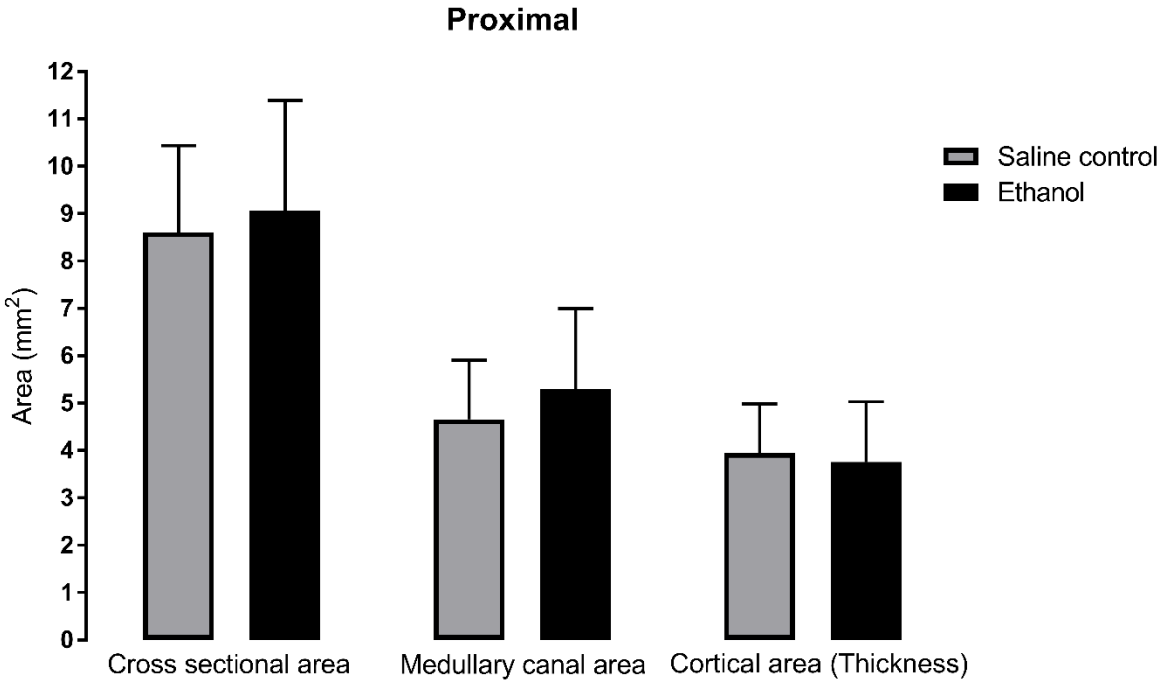


Figure 5.10: Humerus proximal cross-sectional area, medullary canal area and cortical thickness at 12 weeks of age. The means at the 25th percentile mark given for the two groups studied. Error bars represent standard deviation.

Midshaft (50th percentile mark)

The midshaft cross-sectional area was different in the two groups studied. The ethanol group had a lower cross-sectional area mean of 6.19mm^2 ±0.82 than the saline which had a mean of (6.631mm^2 ±1.08). There were no statistical group differences detected (p=0.23) (Fig. 5.11). The medullary canal area was smaller in the ethanol group (mean = 2.16mm^2 ±0.31) than the saline group (mean = 2.51mm^2 ±0.62). Significant differences in the medullary canal area were observed between the ethanol and saline controls (p=0.018). Regarding the cortical area (thickness) in this region, the ethanol group (mean = 4.04mm^2 ±0.79) exhibited a lower value compared to the saline (mean = 4.13mm^2 ±0.89) (Fig. 5.11). No significant differences in the cortical area (thickness) were detected among the three groups (p=0.59).

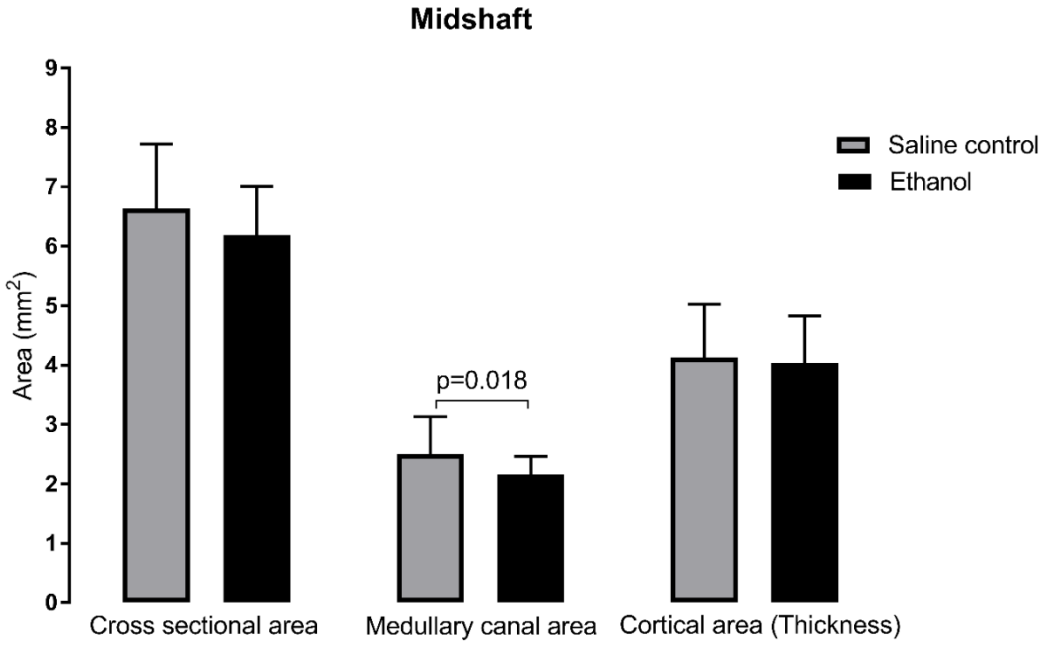


Figure 5.11: Humerus midshaft cross-sectional area, medullary canal area and cortical thickness at 12 weeks of age. The means at the 50th percentile mark given for the two groups studied. Error bars represent standard deviation.

Distal (75th percentile mark)

The distal cross-sectional area was similar in the ethanol group (mean = 6.00mm^2 ±1.24) compared to the saline controls (mean = 6.08mm^2 ±1.12) (p=0.82). (Fig. 5.12). The distal medullary canal appeared larger in the ethanol group (mean = 1.82mm^2 ±0.83) in comparison to the saline (mean = 1.59mm^2 ±0.63) however, these differences were not significant (p=0.28) (Fig. 5.12). With respect to the cortical area (thickness) in this region, the ethanol group (mean = 4.18mm^2 ±1.31) exhibited a marginally lower value compared to the saline groups (mean = 4.49mm^2 ±1.14) (p=0.40) (Fig. 5.12).

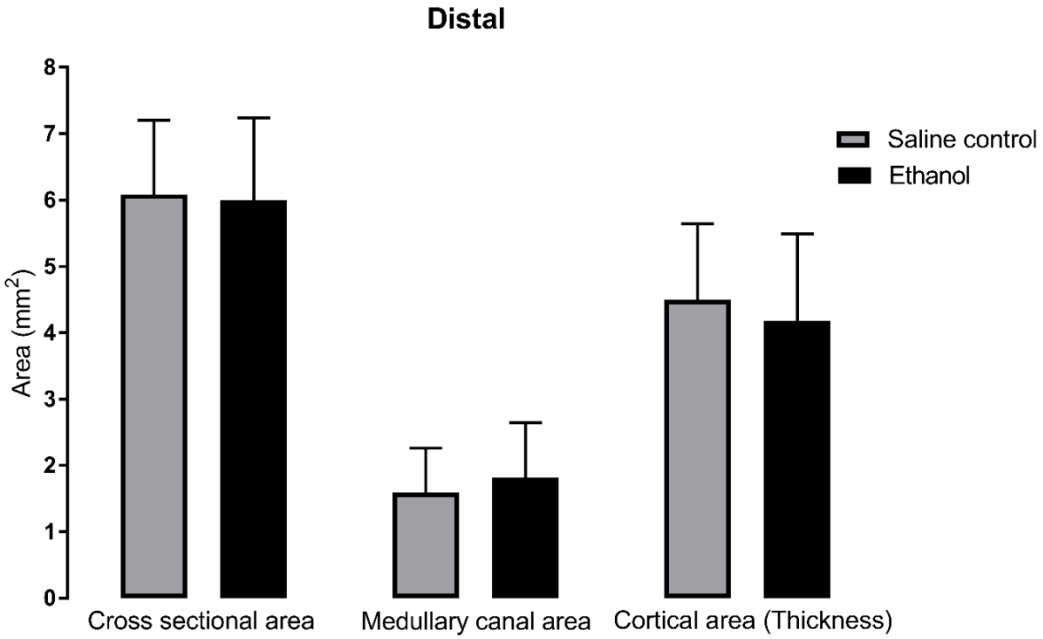


Figure 5.12: Humerus distal cross-sectional area, medullary canal area and cortical thickness at 12 weeks of age. The mean values at the 75th percentile mark given for the two groups studied. Error bars represent standard deviation.

Tensile strength of the humerus using 3-point bending tests

We detected no group differences in the bone weight between the saline controls and the ethanol group (p=0.65). The bones head diameter in the ethanol group than the saline controls. However, no significant differences were detected between the two groups (p=0.98). The maximum force and break force were greater in the ethanol group than the saline controls but not statistically significant (p=0.79 and p=0.77, respectively). With respect to the amount of time required to fracture the bones when applying force (maximum time), the 2 groups exhibited similarities (p=0.33) (Table 5.3). The energy to fracture was not different between the groups (p=0.54).

Table 5.3: Osteometric measurements and tensile strength of the humerus

		N	Mean	SD
Bone weight (g)	Saline control	9	0.489	0.078
	Ethanol	10	0.532	0.269
Head diameter (mm)	Saline control	9	4.717	0.373
	Ethanol	10	4.713	0.239
Maximum force (N)	Saline control	9	66.29	17.26
	Ethanol	10	68.35	15.26
Maximum displacement (mm)	Saline control	9	0.788	0.184
	Ethanol	10	0.826	0.141
Maximum time (Sec)	Saline control	9	10.71	3.543
	Ethanol	10	9.908	1.696
Break force (N)	Saline control	9	65.80	17.75
	Ethanol	10	68.03	15.19
Energy to fracture	Saline control	9	25.74	8.964
	Ethanol	10	28.07	7.479

5.3.3 Femur

Femur bone length at 12 weeks of age

The mean full bone length of the femur was similar among the two groups in the study (ethanol, mean = 34.20mm ±1.15; saline controls, mean = 34.95mm ±1.95) (p=0.31) (Fig. 5.13a). However, group differences in the biomechanical length occurred, being shorter in the (ethanol, mean = 26.87mm ±1.57) than the saline controls (mean = 29.29mm ±1.79) (p=0.008) (Fig. 5.13b).

Femur bicondylar breadth at 12 weeks of age

The bicondylar breadth showed marginal differences between the two groups in the study (Fig. 5.13c). The ethanol group (mean = 6.59mm ±0.412) had smaller but not significant bicondylar breadth than the saline controls (mean = 6.86 ±0.95) (p=0.165).

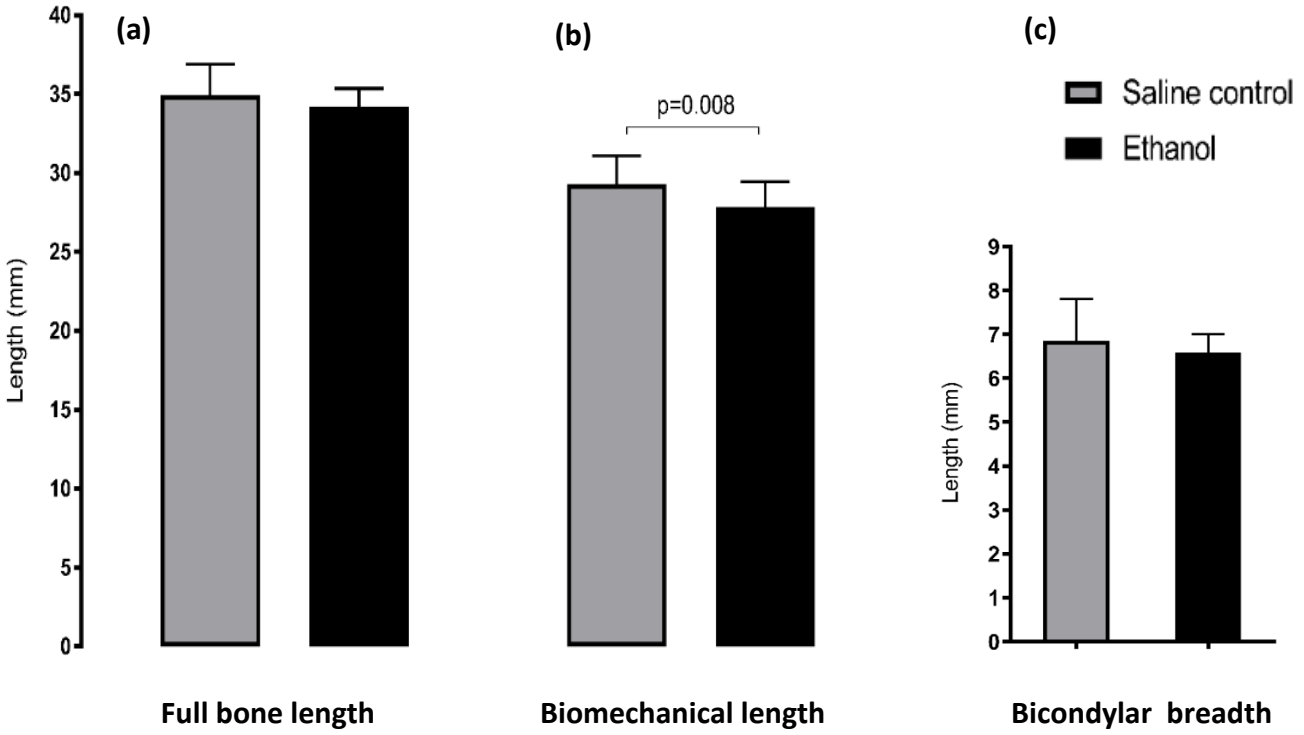


Figure 5.13: Femur osteometric measurements at 12 weeks of age. (a), full bone length; (b), biomechanical length; (c), bicondylar breadth. The lengths are given as means for the saline controls and the ethanol group. Error bars indicate standard deviation.

Femur bone to total volume ratio at 12 weeks of age (BV/TV)

In the proximal epiphysis, group differences in the bone to total volume ratio (BV/TV) were significantly smaller in the ethanol group (mean = 81.22% ±3.96) than the saline controls (mean = 85.17% ±5.39) (p=0.007) (Fig. 5.14). Similarly, the distal epiphysis displayed a marginally lower bone to total volume ratio (BV/TV) in the ethanol group (mean = 78.01% ±5.16) than the saline controls (mean = 76.48% ±7.71) with no significant differences detected (p=0.495) (Fig. 5.14).

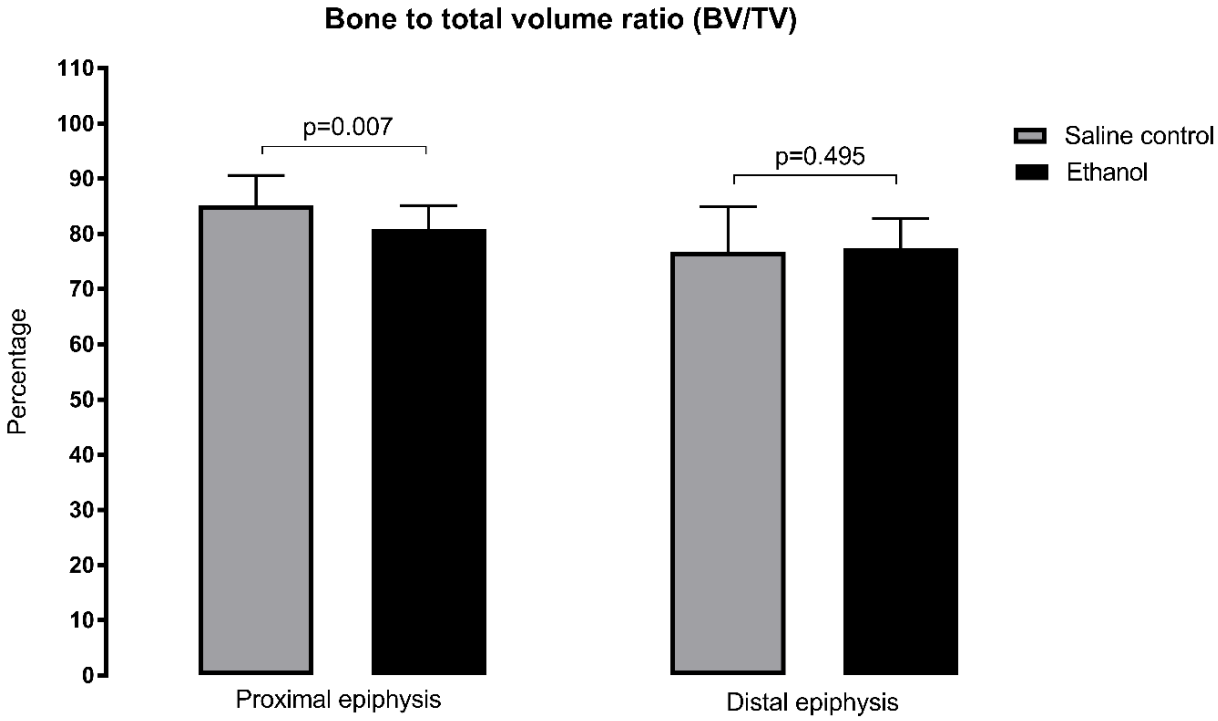


Figure 5.14: Femur bone to total volume ratio (BV/TV) at 12 weeks of age. The mean values are given for the proximal and distal epiphysis in the saline controls and the ethanol group. Error bars indicate standard deviation.

.

Femur trabecular thickness (TbTh) at 12 weeks of age

The trabecular thickness (TbTh) was similar in the study groups for both the proximal and distal extremities of the femur. In the proximal region, the ethanol group had a mean of 0.56mm ±0.14 and the saline controls had a mean of 0.51mm ±0.11. No significant differences were detected (p=0.48). In a similar pattern, the distal region the trabecular thickness did not show major differences in the ethanol group (mean = 0.36±0.13) and saline controls (mean = 0.34mm ±0.14) (p=0.41) (Fig. 5.15).

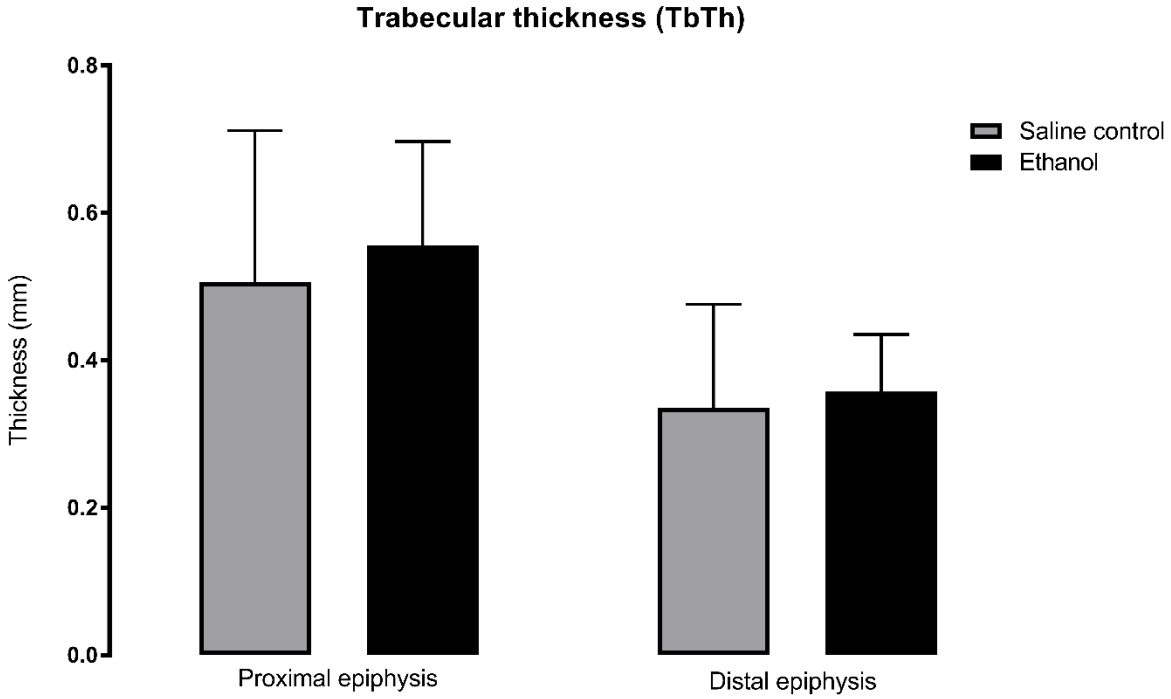


Figure 5.15: Femur trabecular thickness (TbTh) at 12 weeks of age. The mean values are given for the proximal and distal epiphysis in the saline controls and the ethanol group. Error bars indicate standard deviation.

Femur trabecular number (TbN) at 12 weeks of age

Trabecular distribution assessed by study group showed a varied pattern when stratified by the proximal and distal epiphyseal ends of the femur. In the proximal region the trabecular number (TbN) was not statistically different for the ethanol (mean = 1.71 ±0.43) compared to the saline group (mean = 2.01± 0.65) (Fig. 5.16) (p=0.079). Conversely, the distal epiphysis, exhibited fewer trabeculae (TbN) in the ethanol group (mean=2.14 ±0.26) than the saline (mean = 2.56± 0.67) (p=0.007) (Fig. 5.16).

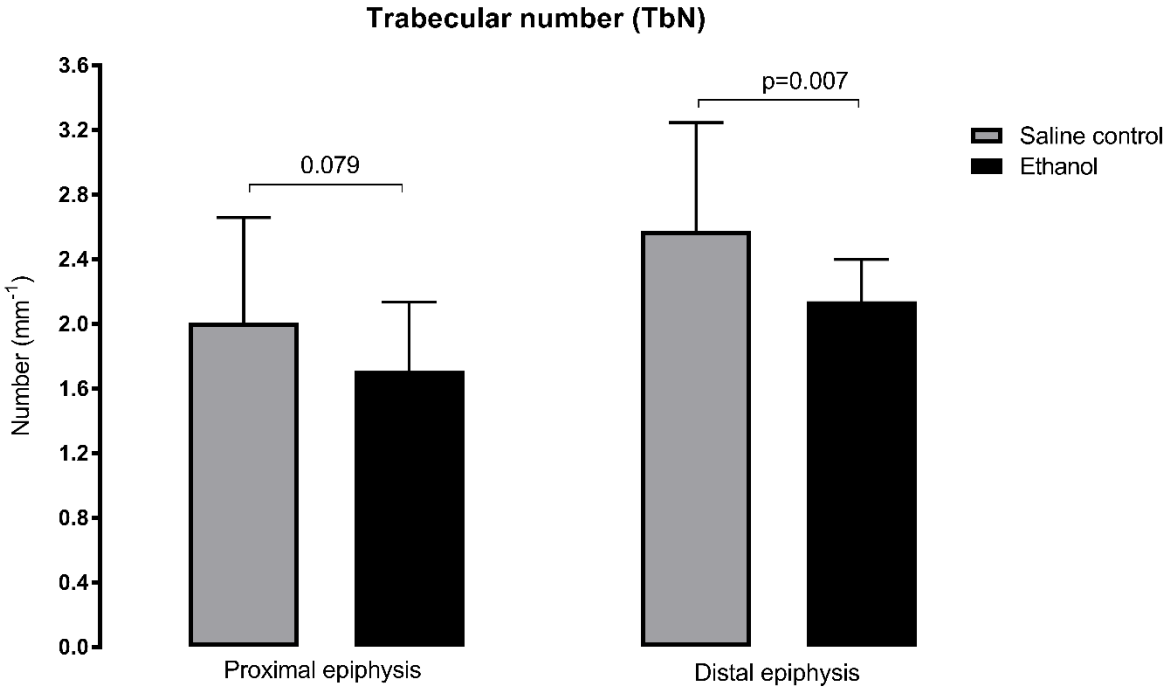


Figure 5.16: Femur trabecular number (TbN) at 12 weeks of age. The mean values are given for the proximal and distal epiphysis in the saline controls and the ethanol group. Error bars indicate standard deviation.

Femur trabecular spacing (TbSp) at 12 weeks of age

The mean trabecular spacing (TbSp) was widest in the ethanol group than saline controls in both epiphyseal ends. In the proximal epiphysis, it was significantly greater in the ethanol group (mean = 0.078mm ±0.01) than the saline controls (mean = 0.066mm ±0.01) ($p<0.001$) (Figs. 5.17 and 5.18 a and b). Similarly, the distal epiphysis, had significantly greater trabecular spacing (TbSp) for the ethanol group (mean = 0.086mm ±0.01) compared to saline (mean = 0.079mm ±0.01) ($p=0.033$) (Figs. 5.17 and 5.18 c and d).

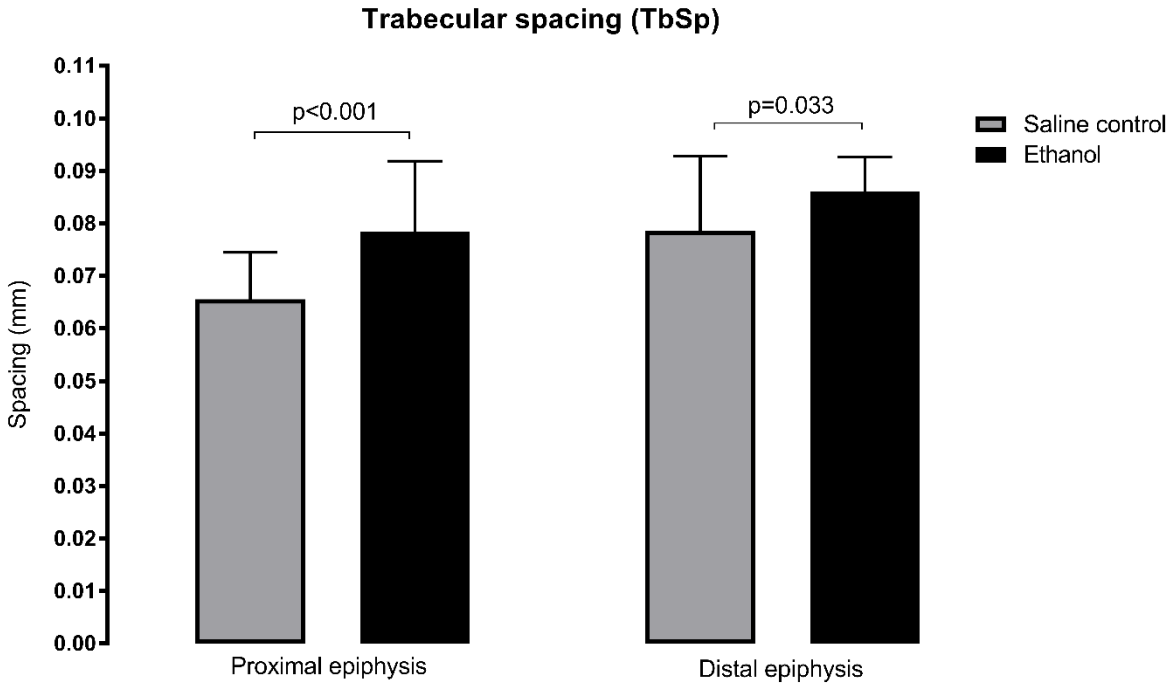


Figure 5.17: Femur trabecular spacing (TbSp) at 12 weeks of age. The mean values are given for the proximal and distal epiphysis in the saline controls and the ethanol group. Error bars indicate standard deviation.

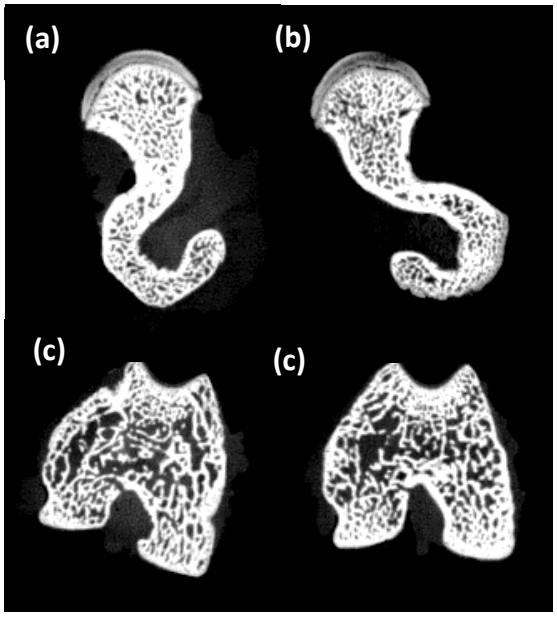


Figure 5.18: Trabecular morphology in the femur at 12 weeks of age. (a), proximal end of saline control showing more trabeculae and less spacing; (b), proximal end of the ethanol group showing fewer trabeculae and wider spacing; (c), distal end of saline control showing more trabeculae and less spacing; (d), distal end of the ethanol group showing fewer trabeculae and wider spacing.

5.3.4 Femur cross-sectional area, cortical area (thickness) and medullary canal area at 12 weeks of age

Proximal (25th percentile mark)

The proximal cross-sectional area was smaller in the ethanol group (mean = 12.43mm^2 ±1.62) than the saline controls (mean = 13.81mm^2 ±1.67) (p=0.014). We also observed a smaller medullary canal area in the ethanol group (3.59 mm^2 ±0.50) compared to the saline controls (mean = 4.75mm^2 ±1.09) (p<0.001). With respect to the cortical area (thickness) in this region, the ethanol group (mean = 14.79 mm^2 ±2.99) only exhibited a marginally lower value compared to the saline controls (mean = 14.83 mm^2 ±2.76) (p=0.36) (Fig. 5.19).

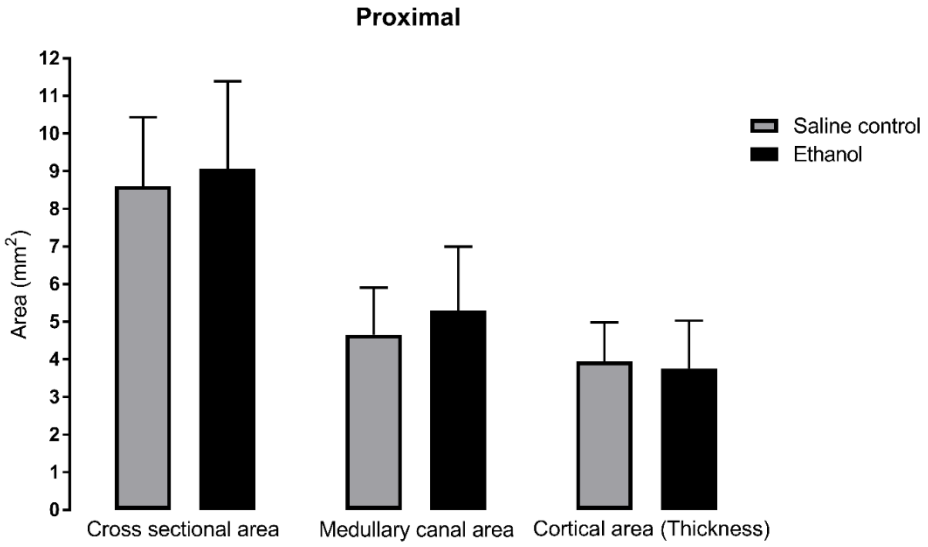


Figure 5.19: Femur proximal cross-sectional area, medullary canal area and cortical thickness at 12 weeks of age. The means at the 25th percentile mark given for the two groups studied. Error bars represent standard deviation.

Midshaft (50th percentile mark)

The midshaft cross-sectional area varied in the two groups studied with the ethanol group showing a slightly lower and not significant mean of 10.89mm^2 ±1.51 than the saline controls (mean = 11.78mm^2 ±1.39) (p=0.06) (Fig. 5.20). Conversely, the medullary canal area in the ethanol (mean = 4.75 ±1.36) had a significantly smaller medullary canal area than the saline group (mean = 5.33mm^2 ±1.46) (p=0.018) (Fig. 5.20). Regarding cortical area (thickness) in this region, the ethanol group (mean = 6.29mm^2 ±0.99) exhibited only a marginally lower value compared to the saline (mean = 6.59mm^2 ±1.05) (Fig. 5.20) (p=0.33).

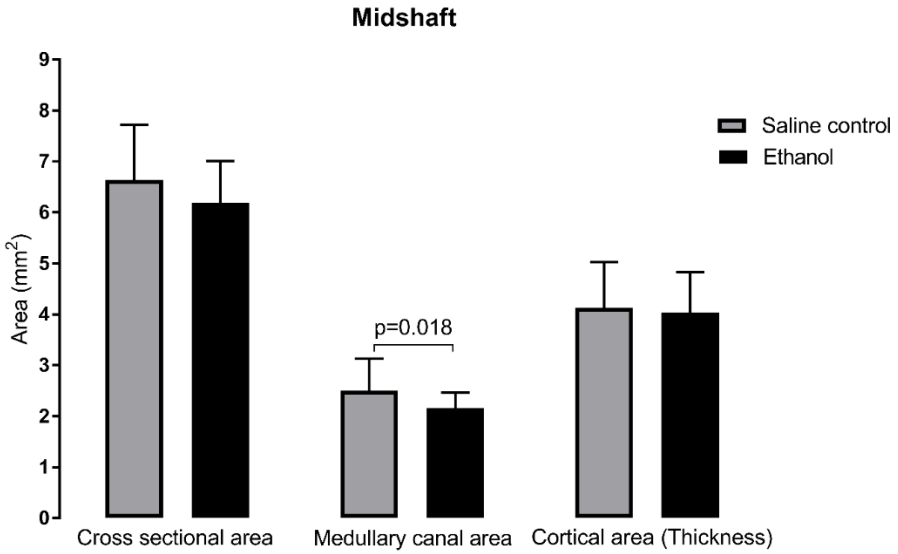


Figure 5.20: Femur midshaft cross-sectional area, medullary canal area and cortical thickness at 12 weeks of age. The means at the 50th percentile mark given for the two groups studied. Error bars represent standard deviation.

Distal (75th percentile mark)

The distal cross-sectional area was similar in the ethanol group (mean = 14.79mm^2 ±2.99) compared to the saline controls (mean = 14.83mm^2 ±2.77) (p=0.99) (Fig. 5.21). Also, the medullary canal area was similar between the groups (ethanol; mean = 9.36mm^2 ±2.48, saline controls; mean = 9.28mm^2 ±2.05) (p=0.95) (Fig. 5.21). This observation of similarity between the ethanol group and saline controls continued for the cortical area (thickness) in this bone region (mean = 5.43mm^2 ±1.15; and 5.55mm^2 ±1.08, respectively).

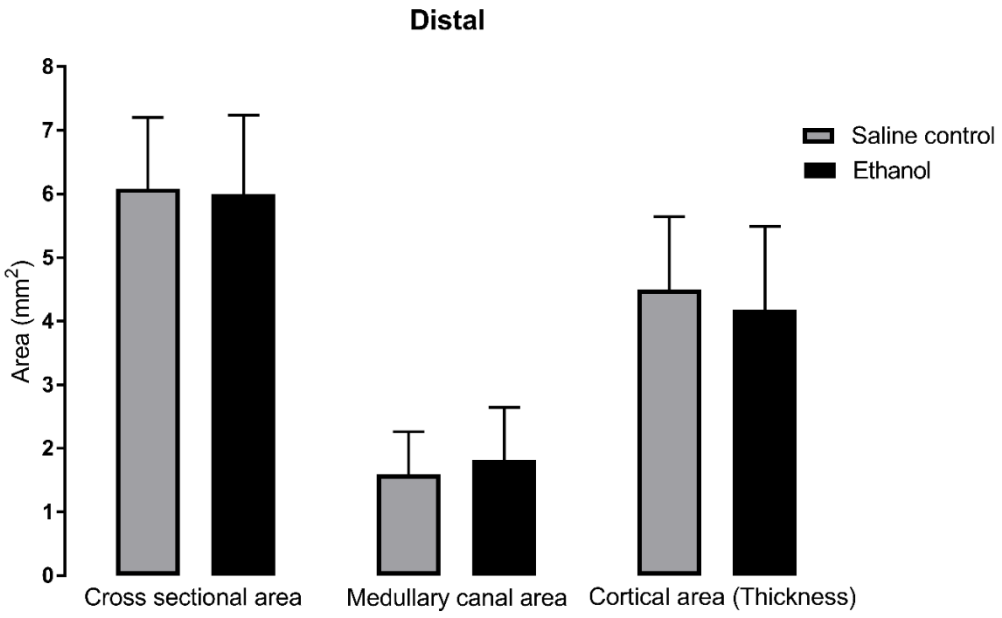


Figure 5.21: Femur distal cross-sectional area, medullary canal area and cortical thickness at 12 weeks of age. The means at the 75th percentile mark given for the two groups studied. Error bars represent standard deviation.

Tensile strength of the femur using 3-point bending tests

We observed a marginally lower and no significant bone weight in the ethanol group than the saline control as indicated in table 5.4 (p=0.78). Also, the maximum force and break force were similar in the ethanol group and the saline controls (p=0.98 and p=0.67, respectively). With respect to the maximum time required to fracture, the ethanol group displayed a lower value than saline controls (Table 5.4). Again, there were no statistical group differences detected (p=0.73). The energy to fracture was appeared to be lower in the ethanol group than the saline control but not statistically significant (p=0.71).

Table 5.4: Osteometric measurements and tensile strength of the femur.

		N	Mean	SD
Bone weight (g)	Saline control	10	1.034	0.2
	Ethanol	10	1.011	0.155
Maximum Force (N)	Saline control	10	86.33	10.89
	Ethanol	10	86.19	11.61
Maximum Displacement (mm)	Saline control	10	1.598	0.459
	Ethanol	10	1.519	0.555
Maximum Time (Sec)	Saline control	10	19.16	5.506
	Ethanol	10	18.22	6.662
Break Force(N)	Saline control	10	85.75	10.86
	Ethanol	10	83.67	10.26
Energy to fracture	Saline control	10	68.06	20.62
	Ethanol	10	63.93	27.03

5.3.5 Major parameters for the ethanol and saline controls

Principal components analysis was conducted to assess how femur and humerus morphology parameters clustered. These variables were the bone length, BV/TV, TbTh, TbN, TbSp. Two components were used based on the eigenvalues above 1 criterion. After rotation, the first component accounted for 91.4% of the variance, and the second component accounted for 8.6% of the variance. In component 1 Femur BV/TV and TbSp, Femur biomechanical length, Humerus BV/TV and TbSp, Femur Distal TbN, Humerus length, Humerus TbN (Table 5.5 and Fig. 5.22).

Table 5.5: Principal components analysis of femur and humerus. The contributing variables are arranged in descending order according to component 1, with major contributors in bold (above ±0.3).

Parameter	PC 1	PC 2
Femur Distal BV/TV	**0.971**	0.238
Femur biomechanical length	**0.445**	0.060
Femur Proximal BV/TV	**0.435**	0.150
Humerus Proximal BV/TV	**0.423**	0.383
Humerus Proximal TbN	**0.405**	-0.137
Femur Distal TbN	**0.370**	-0.018
Humerus length	**0.350**	0.087
Humerus Distal TbN	**0.326**	0.303
Humerus epicondylar breadth	0.299	-0.026
Femur bicondylar breadth	0.230	-0.109
Femur length	0.216	0.051
Femur Proximal TbN	0.108	0.232
Humerus Distal TbTh	0.101	-0.369
Femur Proximal TbTh	-0.014	-0.149
Humerus Proximal TbTh	-0.049	0.036
Femur Distial TbTh	-0.058	0.011
Femur DistTbSp	**-0.318**	-0.017
Humerus ProxTbSp	**-0.394**	-0.047
Humerus Distal TbSp	**-0.418**	-0.075
Femur Proximal TbSp	**-0.572**	-0.067

Humerus Distal BV/TV	**-0.933**	0.359

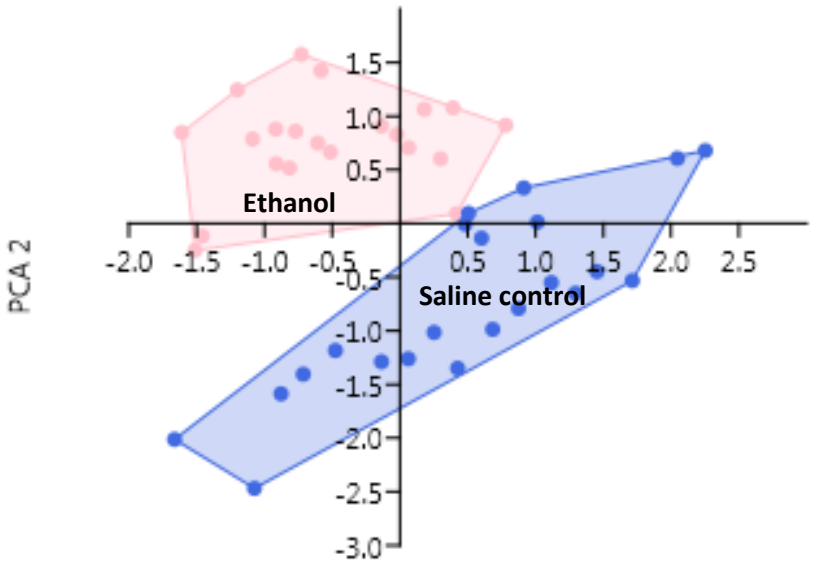


Figure 5.22: Principal component analysis. Indicating the level of correlation between the ethanol group and saline control for the femur and humerus.

5.4 DISCUSSION

In this chapter, we tested the theory that gestational alcohol exposure has detrimental effects on skeletal elements lasting through adult life using a rat model of binge drinking throughout pregnancy. These effects are known to be characterised by shorter, weaker and osteoporotic bones that have a high propensity for fracture (Diamond et al., 1989; Sampson et al., 1996; Osterhoff et al., 2016). Since these effects may be different per skeletal element, we have used the humerus and the femur in the current study as these 2 bones are less commonly investigated regarding gestational alcohol exposure (Simpson et al., 2005; Snow and Keiver, 2007). We found that humeri were shorter, whereas only a shorter biomechanical length was observed in the femur. The trabecular morphometric parameters were smaller for the ethanol group with larger trabecular spacing. In both, the humerus and femur, cortical and medullary dimensions remained unaffected in the proximal and distal regions. In contrast, a smaller medullary canal thickness occurred in the midshaft of both bones for the ethanol group.

Having found shorter humeri in this study corroborates previous study findings that gestational alcohol results in shorter bones. Although the full femoral length was not significantly shorter in our study, the biomechanical length was shorter in the ethanol group. This is important to note because the biomechanical length represents the parts of the femur responsible for load-bearing. These findings support the idea that gestational ethanol exposure results in shorter bones, potentially translating to short stature as seen in FAS children (O'Leary, 2004)

Both the humerus and the femur showed fewer trabeculae that were more widely spaced in the ethanol group. This was accompanied by a smaller bone to volume ratio (BV/TV) in the ethanol group for both bones. Therefore, at 12 weeks of age after prenatal alcohol exposure in the current study, the trabecular morphometric parameters were affected in a similar manner and extent in both humerus and the femur. These 2 bones are not widely studied as most studies on prenatal alcohol exposure focus on the tibia, radius and ulna (Weinberg et al., 1990; Keiver et al., 1996; Keiver and Weinberg, 2004).

The effects on the humerus and femur are variable among the studies (Weinberg et al., 1990; Keiver et al., 1996; Snow and Keiver, 2007). In contrast, our study has shown that both the humerus and femur were affected in a similar manner even up to 12 weeks of postnatal life following gestational alcohol exposure. We, therefore, recommend that the humerus can equally be used for such studies.

A smaller medullary canal area was observed in the midshaft of both the humerus and femur. This could have compensated for possible bone weakness as the cortical thickness was proportionally larger with a reduction in the medullary canal area. Since the midshaft is also the part that was tested for strength in 3-point bending tests, this could explain why we did not find group differences in bone strength. This finding of a small medullary canal area obtained in our study fails to support the theory that gestational alcohol causes weaker bones. However, it supports the idea of potential catch up growth in children born small for age due to mothers drinking in pregnancy.

Studies suggest that children of mothers who drink in pregnancy may have a recovery period in postnatal life if nutritional interventions are provided (Abel, 1982; Shankar et al., 2007). This stems from the proposition that mothers who continue to drink in pregnancy tend to belong to the lower socioeconomic status which affects their ability to provide adequate nutrition to their offspring both during gestation and in postnatal life (May et al., 2013). It is possible that the rat chow provided to all the animals in the study may have mitigated the detrimental effects of gestational alcohol exposure, resulting in the observed minor group differences at the postnatal age of 12 weeks.

In the 12-week-old groups, principal components analysis revealed that BV/TV, TbN and TbSp were the most affected parameters in both the humerus and femur. These are the parameters that also showed significant differences between the groups. This finding suggests that the previously reported bone weakening that occurs in bones of individual exposed to alcohol during gestation may be through the disturbances in trabecular morphology.

5.4.1 Conclusions

Alcohol resulted in shorter bones in our study. Both the humerus and the femur exhibited that gestational alcohol exposure causes thinner trabeculae that are more widely spaced and with a smaller bone to volume ratio (BV/TV). A similar finding was made on both the humerus and femur, suggesting that either the humerus or the femur is a suitable candidate for similar studies. However, the tensile strength was similar in the ethanol and saline groups, supporting the proposition of postnatal recovery when adequate nutrition is provided.

Chapter 6

General discussion and conclusions

6.0 GENERAL DISCUSSION

We sought to investigate whether bone growth, development and osseous tissue structural integrity disturbances would persist through postnatal life in 3 and 12-week-old humerus and femur in a binge drinking rat model. To achieve this, we started by evaluating body size parameters of the pups exposed to gestational alcohol. To assess whether gestational alcohol causes stunted growth through disturbances of epiphyseal growth plate chondrocyte activity, we immunolabelled these chondrocytes for Ki-67 protein expression. We then evaluated whether exposure to gestational alcohol affects bone growth and development through inhibiting chondrocyte multiplication by anti TGFβ1 antibody immunolabeling. Then, we used three-dimensional micro-focus X-ray computed tomography (3D- μCT) to assess trabeculae thickness, volume, number and spacing in the proximal and distal epiphysis of the femur and humerus. Finally, we tested the theory that gestational alcohol exposure increases fracture risk (weakens bones) by using 3-point bending tests to assess bone strength.

Our study queried the extent to which intrauterine alcohol exposure would affect bone growth and development in a rat model of moderate binge drinking. This model is appropriate in the South African context where binge drinking is common (Conover and Jones, 2012). No group differences in weight gain, food intake, gestation duration and litter size were observed despite one group receiving alcohol. In contrast, the pups had a smaller average crown rump length (CRL) in the ethanol group at birth up to the third week of life. However, this smaller CRL observed in the ethanol group did not persist in the 12-week-old groups. This supports the proposition that the effects of prenatal exposure may be mitigated in postnatal life. Since all animals in the study received balanced nutrition, we attribute this lack of adverse ethanol effects in the 12-week-old rats to the good diet (rat chow). However, in society, woman who drink during pregnancy tend to have poor nutrition both in pregnancy and postpartum (Shankar et al., 2007). This (poor nutrition) may potentially prevent amelioration of gestational alcohol effects in later life.

Growth plate size and cell proliferation

Previous studies attributed the stunted growth observed in offspring of mothers who conceded to drinking during pregnancy to a smaller epiphyseal growth plate size (Miralles-Flores and Delgado-Baeza, 1992). Other researchers (Snow and Keiver, 2007) also found fewer chondrocytes in the epiphyseal growth plate of offspring exposed to gestational alcohol using animal studies. Similarly, our study made the same findings of smaller epiphyseal growth plates with fewer chondrocytes in the pups from the ethanol treated group. With this knowledge, we then proposed and tested the that theory that epiphyseal growth plate chondrocyte proliferation is inhibited by exposure to alcohol during gestation. Using immunohistolochemical methods (Ki-67), we showed that exposure to alcohol during gestation results in decreased chondrocyte proliferation in the epiphyseal growth plate. The findings in the present study were made in both the femur and humerus.

Osteometric dimensions of the humerus and femur were included in the parameters to facilitate the estimation of bone size. This follows from the existing literature showing that exposure to gestational alcohol results in short stature (Snow and Keiver, 2007; Popova et al., 2017). The humerus length remained unaffected both at 3 and 12-week groups as no group differences were detected. In contrast, the ethanol group exhibited shorter femora in the 3-week group although no differences were observed in the 12-week-old groups. Our results also support the idea of possible catch up growth when good nutrition is provided to FAS children (Shankar et al., 2007). Also, the dose of alcohol administered in the current study was moderate (25.2%), a higher dosage of 36%, may affect the outcome differently.

TGFβ1 antibody was utilized to quantify chondrocytes expression of this cytokine. We found that TGFβ1 immunopositive chondrocytes were fewer in the alcohol group. This was coupled with smaller epiphyseal growth plates containing fewer chondrocytes and displaying compromised proliferation rates in the ethanol group. With these findings, we propose that intrauterine alcohol exposure inhibits TGFβ1 expression, leading to fewer chondrocytes that also proliferate at a slower rate in the epiphyseal growth plates. We

suggest that this is one of the plausible ways in which intrauterine alcohol exposure causes a shorter stature as seen in FAS children.

Parameters most affected by prenatal ethanol exposure

In the 3-week-old samples, we found differences in the main parameters that determined group membership into either ethanol or saline control for the humerus and femur using binary logistic regression. In the humerus the distal BV/TV and trabecular number (TbN) were the main parameters that determined group membership. This means that these two parameters (distal BV/TV and TbN) are affected the most in gestational alcohol exposure. The distal bone parameters varied more between the groups. This may explain why none of the samples were misclassified in the distal part. In contrast, no proximal trabecular parameters could be singled out as crucial for correct group membership assignment into ethanol or saline. This means that group variations were minimal with respect to the proximal bone parameters. Therefore, this could mean that prenatal alcohol exposure affected the humerus extremities differently, with the distal being affected the most.

With respect to the femur, binary logistic regression revealed that the shaft volume, length and proximal cortical thickness were the main parameters that determined group membership into either ethanol or saline control. This means that these three parameters are affected the most in gestational alcohol exposure. When using the proximal trabeculae morphometric parameters more saline control were misclassified as belonging to the ethanol group. This suggest that there was less group variation in these parameters. This in turn suggests that the intrauterine ethanol effects in the femur may be minimal for the proximal aspect of the bone. Our results show that, in the humerus, trabecular morphometry was disturbed the most whereas external dimensions were affected the most in the femur. This further supports the theory that prenatal alcohol exposure affects various skeletal elements differently.

In the 12-week-old groups, principal components analysis revealed that BV/TV, TbN and TbSp were the most affected parameters in both the humerus and femur. This agrees with

our hypothesis that prenatal alcohol exposure would cause fewer, more spaced out trabecular with a lower bone to total volume ratio. Only in the humerus was length part of the principal components. This shows that in our model of binge drinking, the effects of alcohol in fetal stages persisted to postnatal week 12. These findings support the idea that a recovery from gestational alcohol effects in postnatal life is not always possible.

Our study is the first to have studied bone strength at postnatal week 12 in samples from rats exposed to ethanol during gestation. We did not find differences in bone strength using 3-point bending tests in the ethanol group and saline controls in this study. This agrees with the observation that cortical thickness and medullary canal area did not contribute to the principal components for the ethanol and saline controls. However, our findings do not support the observation that FAS children have bones prone to fracture. This may be due to the daily single dosage of alcohol given unlike having the alcohol in drinking water which ensures multiple alcohol intake per day.

6.1 CONCLUSIONS

1. Binge drinking affects offspring CRL at birth to at least 3 weeks postnatally but not at 12 weeks after birth.

2. Exposure to alcohol during gestation results in a smaller epiphyseal growth plate size with decreased chondrocyte proliferation.

3. Intrauterine alcohol exposure affects bone development and trabecular morphological properties through inhibiting the expression of TGFβ-1 in epiphyseal growth plate chondrocytes.

4. Our study partly supports the proposition that there is potential for bone health recovery in postnatal life if a diet with adequate nutrition is provided post weaning.

5. Our results on trabecular morphometric parameters suggest that the epiphyseal ends of the bone tend to suffer the detrimental effects of gestational exposure to alcohol through the adult like (12 weeks postnatal life in the present study).

6. In the humerus (at age 3 weeks) the distal BV/TV and trabecular number (TbN) were the main parameters affected the most by gestational alcohol exposure, as shown by binary logistic regression.

7. In the femur (at age 3 weeks), binary logistic regression revealed that that shaft volume, length and proximal cortical thickness were the main parameters affected the most in gestational alcohol exposure.

8. In the 12-week-old groups, principal components analysis revealed that BV/TV, TbN and TbSp were the most affected parameters in both the humerus and femur

7.0 REFERENCES

Abel EL. 1982. Consumption of alcohol during pregnancy: a review of effects on growth and development of offspring. Hum Biol 54:421-453.

Abel EL, Dintcheff BA. 1978. Effects of prenatal alcohol exposure on growth and development in rats. J Pharmacol Exp Ther 207:916-921.

Abel EL, Hannigan JH. 1995. Maternal risk factors in fetal alcohol syndrome: provocative and permissive influences. Neurotoxicol Teratol 17:445-462.

Adebsi S. 2005. Alcohol effects on embryonal bone growth. Niger J Surg Res 7:152-158.

Bagi CM, Hanson N, Andresen C, Pero R, Lariviere R, Turner CH, Laib A. 2006. The use of Micro-CT to evaluate cortical bone geometry and strength in nude rats: correlation with mechanical testing, pQCT and DXA. Bone 38:136-144.

Baron R, Tross R, Vignery A. 1984. Evidence of sequential remodeling in rat trabecular bone: morphology, dynamic histomorphometry, and changes during skeletal maturation. Anat Rec 208:137-145.

Beyers N, Moosa A. 1978. The fetal alcohol syndrome. S Afr Med J 54:575-578.

Bismar H, Kloppinger T, Schuster EM, Balbach S, Diel I, Ziegler R, Pfeilschifter J. 1999. Transforming growth factor beta (TGF-beta) levels in the conditioned media of human bone cells: relationship to donor age, bone volume, and concentration of TGF-beta in human bone matrix in vivo. Bone 24:565-569.

Bonewald LF. 2011. The amazing osteocyte. J Bone Miner Res 26:229-238.

Boskey AL, Coleman R. 2010. Aging and bone. J Dent Res 89:1333-1348.

Bouxsein ML, Boyd SK, Christiansen BA, Guldberg RE, Jepsen KJ, Muller R. 2010. Guidelines for assessment of bone microstructure in rodents using micro-computed tomography. J Bone Miner Res 25:1468-1486.

Broulik P, Vonrova J, Ruzicka P, Sedlacek R, Zima T. 2010. The effect of chronic alchol administration on bone mineral content and bone strength in male rats. Physiol Res 59:599-601.

Burdan F, Szumilo J, Korobowicz A, Farooquee R, Patel S, Patel A, Dave A, Szumilo M, Solecki M, Klepacz R, Dudka J. 2009. Morphology and physiology of the epiphyseal growth plate. Folia histochemica et cytobiologica 47:5-16.

Cederbaum AI. 2012. Alcohol metabolism. Clin Liver Dis 16:667-685.

Chapurlat RD, Confavreux CB. 2016. Novel biological markers of bone: from bone metabolism to bone physiology. Rheumatology 55:1714-1725.

Chaudhuri JD. 2000. Alcohol and the developing fetus: a review. Med Sci Monit 6:1031-1041.

Chen G, Deng C, Li Y. 2012. TGF-B and BMP signaling in osteoblast differentiation and bone formation. Int J Biol Sci 8:272-288.

Chen H, Hayakawa D, Emura S, Ozawa Y, Taguchi H, Yano R, Shoumura S. 2001. Effects of ethanol on the ultrastructure of the hamster femur. Histol Histopathol 16:763-770.

Chudley AE, Conry J, Cook JL, Loock C, Rosales T, LeBlanc N, Public Health Agency of Canada's National Advisory Committee on Fetal Alcohol Spectrum D. 2005. Fetal alcohol spectrum disorder: Canadian guidelines for diagnosis. CMAJ 172:S1-S21.

Conover E, Jones K. 2012. Safety concerns regarding binge drinking in pregnancy: A review. Birth defects research: Part A, Clinical and molecular teratology. Clin Mol Teratol 94:570-575.

Cooper C, Eriksson JG, Forsen T, Osmond C, Tuomilehto J, Barker DJ. 2001. Maternal height, childhood growth and risk of hip fracture in later life: a longitudinal study. Osteoporos Int 12:623-629.

Croxford J, Viljoen D. 1999. Alcohol consumption by pregnant women in the Western Cape. S Afr Med J 89:962-965.

Day N, Jasperse D, Richardson G, Robies N, Sambamoorthi U, Taylor P, Scher M, Stoffer D, Cornelius M. 1989. Prenatal exposure to alcohol: effect on infant growth and morphological characteristics. Pediatrics 84:536-541.

Del Fattore A, Teti A, Rucci N. 2012. Bone cells and the mechanisms of bone remodelling. Frontiers in bioscience (Elite edition) 4:2302-2321.

Diamond T, Stiel D, Lunzer M, Wilkinson M, Posen S. 1989. Ethanol reduces bone formation and may cause osteoporosis. The American journal of medicine 86:282-288.

Diez A, Serrano S, Cucurull J, Marinoso L, Bosch J, Puig J, Nogues X, Aubia J. 1997. Acute effects of ethanol on mineral metabolism and trabecular bone in Sprague-Dawley rats. Calcif Tissue Int 61:168-171.

Driver J, Weber CE, Callaci JJ, Kothari AN, Zapf MA, Roper PM, Borys D, Franzen CA, Gupta GN, Wai PY, Zhang J, Denning MF, Kuo PC, Mi Z. 2015. Alcohol inhibits osteopontin-dependent transforming growth factor-beta1 expression in human mesenchymal stem cells. J Biol Chem 290:9959-9973.

Erben RG. 1996. Trabecular and endocortical bone surfaces in the rat: modeling or remodeling? Anat Rec 246:39-46.

Ertem K, Kekilli E, Elmali N, Ceylan F. 2006. The effects of alcohol exposure during intrauterine and postnatal period on bone mineral density and bone growth and body weight in rats' virgin offspring. Eur J Gen Med 3:54-57.

Farr JN, Khosla S. 2015. Skeletal changes through the lifespan: from growth to senescence. Nat Rev Endocrinol 11:513-521.

Fitzpatrick JP, Elliott EJ, Latimer J, Carter M, Oscar J, Ferreira M, Olson HC, Lucas B, Doney R, Salter C, Peadon E, Hawkes G, Hand M. 2012. The Lililwan project: study protocol for a population-based active case ascertainment study of the prevalence of fetal alcohol spectrum disorders (FASD) in remote Australian Aboriginal communities. BMJ Open 2:e000968.

Godfrey K, Walter K, Robinson S, Taylor P, Shore S, Wheeler T, Cooper C. 2001. Neonatal bone mass influence of parental birthweight, maternal smoking,body composition,and activity during pregancy. J Bone Miner Res 16:1694-1703.

Hadjidakis DJ, Androulakis II. 2006. Bone remodeling. In: George C, George M, George PC, editors. Women's health and disease: gynecologic, endocrine, and reproductive issues: Wiley. p 385-396.

Hogan HA, Sampson HW, Cashier E, Ledoux N. 1997. Alcohol consumption by young actively growing rats: a study of cortical bone histomorphometry and mechanical properties. Alcohol Clin Exp Res 21:809-816.

Hoyme HE, Kalberg WO, Elliott AJ, Blankenship J, Buckley D, Marais AS, Manning MA, Robinson LK, Adam MP, Abdul-Rahman O, Jewett T, Coles CD, Chambers C, Jones KL, Adnams CM, Shah PE, Riley EP, Charness ME, Warren KR, May PA. 2016. Updated clinical guidelines for diagnosing fetal alcohol spectrum disorders. Pediatrics 138:e20154256.

Hoyme HE, May PA, Kalberg WO, Kodituwakku P, Gossage JP, Trujillo PM, Buckley DG, Miller JH, Aragon AS, Khaole N, Viljoen DL, Jones KL, Robinson LK. 2005. A practical clinical approach

to diagnosis of fetal alcohol spectrum disorders: clarification of the 1996 institute of medicine criteria. Pediatrics 115:39-47.

Hsu JT, Wang SP, Huang HL, Chen YJ, Wu J, Tsai MT. 2013. The assessment of trabecular bone parameters and cortical bone strength: a comparison of micro-CT and dental cone-beam CT. J Biomech 46:2611-2618.

Idrus NM, Breit KR, Thomas JD. 2017. Dietary choline levels modify the effects of prenatal alcohol exposure in rats. Neurotoxicol Teratol 59:43-52.

Jacobson JL, Jacobson SW, Sokol RJ, Ager JW, Jr. 1998. Relation of maternal age and pattern of pregnancy drinking to functionally significant cognitive deficit in infancy. Alcohol Clin Exp Res 22:345-351.

Jones G, Dwyer T. 2000. Birth weight,birth length,and bone density in prepubertal children: evidence for an association that may be mediated by genetic factos. Calcif Tissue Int 67:304-308.

Jones K, Smith D, Ulleland C, Streissguth P. 1973. Pattern of malformation in offspring of chronic alcohol mothers. Lancet 1:1267-1271.

Kanaan R, A Kanaan L. 2006. Transforming growth factor β1, bone connection. Med Sci Monit 12:RA164-169.

Kanis JA, Borgstrom F, De Laet C, Johansson H, Johnell O, Jonsson B, Oden A, Zethraeus N, Pfleger B, Khaltaev N. 2005. Assessment of fracture risk. Osteoporos Int 16:581-589.

Kasagi S, Chen W. 2013. TGF-beta1 on osteoimmunology and the bone component cells. Cell Biosci 3:4.

Katwan E, Adnams C, London L. 2011. Childhood behavioural and developmental disorders: association with maternal alcohol consumption in Cape Town, South Africa. S Afr Med J 101:724, 726-727.

Keiver K, Ellis L, Anzarut A, Weinberg J. 1997. Effect of prenatal ethanol exposure on fetal calcium metabolism. Alcohol Clin Exp Res 21:1612-1618.

Keiver K, Herbert L, Weinberg J. 1996. Effect of maternal ethanol consumption on maternal and fetal calcium metabolism. Alcohol Clin Exp Res 20:1305-1312.

Keiver K, Weinberg J. 2003. Effect of duration of alcohol consumption on calcium and bone metabolism during pregancy in the ra. Alcohol Clin Exp Res 27:1507-1519.

Keiver K, Weinberg J. 2004. Effect of duration of maternal alcohol consumption on calcium metabolism and bone in the fetal rat. Alcohol Clin Exp Res 28:456-467.

Kierszenbaum AL, Tres LL. 2012. Histology and cell biology : An introduction to pathology, 3rd ed. Philadelphia, PA: Saunders.

Kini U, Nandeesh BN. 2012. Physiology of bone formation, remodeling, and metabolism. In: Fogelman I, Gnanasegaran G, van der Wall H, editors. Radionuclide and Hybrid Bone Imaging. Berlin, Heidelberg: Springer p29-57.

Koren G. 2012. The first description of fetal alcohol syndrome by French pediatrician Paul Lemoine. Journal of population therapeutics and clinical pharmacology = Journal de la therapeutique des populations et de la pharamcologie clinique 19:e223.

Koren G, Nulman I, Chudley AE, Loocke C. 2003. Fetal alcohol spectrum disorder. CMAJ 169:1181-1185.

Kotha SP, Guzelsu N. 2007. Tensile behavior of cortical bone: dependence of organic matrix material properties on bone mineral content. J Biomech 40:36-45.

Lee M, Leichter J. 1980. Effect of litter size on the physical growth and maturation of the offspring of rats given alcohol during gestation. Growth 44:327-335.

Lemoine P, Harousseau H, Borteyru JP, Menuet JC. 2003. Children of alcoholic parents: observed anomalies: discussion of 127 cases. Ther Drug Monit 25:132-136.

Leppanen O, Sievanen H, Jokihaara J, Pajamaki I, Jarvinen TL. 2006. Three-point bending of rat femur in the mediolateral direction: introduction and validation of a novel biomechanical testing protocol. J Bone Miner Res 21:1231-1237.

Liangpunsakul S, Crabb DW, Qi R. 2010. Relationship among alcohol intake, body fat, and physical activity: a population-based study. Annals of epidemiology 20:670-675.

Lui JC, Nilsson O, Baron J. 2011. Growth plate senescence and catch-up growth. Endocr Dev 21:23-29.

Maddalozzo GF, Turner RT, Edwards CH, Howe KS, Widrick JJ, Rosen CJ, Iwaniec UT. 2009. Alcohol alters whole body composition, inhibits bone formation, and increases bone marrow adiposity in rats. Osteoporos Int 20:1529-1538.

Margolis DS, Kim D, Szivek JA, Lai LW, Lien YH. 2006. Functionally improved bone in calbindin-D28k knockout mice. Bone 39:477-484.

Marrs JA, Clendenon SG, Ratcliffe DR, Fielding SM, Liu Q, Bosron WF. 2010. Zebrafish fetal alcohol syndrome model: effects of ethanol are rescued by retinoic acid supplement. Alcohol 44:707-715.

Martin EA, Ritman EL, Turner RT. 2003. Time course of epiphyseal growth plate fusion in rat tibiae. Bone 32:261-267.

Martin RM, Correa PH. 2010. Bone quality and osteoporosis therapy. Arq Bras Endocrinol Metabol 54:186-199.

Martini F, Nath JL, Bartholomew EF. 2015. Fundamentals of anatomy & physiology: Pearson.

Maurel D, Boisseau N, Benhamou C, Jaffre C. 2012a. Cortical bone is more senstive to alcohol dose effects than trabecular bone in the rat. Bone 79:492-499.

Maurel DB, Boisseau N, Benhamou CL, Jaffre C. 2012b. Alcohol and bone: review of dose effects and mechanisms. Osteoporos Int 23:1-16.

Maurel DB, Jaffre C, Rochefort GY, Aveline PC, Boisseau N, Uzbekov R, Gosset D, Pichon C, Fazzalari NL, Pallu S, Benhamou CL. 2011. Low bone accrual is associated with osteocyte apoptosis in alcohol-induced osteopenia. Bone 49:543-552.

May PA, Blankenship J, Marais AS, Gossage JP, Kalberg WO, Barnard R, De Vries M, Robinson LK, Adnams CM, Buckley D, Manning M, Jones KL, Parry C, Hoyme HE, Seedat S. 2013. Approaching the prevalence of the full spectrum of fetal alcohol spectrum disorders in a South African population-based study. Alcohol Clin Exp Res 37:818-830.

McCalden RW, McGeough JA, Barker MB, Court-Brown CM. 1993. Age-related changes in the tensile properties of cortical bone. The relative importance of changes in porosity, mineralization, and microstructure. The Journal of bone and joint surgery American volume 75:1193-1205.

Mikosch P. 2014. Alcohol and bone. Wien Med Wochenschr 164:15-24.

Miralles-Flores C, Delgado-Baeza E. 1992. Histomorphometric analysis of the epiphyseal growth plate in rats after prenatal alcohol exposure. J Orthop Res 10:325-336.

Naassila M, Pierrefiche O. 2019. GluN2B subunit of the NMDA receptor: the keystone of the effects of alcohol during neurodevelopment. Neurochem Res 44:78-88.

Nilsson O, Baron J. 2004. Fundamental limits on longitudinal bone growth: growth plate senescence and epiphyseal fusion. Trends Endocrinol Metab 15:370-374.

Nwaogu IC. 2002. Foetal alcohol syndrome: growth rate of bones in rats. J Appl Anim Res 22:249-253.

O'Leary CM. 2004. Fetal alcohol syndrome: diagnosis, epidemiology, and developmental outcomes. J Paediatr Child H 40:2-7.

Olivier L, Curfs LM, Viljoen DL. 2016. Fetal alcohol spectrum disorders: prevalence rates in South Africa. S Afr Med J 106:S103-106.

Osterhoff G, Morgan EF, Shefelbine SJ, Karim L, McNamara LM, Augat P. 2016. Bone mechanical properties and changes with osteoporosis. Injury 47 Suppl 2:S11-20.

Oyedele O, Kramer B. 2008. Acute ethanol administration causes malformations but does not affect cranial morphometry in neonatal mice. Alcohol 42:21-27.

Palmer C. 1985. Fetal alcohol effects: incidence and understanding in the Cape. S Afr Med J 68:779-780.

Pan Z, Zhang X, Shangguan Y, Hu H, Chen L, Wang H. 2016. Suppressed osteoclast differentiation at the chondro-osseous junction mediates endochondral ossification retardation in long bones of Wistar fetal rats with prenatal ethanol exposure. Toxicol Appl Pharmacol 305:234-241.

Pattern A, Fontaine C, Christie B. 2014. A comparison of the different animal models of fetal alcohol spectrum disorders and their use instudying complex behaviors. Front Pediatr 2:1-19.

Payton CG. 1933. The growth of the epiphyses of the long bones in the madder-fed pig. J Anat 67:371-381.

Peltzer K, Pengpid S. 2019. Maternal alcohol use during pregnancy in a general national population in South Africa. S Afr J Psychiatr 25:1236.

Petrelli B, Weinberg J, Hicks GG. 2018. Effects of prenatal alcohol exposure (PAE): insights into FASD using mouse models of PAE. Biochem Cell Biol 96:131-147.

Popova S, Lange S, Probst C, Parunashvili N, Rehm J. 2017. Prevalence of alcohol consumption during pregnancy and fetal alcohol spectrum disorders among the general and Aboriginal populations in Canada and the United States. Eur J Med Genet 60:32-48.

Raggatt LJ, Partridge NC. 2010. Cellular and molecular mechanisms of bone remodeling. J Biol Chem 285:25103-25108.

Ramadoss J, Hogan HA, Given JC, West JR, Cudd TA. 2006. Binge alcohol exposure during all three trimesters alters bone strength and growth in fetal sheep. Alcohol 38:185-192.

Ramchandani VA, Bosron WF, Li TK. 2001. Research advances in ethanol metabolism. Pathologie Biologie 49:676-682.

Robey P, Boskey A. 2009. Chapter 6. The composition of bone. In: Clifford JR, editor. Primer on the metabolic bone diseases and disorders of mineral metabolism: John Wiley & Sons, Inc. p 32-38.

Rosett HL. 1980. A clinical perspective of the fetal alcohol syndrome. Alcohol Clin Exp Res 4:119-122.

Sampson HW, Perks N, Champney TH, DeFee B, 2nd. 1996. Alcohol consumption inhibits bone growth and development in young actively growing rats. Alcohol Clin Exp Res 20:1375-1384.

Sanchis R, Sanchotello M, Guerri C. 1986. The effects of chronic alcohol-consumption on pregnant rats and their offspring. Alcohol Alcoholism 21:295-305.

Schneider ML, Moore CF, Barr CS, Larson JA, Kraemer GW. 2011. Moderate prenatal alcohol exposure and serotonin genotype interact to alter CNS serotonin function in rhesus monkey offspring. Alcohol Clin Exp Res 35:912-920.

Schnitzler CM, Solomon L. 1984. Bone changes after alcohol abuse. S Afr Med J 66:730-734.

Sebastiani G, Borras-Novell C, Casanova MA, Pascual Tutusaus M, Ferrero Martinez S, Gomez Roig MD, Garcia-Algar O. 2018. The effects of alcohol and drugs of abuse on maternal nutritional profile during pregnancy. Nutrients 10:1008.

Shankar K, Ronis MJ, Badger TM. 2007. Effects of pregnancy and nutritional status on alcohol metabolism. Alcohol Res Health 30:55-59.

Simpson M, Duggal S, Keiver K. 2005. Prenatal alcohol exposure has differential effects on fetal growth and skeletal ossification. Bone 36:521-532.

Sivaraj KK, Adams RH. 2016. Blood vessel formation and function in bone. Development 143:2706-2715.

Snow ME, Keiver K. 2007. Prenatal ethanol exposure disrupts the histological stages of fetal bone development. Bone 41:181-187.

Sokol RJ, Delaney-Black V, Nordstrom B. 2003. Fetal alcohol spectrum disorder. JAMA 290:2996-2999.

Streissguth A, Aase J, Clarren S, Randels S, LaDue R, Smith D. 1991. Fetal alcohol syndrome in adolscents and adults. JAMA 265:1961-1967.

Tang Y, Wu X, Lei W, Pang L, Wan C, Shi Z, Zhao L, Nagy TR, Peng X, Hu J, Feng X, Van Hul W, Wan M, Cao X. 2009. TGF-beta1-induced migration of bone mesenchymal stem cells couples bone resorption with formation. Nature medicine 15:757-765.

Thomas SE, Kelly SJ, Mattson SN, Riley EP. 1998. Comparison of social abilities of children with fetal alcohol syndrome to those of children with similar IQ scores and normal controls. Alcohol Clin Exp Res 22:528-533.

Tomlinson M, O'Connor MJ, le Roux IM, Stewart J, Mbewu N, Harwood J, Rotheram-Borus MJ. 2014. Multiple risk factors during pregnancy in South Africa: the need for a horizontal approach to perinatal care. Prev Sci 15:277-282.

Turner R, Kidder L, Kennedy A, Evans G, Sibonga J. 2001. Moderate alcohol consumption suppress bone turnover in adults female rats. J Bone Miner Res 16589-16594.

Turner RT. 2000. Skeletal response to alcohol. Alcohol Clin Exp Res 24:1693-1701.

Urban M, Chersich MF, Fourie LA, Chetty C, Olivier L, Viljoen D. 2008. Fetal alcohol syndrome among grade 1 schoolchildren in Northern Cape Province: prevalence and risk factors. S Afr Med J 98:877-882.

Urban MF, Olivier L, Viljoen D, Lombard C, Louw JG, Drotsky LM, Temmerman M, Chersich MF. 2015. Prevalence of fetal alcohol syndrome in a South African city with a predominantly Black African population. Alcohol Clin Exp Res 39:1016-1026.

van der Kraan PM, Blaney Davidson EN, Blom A, van den Berg WB. 2009. TGF-beta signaling in chondrocyte terminal differentiation and osteoarthritis: modulation and integration of signaling pathways through receptor-Smads. Osteoarthr cartilage 17:1539-1545.

Viljoen D, Croxford J, Gossage JP, Kodituwakku PW, May PA. 2002. Characteristics of mothers of children with fetal alcohol syndrome in the Western Cape Province of South Africa: a case control study. J Stud Alcohol 63:6-17.

Watt MH, Eaton LA, Choi KW, Velloza J, Kalichman SC, Skinner D, Sikkema KJ. 2014. "It's better for me to drink, at least the stress is going away": perspectives on alcohol use during pregnancy among South African women attending drinking establishments. Soc Sci Med 116:119-125.

Weinberg J, D`Alquen G, Bezio S. 1990. Interactive effects of ethanol intake and maternal nutritional status on skeletal development of foetal rats. Alcohol 7:384-388.

Weiner S, Traub W, Wagner HD. 1999. Lamellar bone: structure-function relations. Journal of structural biology 126:241-255.

Welch-Carre E. 2005. The neurodevelopmental consequences of prenatal alcohol exposure. Advances in neonatal care : official journal of the National Association of Neonatal Nurses 5:217-229.

Wezeman F, Emanuele M, Emanuele N, MoskolII S, Woods W, Suri M, Steiner J, Lapaglia N. 1999. Chronic alcohol consumption during male rat adolescence impairs skeletal development through effects on oteoblast gene expression, bone mineral density and bone strength. Alcohol Clin Exp Res 23:1534-1542.

Wu M, Chen G, Li YP. 2016. TGF-beta and BMP signaling in osteoblast, skeletal development, and bone formation, homeostasis and disease. Bone Res 4:16009.

Yeni YN, Christopherson GT, Turner AS, Les CM, Fyhrie DP. 2004. Apparent viscoelastic anisotropy as measured from nondestructive oscillatory tests can reflect the presence of a flaw in cortical bone. J Biomed Mater Res 69:124-130.

Zorzano A, Herrera E. 1990. In vivo ethanol elimination in man, monkey and rat: A lack of relationship between the ethanol metabolism and the hepatic activities of alcohol and aldehyde dyhydrogenases. Life Sciences 46:223-230.